NIST Special Publication 250
NIST SP 250-100

Magnetic Resonance Imaging Biomarker Calibration Service: NMR Measurement of Isotropic Water Diffusion Coefficient

Michael A. Boss
Kathryn E. Keenan
Karl F. Stupic
Nikki S. Rentz
Cassandra M. Stoffer
Stephen E. Russek
Amanda A. Koepke
Kevin J. Coakley

This publication is available free of charge from:
https://doi.org/10.6028/NIST.SP.250-100

NIST Special Publication 250
NIST SP 250-100

Magnetic Resonance Imaging Biomarker Calibration Service: NMR Measurement of Isotropic Water Diffusion Coefficient

Michael A. Boss*
Kathryn E. Keenan
Karl F. Stupic
Cassandra M. Stoffer
Stephen E. Russek
Applied Physics Division
Physical Measurement Laboratory

Nikki S. Rentz
Boulder Safety, Health, and Environment Division
Office of Safety, Health and Environment

Amanda A. Koepke
Kevin J. Coakley
Statistical Engineering Division

**Former NIST employee; all work for this publication was done while at NIST.*

This publication is available free of charge from:
https://doi.org/10.6028/NIST.SP.250-100

March 2023

U.S. Department of Commerce
Gina M. Raimondo, Secretary

National Institute of Standards and Technology
Laurie E. Locascio, NIST Director and Under Secretary of Commerce for Standards and Technology

NIST SP 250-100
March 2023

Publication History
Approved by the NIST Editorial Review Board on 2022-11-19

How to Cite this NIST Technical Series Publication
Boss MA, Keenan KE, Stupic KF, Rentz NS, Stoffer CM, Koepke A, Coakley KJ, Russek SE (2023) Magnetic Resonance Imaging Biomarker Calibration Service: NMR Measurement of Isotropic Water Diffusion Coefficient. (National Institute of Standards and Technology, Boulder, CO), Special Publication (SP) NIST SP 250-100. https://doi.org/10.6028/NIST.SP.250-100

NIST Author ORCID iDs
M. Boss: 0000-0002-9492-767X
K. Keenan: 0000-0001-9070-5255
K. Stupic: 0000-0001-8356-1660
N. Rentz: 0000-0002-7328-5639
C Stoffer: 0000-0003-2619-546X
S. Russek: 0000-0002-8788-2442
K. Coakley: 0000-0003-3787-2577
A Koepke: 0000-0001-9515-0383

Contact Information
stephen.russek@nist.gov

Abstract

This document describes a calibration service to measure the water diffusion coefficient, or diffusivity, in reference materials and tissue mimics using nuclear magnetic resonance (NMR) techniques. This calibration is restricted to materials which exhibit isotropic Gaussian water diffusion. The measurement uses the water proton spin as a tag and standard NMR gradient techniques to measure diffusion of the proton magnetization, which, in low viscosity fluids, is largely determined by the physical motion of water molecules. The calibrated materials are meant to be used in phantoms (calibration devices) to verify the accuracy of magnetic resonance imaging (MRI)-based water diffusion measurements. The local diffusion coefficient (often referred to as the apparent diffusion coefficient in complex materials) and other associated parameters, are used as image-based biomarkers to assess the state of tissue cellular density, detect tissue anomalies, characterize tumor type, evaluate treatment efficacy, and assess neural connectivity and neural tissue degeneration. A biomarker, as defined by the U.S. Food and Drug Administration, is “a characteristic that is objectively measured and evaluated as an indicator of normal biological processes, pathogenic processes, or biological responses to a therapeutic intervention.” (1) Diffusion coefficients, which describe the rate that water protons move due to random thermal motion, are phenomenological parameters that must be carefully defined and measured to enable rigorous quantification and their use as biomarkers for clinical decision making. Diffusion parameters, in addition to being dependent on local material properties, are dependent on environmental parameters such as temperature, which must be controlled and precisely and accurately measured.

Keywords

Biomarker; magnetic resonance imaging; MRI; MRI phantoms; NMR; nuclear magnetic resonance; proton magnetization diffusion; water diffusion.

Table of Contents

List of Tables

List of Figures

1. Introduction

This calibration service provides traceable measurements of the isotropic water diffusion coefficient *D*, in materials used in magnetic resonance imaging (MRI) phantoms (calibration artifacts) at a specified field strength and temperature. The diffusion measurements complement existing measurement services that provide traceable proton spin magnetization relaxation time measurements for MRI phantom materials (2). The self-diffusion coefficient is a measure of the mean square displacement of water molecules due to random thermal motion. For classical Gaussian diffusion[a] in three dimensions and in the absence of any driving fields or concentration gradients, the distance travelled by a water molecule, $r_i = |\vec{r}_i(t) - \vec{r}_i(t=0)|$, in time t and direction $\hat{n}$, is given by $\langle r_i^2 \rangle = 6\hat{n} \cdot \overline{\overline{D}} \cdot \hat{n}t$, where $\vec{r}_i(t)$ is the position of water molecule *i*, and the average is over an ensemble of similar water molecules. For complex materials, diffusion may be anisotropic and the water diffusivity, $\overline{\overline{D}}$, is a second rank tensor. For this measurement service, we restrict measurements to materials whose diffusion is Gaussian, isotropic and characterized by a scalar value *D*. Due to the design of the measurement cell and gradient calibration procedure, *D* is usually measured along 2 axes perpendicular to the magnetic field and the reported self-diffusion coefficient is the average of these measurements. The geometric calibration of the magnetic field gradients along the field axis is not as precise, and the calibration of the gradient along the field axis is done using an isotropic calibrant such as water, with the calibrant's value taken as the measured transverse diffusivity. Measurement of the diffusivity along the field axis may be done if there is reason to believe the material is anisotropic and the full diffusion tensor needs to be measured.

The measurements are based on a variable-field, variable-temperature, nuclear magnetic resonance (NMR) system with 3-axis magnetic field gradients (2). The parameter measured is proton magnetization diffusivity (3) which for low viscosity liquids with large diffusion coefficients (> 10^{-12} m^2/s), is equal to the water diffusion coefficient within the stated uncertainty.[b] The effect of spin diffusion due to exchange and dipolar interactions, which do not involve water motion, are negligeable as discussed in Sec. 6.4.

NMR and MRI systems are qualitatively similar; however, given the smaller sample volumes in NMR systems, key parameters such as radio frequency (RF) field intensity, magnetic field distortions, and the timing of RF pulses can be better controlled and made more precise. Gradient amplitudes and gradient slew rates can be much larger. Most importantly, NMR systems allow the proton spin signal to be spectrally resolved so that the signal from water protons can be separated from the signal of protons on other molecules within the material. Hence, NMR is a better system for primary measurements of many key MRI biomarkers. The corresponding MRI biomarker is usually referred to as the apparent diffusion coefficient (ADC) of water. Tissues have considerable complexity with populations of water in many

[a] Water molecules are fundamentally indistinguishable, and the classical definition of self-diffusion is not well posed. Classical diffusion requires the ability to tag a particle without altering it. Water can be tagged either by replacing an atom with a different isotope, e.g., using deuterated water or by using the nuclear spin. These techniques require corrections to obtain the water-self diffusion coefficient, which for the case of spin-tagging for water based biological materials, is small.

[b] Here, we define the standard uncertainty for a measurand m, as a positive number, u_c, and define a coverage interval with approximately a 68 % level of confidence as $m \pm u_c$. The coverage interval, as discussed in Section 6, is an element in an ensemble of uncertainty estimations for a given parameter obtained through repeated experiments or simulations. The coverage intervals for all experimental parameters are given by $m \pm u_c$ except when it is explicitly stated that we are reporting an expanded uncertainty $U = ku_c$, where $k = 2$.

different environments with membranes and barriers. Tissues may show multiple water diffusion coefficients, non-Gaussian diffusion, as well as strong dependence of diffusion on the measurement time and length scale. This measurement service is restricted to materials showing single component Gaussian diffusion over the range of the measurements reported. The measurement range is specified by the range of temperatures, the applied spin-gradient wavevectors used in the experiments and the associated parameter, b, which is a measure of the size of and exposure to the gradient pulses.

2. Calibration Service Summary

The diffusion measurements are performed in an NMR system at clinical MRI magnetic fields of 1.5 T, 3.0 T, and 7.0 T, with variable sample temperatures between 0 °C to 50 °C. While pure-water diffusion is not field dependent, measurement at clinical magnetic fields allows other important MRI biomarker parameters, such as the longitudinal spin relaxation time T_1 , and transverse spin relaxation time T_2 , which are field dependent, to be measured concurrently. The customer's aqueous solutions are sent to NIST, and the customer specifies the desired measurement fields and sample temperatures. The sample volume for measurement is approximately 20 µl. It is recommended that at least 20 ml be provided by the customer to ensure that several samples can be taken and to minimize effects due to evaporation or surface contamination when the bottle is opened, and pipettes inserted. The dynamics of the magnetic moment of the customer's material solutions must conform with the Bloch Torrey equations (3) as described in Sec. 3. The samples must be stable for the duration of the measurement process. At the completion of the calibration measurements, the unused material under test and a calibration report are sent to the customer. The calibration report summarizes the results of the measurements and provides a statement of the total measurement uncertainty. This document provides the reference for the isotropic water diffusion measurements that are part of the NIST Calibration Services.

The NMR system calibration is detailed in Secs. 4 and 5, with a short summary given here. The NMR time base is calibrated with a rubidium frequency standard that is first verified against a NIST-traceable rubidium atomic clock. The temperature is monitored using a non-magnetic fiber optic or resistance thermometer that is calibrated against two NIST-traceable platinum resistance thermometers. The average DC magnetic field magnitude at the sample position,[c] is determined after shimming[d] with an uncertainty less than 1 µT by the resonant frequency of protons in water based on the Committee on Data for Science and Technology (CODATA) value of the water proton gyromagnetic ratio (4). The RF probe is tuned and matched for the sample type being measured. The NMR RF power calibration is done before each series of measurements using nutation experiments described in Sec. 4.1. The intrinsic instrument linewidth, the minimum linewidth obtainable by the system, is measured on narrow linewidth samples such as deionized water in the standard sample configuration. The instrument linewidth, after shimming, is less than 2 Hz full width at half-maximum (FWHM). The diffusion measurements use a special cell with a localized sample volume, which has less homogeneity that a standard NMR capillary cell. This results in additional inhomogeneous

[c] The local field experienced by a water proton in a sample may differ from the B_0 field by several ppm depending on the susceptibility and configuration of sample inserted. The local field is a combination of B_0 field, applied gradient fields, magnetic fields generated by the sample and sample container, microscopic fields, and other environmental fields.
[d] Shimming refers to homogenizing the magnetic field around the sample by adjusting the currents in a set of superconducting and room temperature shim coils. Our system has 9 superconducting and 17 room temperature shim coils.

line broadening. The inhomogeneous broadening for diffusion measurements is required to be less than 10 Hz and is typically between 2 Hz and 7 Hz. The most important calibrations are the gradient strengths, which are calibrated by measuring the frequency widths, Δf, in one dimensional (1D) images of the precisely machined cylindrical sample cell. The spread in observed resonance frequencies is related to the gradient strength by $\Delta f_i = \gamma_{wp} G_i d_i$, where $\gamma_{wp}$is the water proton gyromagnetic ratio and $G_i, d_i$are the gradient strength and cell dimension in the *i* direction. The sample cell dimensions are determined using X-ray micro-computed-tomography (microCT) and optical microscopy, which are calibrated using a precision sphere with a NIST-traceable diameter.

The diffusion measurements include precise temperature control since diffusion is a thermally driven process and has considerable temperature dependence. There are tradeoffs in the ability to simultaneously minimize uncertainties in NMR-based parameters and sample temperature. The sample thermometer must be as close as possible to the sample, but not perturb the NMR measurements. Diffusion coefficients are measured at several different temperatures to obtain the temperature variation and temperature-related uncertainty. The biggest components of the uncertainty arise from temperature, gradient calibration, and eddy current correction uncertainties. Our measurement protocol is similar to, and based on, many previous studies in the literature. (5-10)

3. Theory of Measurement

3.1. Diffusion Model and Measurement Equations

The proton spin dynamics of a spin packet[e], located at position $\vec{r}$ in an applied magnetic field B_0 along the *z*-axis, is measured by monitoring the spin-packet magnet moment $\vec{\mu}(\vec{r}, t) = \sum_i \langle \vec{\mu}_i \rangle$,where $\langle \vec{\mu}_i \rangle$ is the expectation value of the magnetic moment operator of the i^{th} proton in the spin packet. The proton magnetization, $\vec{M}(\vec{r}, t)$, is then given by the sum over spin packets divided by the volume of the spin packets. We assume that the time evolution of the local magnetization, in the presence of diffusion, is adequately modeled by the Bloch-Torrey equation (3):

$$\dot{\vec{M}}(\vec{r}, t) = \gamma \vec{M} \times \vec{B}(\vec{r}) + \frac{M_0 - M_z}{T_1}\hat{z} - \frac{\vec{M}_\perp}{T_2} + \nabla \cdot \bar{\bar{D}}(\vec{r}) \nabla (\vec{M} - \vec{M}_0), \quad (1)$$

where $\vec{B} = \vec{B}_0 + \vec{B}_G(t) + \vec{B}_L + \vec{B}_1(t) + \vec{B}_n(t)$ is the magnetic flux density at the spin packet; $\vec{B}_0$ is the macroscopic main field due to the solenoid and shim coils; $\vec{B}_G \cong \vec{g} \cdot \vec{r}\hat{z}$ is the field produced by the gradient coils when energized; $\vec{B}_L$ is the local fields produced by the sample and sample holder; $\vec{B}_1(t)$ is the applied time dependent RF fields; $\vec{B}_n(t)$ is the field created by environmental and thermal noise; T_1 is the longitudinal spin relaxation time; $\vec{M}_t = M_x\hat{x} + M_y\hat{y}$ is the transverse component of the proton moment; and T_2 is the transverse spin relaxation time. $\bar{\bar{D}}(\vec{r})$ is the diffusion tensor, which for the materials considered here, will

[e] A spin packet, often referred to as an isochromat, refers to an ensemble of like spins, which is spatially large on the atomic scale, but very small on the scale of the variations in local magnetic fields. Spins are alike if they belong to the same species, are in the same chemical environment, and are in the same structural environment, e.g., they are all flowing together. We prefer the use of "spin packet" to isochromat, since isochromat originally referred to spins with the same Larmor frequency; we are generalizing to similar spins sharing a similar environment. The numerical calculations, described in Sec. 7, model the sample as a large number of spin packets with different locations, local fields, and properties, each obeying Eq. 1 with different parameters.

have the form $\bar{\bar{D}}(\vec{r}) = D\bar{\bar{I}}$, with $\bar{\bar{I}}$ being the identity matrix. Note, an additional term, $\bar{\bar{D}}_e(\vec{r})$, would be needed to describe spin diffusion mediated by exchange and dipolar coupling, which is not of importance for the samples considered here.

The equilibrium proton magnetic magnetization M_0 of a spin packet is

$$M_0 = \frac{\hbar^2 \gamma_{wp}^2 B_0 N_p}{4 k_b T_s}, \tag{2}$$

where T_s is the sample temperature; N_p is the number of protons per unit volume in the spin packet; $\hbar$ is the reduced Planck constant; andk_b is the Boltzmann constant. The B_0 field is assumed to be much larger than all other field components. For measurements performed under the service described here, B_0 is at least a factor of 10^4 greater that the other listed field components. In the absence of any other fields the magnetization will precess about the B_0 field at the left-handed Larmor frequency:

$$f_0 = \frac{\gamma_{wp}}{2\pi} B_0. \tag{3}$$

The proton magnetization vector can be manipulated by application of RF fields perpendicular to B_0 with a frequency close to the Larmor frequency, which is 63.9 MHz, 128 MHz, and 298 MHz for field values of interest (1.5 T, 3.0 T, and 7.0 T). By application of RF fields (referred to as B_1 fields), the magnetization experiences a torque causing rotation away from B_0 by a tip angle $\alpha \cong \gamma_{wp} B_1 \Delta t$, where Δt is the duration of the RF pulse. After the application of resonant RF pulses, the magnetization will acquire a component in a plane transverse to B_0; where it will precess about B_0 at the Larmor frequency, enabling inductive detection of the nuclear magnetization, and gradually relax back to its equilibrium value.

The Bloch equation is phenomenological and must be applied carefully. It often does not apply to spin systems with spin greater than ½ because, in higher spin systems, there are electric quadrupole moments and many excitation levels with potentially many different relaxation time constants. It does not include the physics required to determine field, temperature, and refocusing time dependence of the relaxation times. It does not apply to systems that have coherent interactions between spins. The Bloch equation formalism can, however, provide a precise description of an ensemble of incoherently interacting spin ½ particles, such as found in water and water-based fluids, when appropriate phenomenological parameters are used.

The Bloch equation does not predict important effects such as spin echoes, multiple relaxation times and diffusion coefficients, and spatial variations due to thermal and sample inhomogeneities. To model this complex structure, a large ensemble of spin packets, each obeying a Bloch equation with different locations and local parameters, is required. We refer to the model using a linear superposition of a large ensemble of spin packets, with varying properties and local fields, each obeying the Bloch-Torrey equation, as the Bloch-Torrey model.

The transverse magnetization of a spin packet can be described as a complex quantity $m = m_x + i m_y$ obeying, in the presence of only the applied and gradient fields, the equation

$$\dot{m}(\vec{r}, t) = -i\gamma B_0 m - i\gamma \vec{g} \cdot \vec{r} m - \frac{m}{T_2} + \nabla \cdot D \nabla m \tag{4}$$

Note, the gradient field term is approximate and does not satisfy the Maxwell equation $\vec{\nabla} \cdot \vec{B} = 0$. The additional field terms, transverse to the applied field axis, required by Maxwells equations have a contribution to the transverse magnetization phase (3) on the order $\varphi = \left|\frac{g(x+iy)}{B_0}\right| < 10^{-4}$ for our gradient amplitudes, sample dimensions and applied field, and are ignored.

After the application of a gradient $\vec{g}(\tau)$, the transverse magnetization will be given by a linear phase gradient $m \propto e^{-i\vec{q}\cdot\vec{r}}$, corresponding to a helical magnetization, with a wave vector given by

$$\vec{q}(t) = \gamma \int_0^t \vec{g}(\tau) d\tau \tag{5}$$

If the gradient induced variation of the magnetization is much larger than other sources of spatial variation of within a sample, the gradient term can be simplified

$$\nabla \cdot D\nabla m \rightarrow -q^2 Dm$$
$$\dot{m}(\vec{r}, t) = -i\gamma B_0 m - i\gamma \vec{g} \cdot \vec{r} m - \frac{m}{T_2} - q^2 Dm \tag{6}$$

Eq. 4 can now be solved giving

$$m(\vec{r}, t) = m_0 e^{-i\gamma B_0 t} e^{-i\vec{q}\cdot\vec{r}} e^{-\frac{t}{T_2}} e^{-D\int_0^t q^2 d\tau} \tag{7}$$

It is customary to define a parameter b given by:

$$b(t) = \int_0^t q^2 d\tau \tag{8}$$

which describes the exponential loss of signal due to diffusion along a q-space time trajectory created by a magnetic field gradient $\vec{g}(t) \cdot \vec{r}\hat{z}$. Physically, the magnetization is wound up into a helical structure with varying pitch and direction, with a corresponding reduction in magnetization, at each time t, due to diffusion of $-q(t)^2 Dm(t)$. For most diffusion measurements, a q-space trajectory is chosen to return to $\vec{q} = 0$. The diffusion coefficient can then be determined from the net decrease in the observed transverse magnetization after the completion of the gradient pulses at time t_f

$$\frac{m(b, t_f)}{m(b = 0, t_f)} = e^{-bD} \tag{9}$$

The observed signal $S(t)$ is the complex-valued inductive voltage generated in the RF coil from the sum over the entire ensemble of spin packets precessing transverse moments and is given by the reciprocity equation (11)

$$S(t) = -i\omega_0 \sum_n C(\vec{r}_n) m_n(\vec{r}_n, t) v_n \tag{10}$$

where $C(\vec{r}_n)$ is the coil sensitivity function, the field per unit current produced by the RF coil at $\vec{r}_n$, the position of the spin packet n, and v_n is the volume of the spin packet. The free induction decay (FID), the signal decay without the presence of any RF or gradient fields, is measured after the application of the gradients. The observed signal consists of induced voltages in the transmit/receive coil with a frequency in the range of range of 1 MHz to 400 MHz, depending on the field strength of the measurement. This signal is mixed with a reference signal at an operator set observe frequency to obtain a signal in the audio frequency range, typically 0.5 kHz to 100 kHz. This signal is digitized to obtain the measured FID. The FID is then Fourier transformed to obtain a spectrum. The spectra are plotted as a function of the relative frequency, with zero frequency being the user set observe frequency. The real part of the water peak is integrated to give a measurand S_{m}, which is proportional to the integrated magnetization of the water protons at t_f after signal decrease due to water diffusion. The measurand S_{m} is ideally given by

$$S_{\mathrm{m}} = S_0 e^{-bD} \tag{11}$$

3.2. Pulsed Gradient Spin Echo Sequence

There are many pulse sequences that can be used to measure magnetization diffusion using gradient pulses. The pulse sequence used here, the pulsed gradient spin echo (PGSE) sequence developed by Stejskal and Tanner (12), shown in Fig. 1, was chosen due to its simplicity, robustness, and ability to evaluate uncertainties.

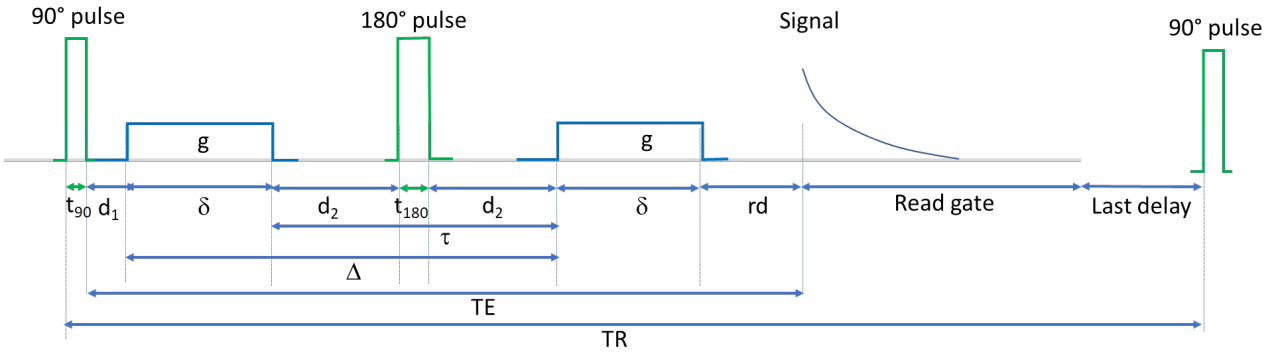

Fig. 1. Pulsed Gradient Spin Echo (PGSE) Sequence

The PGSE sequence uses two equal gradient pulses with a 180° refocusing pulse between them. The critical parameters are the amplitude of the gradient pulse, g; duration of the gradient pulse, δ; the time between gradient pulses, τ; and the repetition time between RF excitations, TR. A typical set of gradient pulses is shown in Fig. 2, along with the calculated q-space trajectories and measured free induction decays (FIDs). The standard values of the pulse sequence parameters used in this measurement service are approximately gradient duration δ = 7 ms, time between the gradients τ = 28 ms, read delay rd = 4 ms, and $TR > 5T_1$. These times, as discussed below, are modified slightly when accounting for gradient rise times, RF pulse durations and gating times. These pulse sequence time parameters were chosen as a compromise between getting high b-values, not having overlarge gradients and eddy currents, and minimizing the time to readout so short T_2 samples can be measured.

For an ideal PGSE sequence, q returns to zero after the end of the second gradient pulse. For the case of rectangular pulses, the b-value after the completion of the gradient pulses can be calculated by analytically integrating Eq. 8 and is given by

$$b = \gamma^2\delta^2 g^2\left(\frac{2}{3}\delta + \tau\right) = \gamma^2\delta^2 g^2\left(\Delta - \frac{1}{3}\delta\right) \text{ where } \Delta = \tau + \delta \tag{12}$$

here, the term proportional to $\frac{2}{3}\delta$ gives the decrease of the magnetization due to diffusive attenuation during the two gradient pulses, and the term proportional to τ gives the decrease of the magnetization due to diffusive attenuation during the interval between the gradient pulses. In general, the gradient pulses have a finite rise time, and the gradient amplitude may not be constant. Other gradient waveforms, $G(t)$, (13) may be chosen to minimize eddy currents and gradient rise-time effects. A general formula for monopolar gradients of arbitrary shape is given by (14)

$$b = \sigma^2\gamma^2\delta^2 g^2(\Delta - 2(\lambda - \kappa)\delta) \tag{13}$$

where $\sigma = \frac{1}{g\delta}\int_0^\delta G(t)dt$ is the gradient pulse shape factor,

$$\lambda = \frac{1}{\gamma g\sigma}\int_0^\delta q(t)dt \tag{14}$$

$$\kappa = \frac{1}{\gamma g\sigma}\int_0^\delta q^2(t)dt \tag{15}$$

Table 1. Gradient pulse shapes, shape factors, and equations for determining b-factors.

Pulse Shape	$\boldsymbol{\sigma}$	$\boldsymbol{\lambda}$	$\boldsymbol{\kappa}$	**b**
rectangular	1	$\frac{1}{2}$	$\frac{1}{3}$	$\gamma^2\delta^2 g^2\left(\Delta - \frac{1}{3}\delta\right)$
trapezoidal pulse with rise/ fall time = ϵ	$1 - \frac{\epsilon}{\delta}$	$\frac{1}{2}$	$\frac{1}{2} - \frac{\sigma}{6} + \frac{\epsilon^3}{60\delta^3\sigma^2} - \frac{\epsilon^2}{12\delta^2\sigma}$	$\gamma^2\delta^2\sigma^2 g^2\left(\Delta - \frac{1}{3}\delta\sigma + \frac{1}{30}\frac{\epsilon^3}{\delta^2\sigma^2} - \frac{1}{6}\frac{\epsilon^2}{\delta\sigma}\right)$
$g\sin\left(\frac{\pi t}{\delta}\right)$	$\frac{2}{\pi}$	$\frac{1}{2}$	$\frac{3}{8}$	$\frac{4}{\pi^2}\gamma^2\delta^2 g^2\left(\Delta - \frac{1}{4}\delta\right)$
$g\sin^2\left(\frac{\pi t}{\delta}\right)$	$\frac{1}{2}$	$\frac{1}{2}$	$\frac{1}{3} + \frac{5}{8\pi^2}$	$\gamma^2\delta^2 g^2\left(\Delta - \frac{1}{3}\delta\right)$

The parameters for standard pulse shapes are given in Table 1. The measured diffusion coefficient must be independent of the gradient pulse shape used, which means that they agree within their combined uncertainties. The uncertainties for different gradient pulse

shapes and pulse sequences can vary since nonidealities, such as output current unfaithfulness and eddy currents can depend on gradient pulse shape. The *b*-value can also be determined by a numerical integration of the measured gradient current waveform.

A discussion of the relative accuracy of using analytical *b*-values verses those calculated from numerical integration is presented in Sec. 4.3. The gradient strengths are adjusted so that there are many cycles within the sample. For the pulse sequence shown in Fig. 2, there is a maximum of $q/2\pi \approx 50$ cycles/mm, whereas the sample size is 3.0 mm. The selected range of *b*-values is typically between 0 to 2000 s/mm^2 and 0 to 10000 s/mm^2 depending on material. The range is selected to ensure that two to four orders of magnitude in signal decrease are observed for accurate determination of the diffusion coefficient. This range of *b*-values covers the range used in most clinical and research scanners.

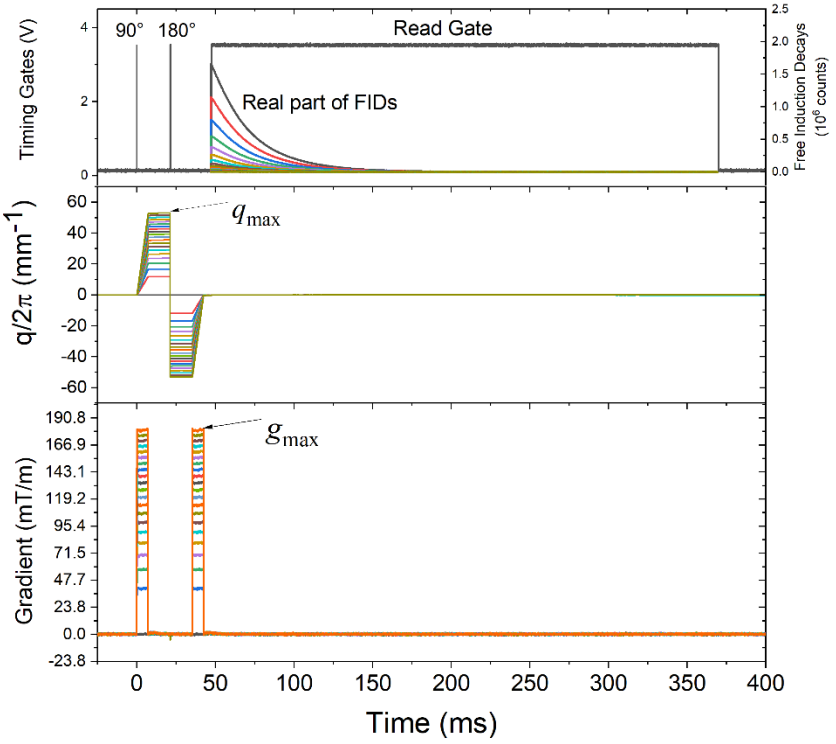

Fig. 2. Pulsed gradient spin echo sequence and recorded free induction decays (real part) for a $CuSO_4$ solution sample at 20 °C with a T_1 = 47.0 ms, T_2= 39.1 ms. The gradient pulses are distributed quadratically to give a uniform b-value spacing, (a) Pulse timing and measured free induction decays. (b) Calculated wavevectors q, normalized by 2π to give the cycles per mm. (c) Recorded gradient pulses from the gradient amplifier current monitors. The PGSE protocol can be characterized, as defined in the figure, by its maximum spin density wavevector q_{max} and its maximum gradient strength g_{max}.

The magnitude of the transverse magnetization at the beginning of the read gate is given by

$$\frac{m_i}{m_0} = e^{-\frac{2\delta+\tau}{T2}} e^{-bD} \tag{16}$$

The measured FID signal is proportional to the magnetic moment $S \propto \frac{m_i}{m_0}$.

The full FIDs, both real and imaginary components, are recorded during the read gate. For a single spin packet, n, in a uniform magnetic field, the FID will be exponentially decaying with a time constant T_2. The FIDs are Fourier transformed to get the spectra, which for exponentially decaying FID, will be Lorentzian with real and imaginary components given by

$$S_n'(\omega) = \frac{S_n(0)T_2}{1 + T_2^2\,(\omega - \omega_0)^2};\; S_n''^{(\omega)} = \frac{S_n(0)T_2^2(\omega - \omega_0)}{1 + T_2^2\,(\omega - \omega_0)^2}, \tag{17}$$

where $\omega = 2\pi f$ is the measurement frequency and ω_0 is the resonance frequency of the proton spin resonance being observed, both relative to the observe frequency. Here, unless otherwise noted, we plot spectra as a function of relative frequency, f, with positive frequencies (faster precession) to the right. This is opposite to a common convention used by chemists that plot lower frequencies to the right.

The measured spectra will be a sum over all spin packets of Lorentzians with a distribution of resonant frequencies due to variations in local field.

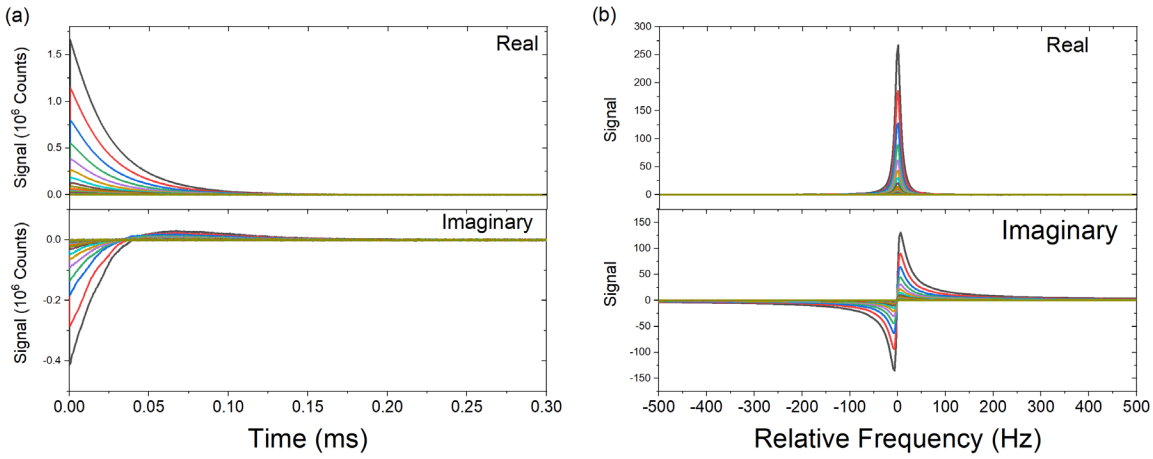

Fig. 3. (a) Real and imaginary components of the free induction decays for the sample and pulsed-gradient spin-echo sequence used in Fig. 2. (b) Real and imaginary components of the spectra.

The FIDs and spectra for a $CuSO_4$ water solution for a PGSE sequence are shown in Fig. 3. We define the measured signal S_m, to be integrated intensity of the real part of the measured spectra. Given an exponential FID, the signal S_m will be given by

$$S_m = \pi S_0 \propto \frac{m_i}{m_0} \tag{18}$$

The normalized signal $S_m/S_m(b = 0)$, is plotted versus b-value, as shown in Fig. 4. The exponential fits give the measured diffusion coefficient $\widehat{D}$. There are other possible measures

of the strength of the signal, which are also proportional to m_i, including the maximum of the amplitude of the FID and the maxima of the spectra. For a system with a single proton environment these will give similar results (see section 4.4.5). The advantage of using the integrated real part of the spectra is that it can spectrally resolve different proton environments, and, since it averages over many points in the spectra through the integration process, is more robust with a higher signal to noise ratio. The signal definition is not dependent on the exact shape of the spectra, however, if there is a significant deviation from a Lorentzian line shape, the separation into real and imaginary components may not be well defined.

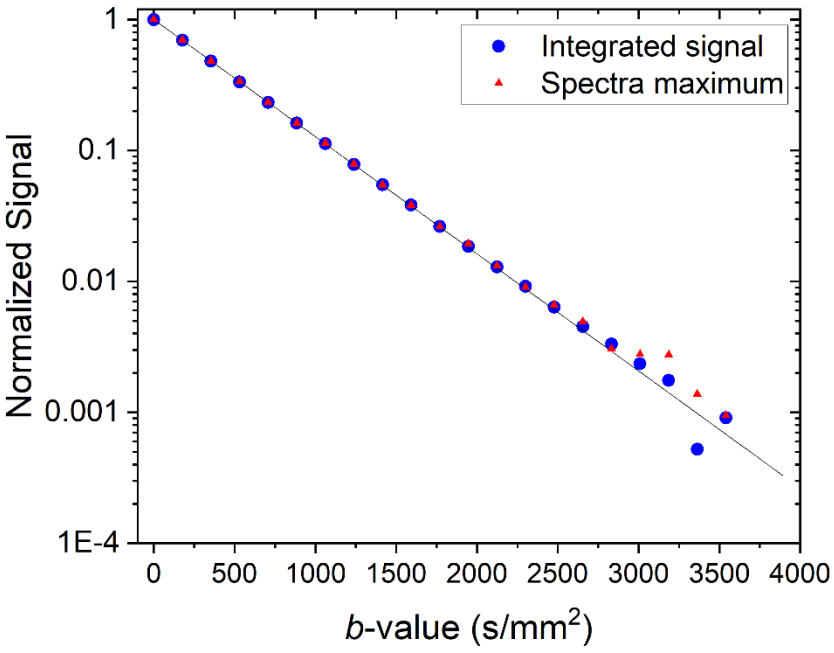

Fig. 4. Normalized signal derived from the integrated spectra and maxima of spectra verses *b*-value. The diffusion coefficients derived from the fit (black lines) are $\hat{D}$ = 2.060 x10^{-3} mm^2/s and $\hat{D}$ = 2.052 x10^{-3} mm^2/s for the integrated and maxima signals, respectively. The standard error of the predicted value of D, from estimated covariance matrix, is typically 0.001 mm^2/s .

4. Sample Geometry and Measurement System

The measurement system, shown in Fig. 5, for proton magnetization diffusion coefficient consists of a superconducting magnet, an NMR probe with receive/transmit coil tuned to the appropriate ^{1}H frequency, an RF amplifier, gradient amplifiers, a console that generates and records RF and gradient signals, a fiber optic thermometer placed next to the sample, and a gas flow system with a heater to control sample temperature. The sample is contained in a precision-machined NMR sample cell and is cylindrical with a 3 mm diameter and 3 mm height.

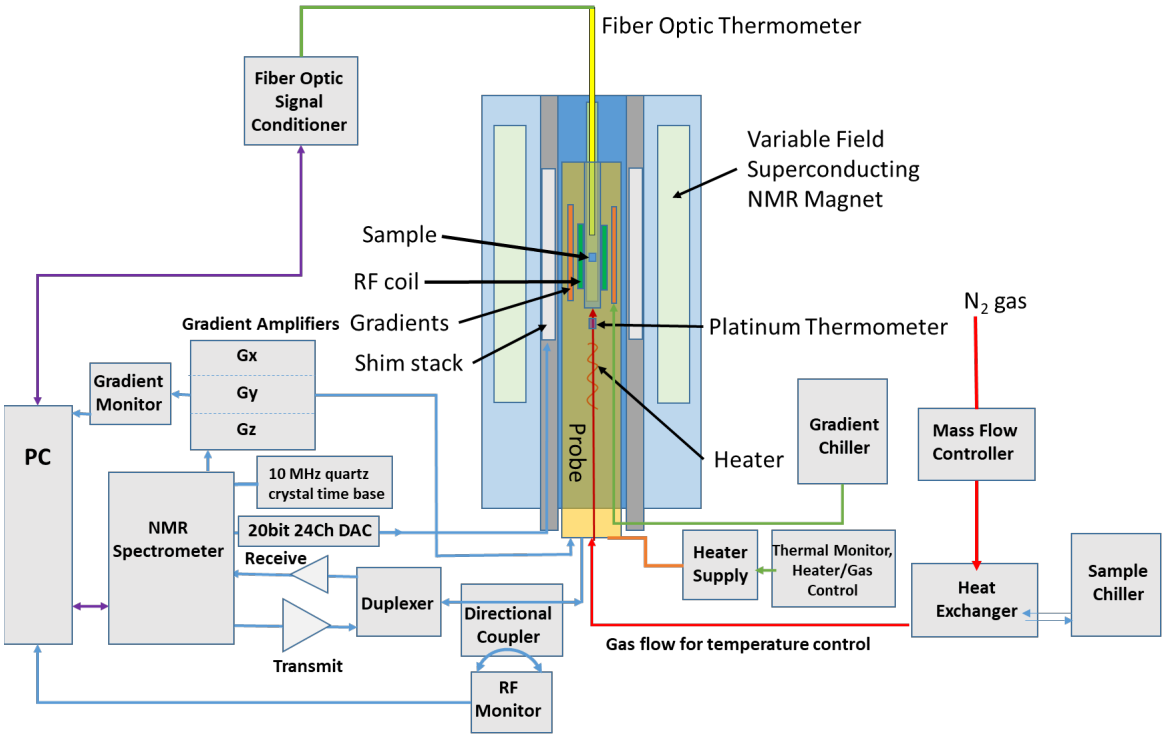

Fig. 5. Schematic diagram of the NIST NMR measurement system.

4.1 NMR system

The NMR system, shown in Fig. 5, was assembled by NIST using commercially available parts. The NMR magnet is Oxford 300-44 project No: 62440; Magnet No: 93894; Cryostat No: DLN0495/30/1. The NMR spectrometer is Tecmag Redstone HF-1 paired with Tecmag TNMR version 3.3.9 software. The NMR probe is Doty DSI-1425, a triaxial gradient probe with low- and high-frequency RF channels for detection of ^{2}H and ^{1}H NMR signals, respectively. The system uses three AE Techron 7224 gradient amplifiers and one Tomco 200 W RF amplifier. The probe is designed to work at frequencies from 42 to 300 MHz corresponding to field strengths of 1 to 7 T. Different tuning wands must be inserted at different operation field strengths, as specified in the manufacturer's instructions. The RF coil is a multi-turn linearly polarized transmit/receive saddle coil with a 14 mm homogenous RF length. The RF coil at maximum power can perform a $\pi/2$ pulse in 8 μs. The probe is set up to take standard 5 mm NMR sample tubes. The gradient coils are cooled with a fluorinated fluid (Fluorinert FC-43), and there is a gas flow/heater system to control the sample temperature. The fiber optic thermometer and controller are an Opsens OTP-M and an AccuSens, respectively. The main solenoid field and superconducting shims are ramped using a Cryomagnetics 4G-100/SHIM superconducting magnet power system. Room temperature shims are set using a Tecmag high-stability 24-channel 20 bit digital to analog converter.

4.1.1 Magnetic Field Ramp and Shimming

The magnet is ramped by insertion of a set of down leads and energized using a superconducting magnet power supply following the manufacturer's operation manual for field ramp rates and energizing procedures. Because the magnet is operated at MRI field values, not at typical NMR field values, the magnet manufacturer does not specify field parameters at all the operation fields. The superconducting shim coils are de-energized during the field ramp by opening all the persistent current switches. Field stability is improved by overshooting the target field value by 2 % and then returning to the desired set point. The resonance of a test sample is measured as the field approaches the desired value to monitor the field magnitude, the field inhomogeneity, and the field stability. The field is stabilized within 100 ppm of the target value. The noise spectrum is monitored to ensure that the sample resonance at the final field value is not close to any noise sources or system resonances.

The magnet is shimmed by ramping the nine superconducting shim coil currents (Z, Z2, Z4, X, Y, ZX, ZY, $X^2–Y^2$, 2XY) to predetermined values for each field strength. Then an automated shimming routine, using the Berger-Braun shimming method (p. 8 of ref. (15)), is run to adjust the 17 values of the room-temperature shim currents. The 17 room temperature shims are Z1, Z2, Z3, Z4, Z5, X, Y, XZ, YZ, XY, X^2-Y^2, Z^2X, Z^2Y, ZXY, $Z(X^2–Y^2)$, X^3, Y^3. The values of the room temperature shims are then used to readjust the superconducting shims to minimize the currents in the room-temperature shim coils. Both the peak width and symmetry of the line width are assessed. The line width of a long capillary of high purity water is required to be less than 1 Hz and the asymmetry, as determined by a Lorentzian fit, is required to be less than 2 %. These measurements are done without spinning of the sample since diffusion calibrations are done with an embedded sample thermometer that precludes spinning of the sample.

The field stability of the system is determined by setting up a 15 h scan that monitors the resonance peak every 10 min. The magnetic field drift should be less than 2 Hz/h or 50 parts per billion/h.

4.1.2 NMR time base verification:

To verify the accuracy of the NMR console oven-controlled crystal oscillator (the system time base that has a nominal frequency 10 MHz), a frequency counter calibrated against a NIST-traceable rubidium frequency reference is used. The measured frequency of the NMR time-base oscillator is 10.000 000 MHz ±5 Hz.

4.1.3 Probe tuning:

To maximize signal, the RF probe resonance condition is verified on a vector network analyzer by monitoring the complex reflection coefficient S_{11}. The RF probe resonance, where minimal RF power is reflected during the S_{11} measurement, is adjusted to within 50 kHz of the NMR frequency of the material under test and the imaging bandwidth 50 kHz lies below -20 dB, as shown in Fig. 6. This ensures the accuracy of the gradient calibration images. The frequency position of the probe resonance is controlled by a variable "Tune"

capacitor. The resonance impedance is adjusted by a variable “Match” capacitor to approximately 50 ohm, which is identified by maximizing the absorption of RF power in the $|S_{11}|$ measurement. The minimum value of $|S_{11}|$ should be below -30 dB.

The tune and matching conditions do not change much with sample or with the sample not inserted. The tuning is done with the first sample of the series in place, and not changed thereafter. A small temperature dependence is observed, as shown in Fig. 7, however tuning in the center of the desired measurement range, typically 20 °C, is sufficient to stay within the specified tuning criteria.

After tuning the RF probe, a nutation experiment is carried out for each sample following the procedure described next.

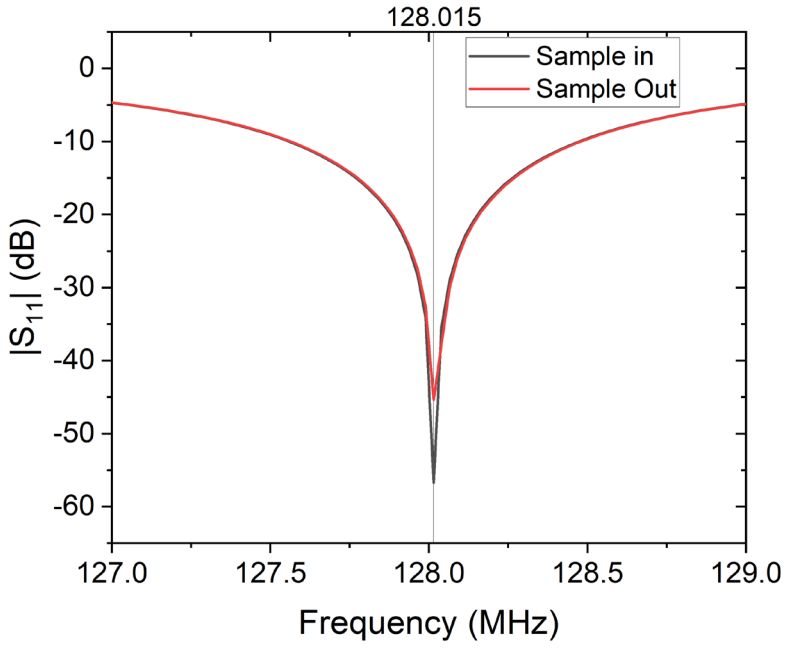

Fig. 6. The magnitude of the reflection coefficient $|S_{11}|$ versus frequency of NMR probe with and without sample inserted

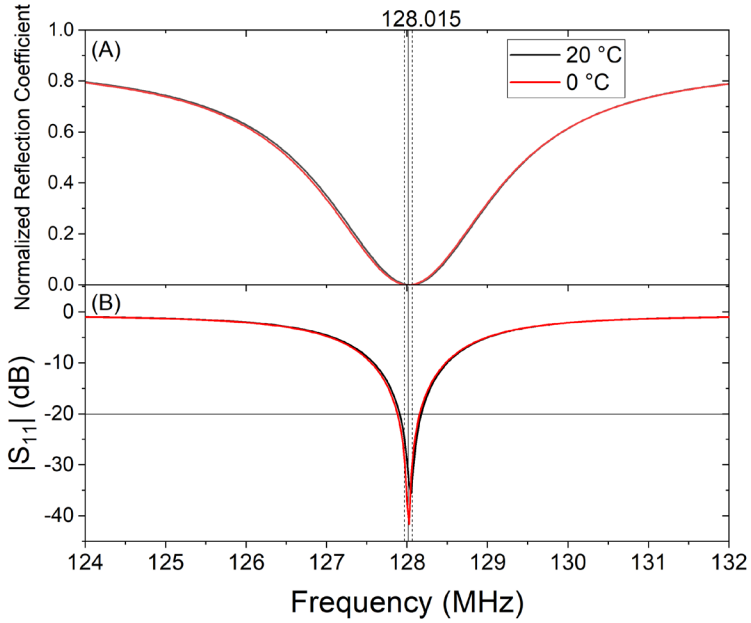

Fig. 7. The magnitude of the reflection coefficient $|S_{11}|$, on a linear (A) and a log scale (B), for the RF coil when the magnetic field is at 3.015 T and the sample temperatures is at 0 °C, and 20 °C. The solid vertical line indicates the proton resonance frequency, and the dashed vertical lines indicate the band width of the calibration images.

4.1.4 NMR radiofrequency (RF) power calibration:

RF power is calibrated using a nutation procedure that records the signal amplitude as a function of RF pulse duration τ_{RF}. The calibration is done using the material under test before each sequence of measurements. The RF pulse amplitude, $B_{1\text{amp}}$, remains fixed. For our NMR system, the RF amplitudes are typically 400 μT to 500 μT, which is much larger than chemical shifts or B_0 distortions. Hence, in the reference frame rotating with the applied RF field, the B_1 field is stationary and lies approximately in the transverse plane. The signal amplitude, S, is defined as the integral of the real part of the spectra obtained from the FIDs. An example of a nutation data set is shown in Fig. 8. For an ideal system, with a constant B_1 amplitude across the sample, we would expect the signal to vary as $S(\tau_{RF}) = S_0 \sin(\gamma B_1 \tau_{RF})$. Since the RF amplitude is not precisely constant over the sample, the signal will decay and can, for a sample well localized in the RF coil, be fit with an exponentially damped sinusoid

$$S(\tau_{RF}) = S_0 e^{-\frac{\tau_{RF}}{\tau}} \sin(\gamma B_1 \tau_{RF}) \tag{19}$$

to obtain an average B_1 and the pulse durations required to tip the spins by 90°, $t_{90} = \frac{\pi}{2\gamma B_1}$, and 180°, $t_{180} = \frac{\pi}{\gamma B_1}$.

The exponential decay time τ is also determined and is required to satisfy $\frac{S(t_{810})}{S(t_{90})} > 0.7$ and $\tau > 22.4t_{90}$, which ensures high B_1 homogeneity over the 3 mm sample.

The variation of B_1 with position along the z-axis can be determined by measuring t_{90} as a function of sample position as shown in Fig. 9a, where $B_1 = \frac{\pi}{2\gamma t_{90}}$. The magnitude of B_1 is fairly constant over the center 8 mm of the coil and the intensity can be accurately fit with a function of the form $B_1 = b_{10}(1 - \left(\frac{(z-z_0)}{c}\right)^4$, where b_{10} is the RF magnetic field in the center of the coil, z_0 is the z axis center of the RF coil and c is a fitting parameter. The uncertainty modeling uses a B_1 nonuniformity given by

$$B_1 = b_{10}\left(1 - \left(\frac{x}{a}\right)^4 - \left(\frac{y}{b}\right)^4 - \left(\frac{(z-z_0)}{c}\right)^4\right) \quad (20)$$

where x, y, z is the position of each spin packet and parameters a, b, c are obtained from position and nutation experiments. The variation in RF power across the sample will lead to a spread in tipping angles in the 180° refocusing pulse in the PGSE sequence that will cause errors in the measured diffusivity. These errors are minimized by using a sample size that is small compared to the homogeneous region of the RF coil.

For this measurement service, the x, y variations of sample center from RF coil center are ignored since the x, y coordinates of the sample are constrained by the insertion of the 5 mm OD sample tube into the 5.2 mm ID probe chamber, giving a worst-case positional variation of ±0.1 mm. The z variation is included since it changes due to operator insertion variations. The insertion depth is determined using a fixed gauge and the sample tube is rigidly held in position to prevent movement due to gas flow used to control temperature. A worst-case variation of ±1 mm in the sample z axis position is assumed and used in the Monte Carlo uncertainty calculations.

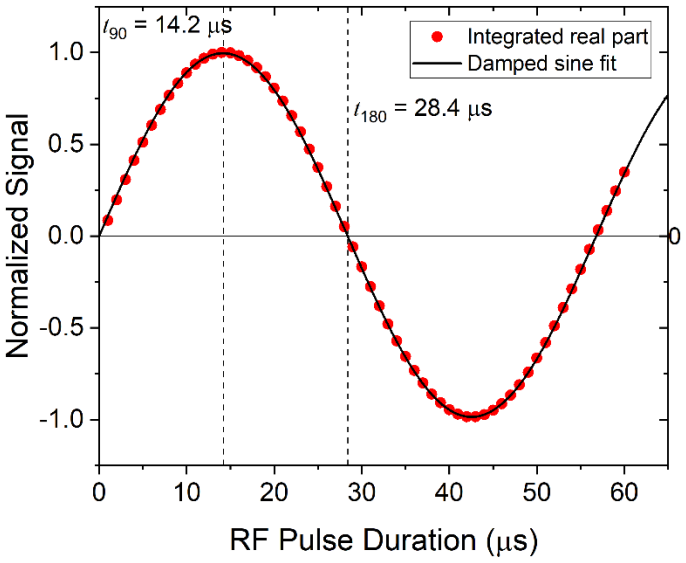

Fig. 8. Nutation data for a 3 mM $CuSO_4$ solution at 20 °C in the diffusion sample cell. The black line is a fit using a damped sinusoid model, which results in t_{90} = 14.2 µs.

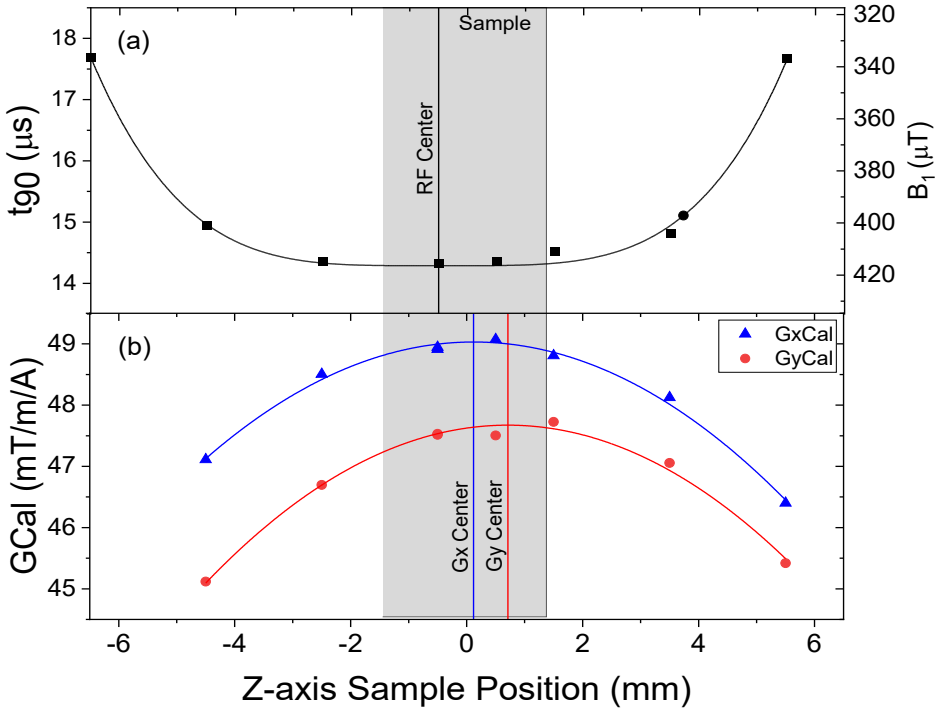

Fig. 9. (a) RF nonuniformity: t_{90}, the time to achieve a 90° rotation of the magnetization, as a function of sample position along the z-axis. The right axis gives the magnitude of the RF field. The solid line is a fit to Eq. 20 with x, y = 0 giving b_{10} = 414.6 µT, c = 9.13 mm. (b) Gradient nonuniformity: gradient calibration as a function of distance along the z-axis. The grey box shows the 3 mm length of the sample. The solid lines are parabolic fits (see Eq. 23) with $G_{0x} = 49.03 \frac{\text{mT}}{\text{A·m}}, \frac{C_x}{G_{0x}} = -0.0018 \frac{1}{\text{mm}^2}$, $G_{0y} = 47.67 \frac{\text{mT}}{\text{A·m}}, \frac{C_y}{G_{0y}} = -0.0020 \frac{1}{\text{mm}^2}$.

4.1.5 NMR instrument linewidth and peak integration:

After equilibration, a single spectrum of American Chemical Society (ACS) reagent-grade water is acquired with eight free-induction decay measurements averaged together. The FID is then Fourier transformed, and phase adjusted to give real and imaginary components of the signal (Fig. 10). The real part of the spectra is fit with a Lorentzian model to determine the approximate FWHM of the single water peak. From this procedure, the minimum linewidth of the instrument was determined to be < 1 Hz for long capillary samples and typically 2 Hz to 5 Hz under the conditions used for measurement service experiments. The linewidth for diffusion measurements is limited by the sample geometry, which consists of a 3 mm diameter, 3 mm long cylindrical sample embedded into a polyphenylene sulfide (PPS) holder. Field distortions due to the susceptibility mismatch between the sample and the PPS cell cannot be fully shimmed out and limit the linewidth.

The measured linewidth, due to the inhomogeneous magnetic field, is much greater than the intrinsic linewidth of water ~ 0.1 Hz. There are significant deviations of the spectral shape from that of single Lorentzian. The spectra consist of a distribution of Lorentzians from an ensemble of spin packets each with different local fields. The uncertainty calculations assume that the distribution of local fields give a worst-case inhomogeneous broadening of 10 Hz. All measured spectra must be shimmed to achieve an inhomogeneous line width of less than 10 Hz.

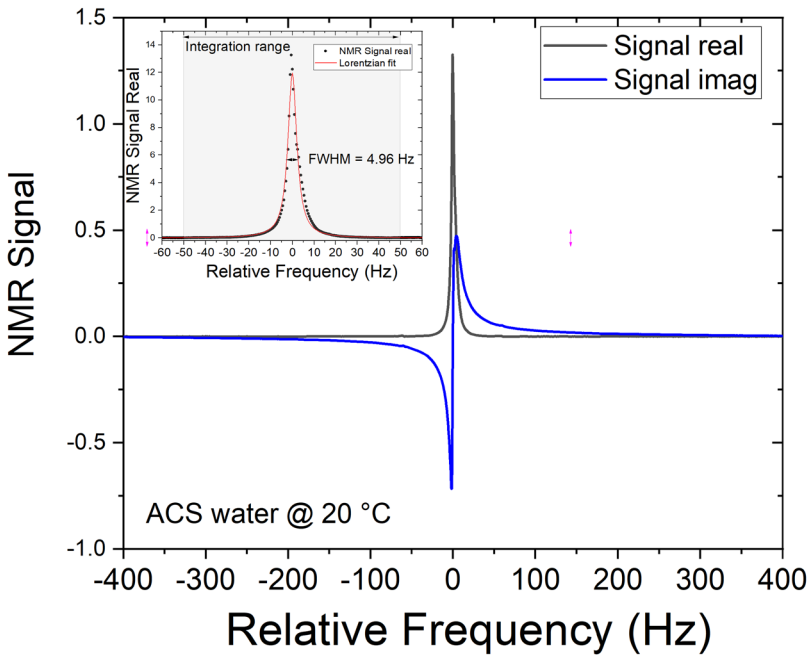

Fig. 10. Real and imaginary components of the spectra for ACS water at 20 °C. The inset shows a Lorentzian fit and gives an approximate line width of 5 Hz.

Many samples measured will contain other organic compounds with signal from chemically distinct protons. The chemical shifts are typically 1- 3 ppm and allow spectroscopically resolving the water protons from other protons on organic molecules. Figure 11 shows a spectrum of a polyvinyl pyrrolidone (PVP) – water solution. The water peak is integrated

over a region of ±10 x FWHM, as shown in the figure. This range is sufficient to capture all the water signal and exclude CH_2, CH_3, protons.

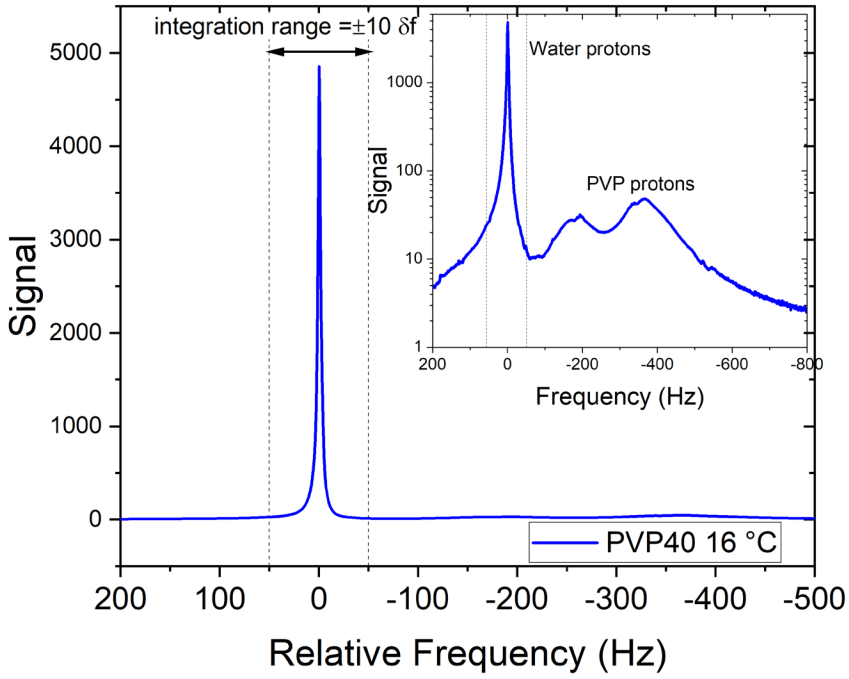

Fig. 11. Spectra from water protons in a 40 % by weight polyvinyl pyrrolidone (PVP) water solution, at 16 °C, showing the region of integration to obtain the water signal. The inset shows the same data on a log scale where the protons on organic PVP molecules are observed. Note, here we plot the negative frequencies on the right to be consistent with the common convention on presenting proton spectra.

4.1.6 **Triaxial gradient system:**

The gradient system consists of Fluorinert-cooled actively shielded triaxial coils with specifications listed in Table 2. The innermost gradient winding is 26.7 mm diameter, and the OD of the outermost shield winding is 37.7 mm. The gradient temperature is continually monitored, along with sample and probe temperatures.

The gradients are driven by a digital ethernet link going from the NMR console to 20 bit Digital-to-Analog Converter (DAC) cards that plug into Techron 7224 amplifiers. The amplifiers have a 300 kHz bandwidth and a 1.1 kW maximum output. The output resolution is 19 bits (±524288) with 1 bit for sign. The gradients are updated every $\Delta t = 2.4\ \mu s$. The gradient output at time $t = n\Delta t$ is given by

$$S_g(n) = DC + A_0 G_a X(n) + \sum_i A_i Y_i(n) \qquad (21)$$

where the gradient DC offset compensates small zero-input gradient currents; $A_0 = 50$ is a system scale factor; G_a, varying from 0 to 100, is the pulse sequence dependent gradient amplitude; $X(n)$, varying from -100 to 100, is the gradient waveform; and $Y_i(n)$is the gradient pre-emphasis.

$$Y_i(n) = int\left(\left(X(n) - X(n-1)\right) + e^{-\frac{n\Delta t}{T_i}} Y_i(n-1)\right) \tag{22}$$

For the diffusion measurements the gradients are left on (enabled) during the entire pulse sequence. The DC offsets are usually set to zero (see Fig. 13) and any gradients that are present in the gradient off state are nulled during the shimming procedure. While having the gradients enabled during the entire pulse sequence may introduce extra noise, it prevents any transients that can be caused by enabling or disabling the gradient amplifiers. Other measurements, such as T_1, T_2, have the gradients disabled and therefore require a separate shimming procedure.

The gradient waveforms are optimized by adjusting the pre-emphasis parameters on the NMR console (Fig. 12). The gradient pre-emphasis is adjusted to remove gradient risetime effects and minimize eddy currents. Eddy currents are also minimized through B_0 compensation. The coefficients are set to minimize the distortion in the phase and magnitude of a post gradient FID. The time constants are identified in the temporal variation of the FID phase. Typically, only one or two time constants are required, with the major one being around 3 ms, for the current actively shielded probe. The gradient pre-emphasis is checked yearly or after any hardware changes.

DC.x	0	DC.y	0	DC.z	0
A0.x	50	A0.y	50	A0.z	50
A1.x	0	A1.y	0	A1.z	0
A2.x	2.6	A2.y	2.7	A2.z	2.5
A3.x	0	A3.y	0	A3.z	0
A4.x	0	A4.y	0	A4.z	0
A5.x	0	A5.y	0	A5.z	0
T1.x	200u	T1.y	200u	T1.z	200u
T2.x	3m	T2.y	3.5m	T2.z	3m
T3.x	20m	T3.y	20m	T3.z	20m
T4.x	200m	T4.y	200m	T4.z	200m
T5.x	2s	T5.y	2s	T5.z	2s

Fig. 12. Gradient pre-emphasis parameters. DC and A1-5 are the DC and AC amplitudes, respectively, used to set the gradient pre-emphasis signals (Eq. 21), whereas T1-5 are the time constants in microseconds (u), milliseconds (m), and seconds (s) used in Eq. 22.

Nonuniformity of the gradients will lead to both error and uncertainty in the measured diffusivity. These errors and uncertainty contributions are minimized by making the sample small and by precise placement of the sample. The gradient uniformity measured along the z-axis is shown in Fig. 9b. The gradient G_x, G_y, G_z and RF centers do not precisely match up and can vary by ±1 mm. The variation in gradient strength can be modeled by Eqns. 23a, 23b and 23c where G_{0x}, A_x, B_x and C_x are adjustable parameters determined from data:

$$G_x = G_{0x} - A_x(x - x_0)^2 - B_x(y - y_0)^2 - C_x(z - z_0)^2, \tag{23a}$$

$$G_y = G_{0y} - A_y(x - x_0)^2 - B_y(y - y_0)^2 - C_y(z - z_0)^2, \tag{23b}$$

$$G_z = G_{0z} - A_z(x - x_0)^2 - B_z(y - y_0)^2 - C_z(z - z_0)^2. \tag{23c}$$

This model is used in the Monte Carlo Bloch simulations to determine uncertainty in diffusivity due to uncertainty in the sample position and the lack of a well-defined gradient value.

The sample z-position, as discussed in the RF power calibration section, may vary by ±1 mm, and the x, y coordinates have a positional variation of ±0.1 mm. The gradient variations along the x, y axes are more difficult to measure, and we rely on calculated profiles provided by the probe manufacturer.

Figure 13 shows the measured diffusion constant as a function of z, using both a fixed gradient calibration at the nominal centered position and with gradient calibrations done at each location, as prescribed in the measurement protocol. The continual recalibration of the gradients gives less error due to variation in sample placement. The maximum variability in the z-axis position of a spin packet relative to the gradient centers is less than ±2 mm, accounting for variation in sample placement and uncertainty in the gradient centers. This gives a potential error in the diffusion coefficient of 0.9 % and is modeled numerically in the uncertainty calculations. The constant gradient recalibration also removes variation due to probe temperature variations and gradient amplifier drift.

Table 2. Gradient properties

Gradient	Nominal Gradient Coefficient (mT/m/A)	Measured Gradient Coefficient[a] (mT/m/A)	Calculated uniformity[b] (%)	Measured uniformity[c] along z (%)	Max continuous[d] current (A)	Max gradient[e] (T/m)	L (mH)	R(W)
X	46.2	48.62 ± 0.23	0.3	0.73	11	5.08	23	1.2
Y	42.5	47.17 ± 0.17	0.5	0.80	11	4.68	21	1.3
Z	54.2	59.81 ± 0.17	0.5	0.80	11	5.96	16	1.2

[a] Gradient strength at the center of the gradient coil with standard uncertainty from a set of repeated measurements. The gradient calibrations will have a small dependence on probe temperature.
[b] Over centered 4 mm spherical volume
[c] Over 4 mm z-distance
[d] Assumes full cooling
[e] at 1 % duty cycle

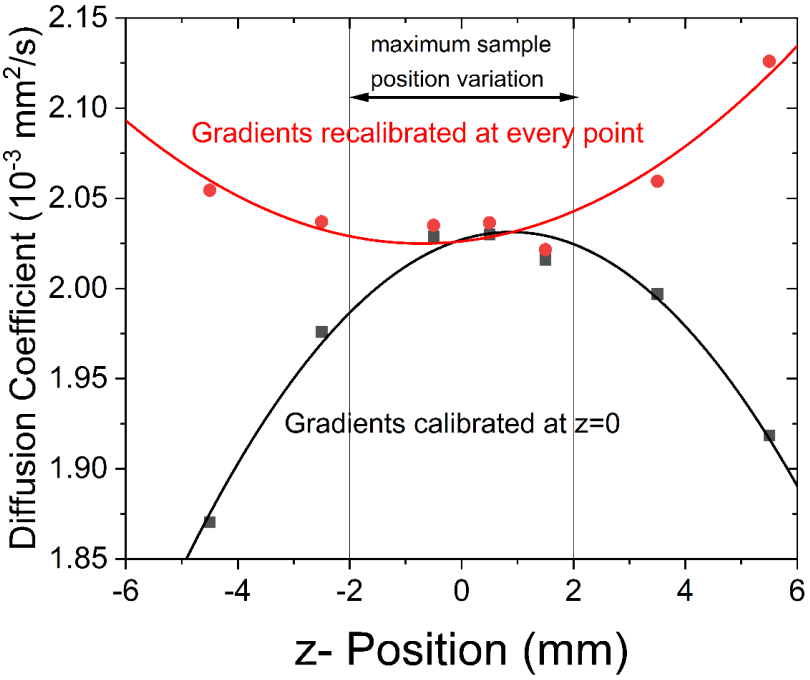

Fig. 13. Diffusion coefficient of water at 20 °C with 3 mM $CuSO_4$ as a function of sample position, using both a single gradient calibration at z = 0, and point by point gradient calibrations.

4.2 Sample cells

The sample cells consist of a two-part precision machined polyphenylene sulfide (PPS) 5 mm diameter rod with a cylindrical sample space with a diameter, at 20 °C, of 3.00 mm ± 0.03 mm and height of 3.00 mm ± 0.05 mm, as shown in Fig. 14. The sample geometry was chosen so that: 1) the sample size is much larger than the characteristic diffusion length; 2) the volume is sufficiently large to prevent surface effects and degradation due to evaporation; 3) samples, including tissue mimics and tissues, can be easily loaded and sealed; 4) the sample dimensions are within the homogenous region of the applied gradients. PPS was used since it is approximately susceptibility matched to water and samples of interest, which prevents artifacts due to susceptibility discontinuities (see Table 3). PPS, further, has low water absorption, good thermal stability, precise machinability, and good chemical resistance. The thermal expansion coefficient of PPS is 3 x 10^{-5} per °C to 5 x 10^{-5} per °C, giving a dimensional variation of 0.4 % over the measurement range of 0 °C to 80 °C.

Table 3. Properties of water, glass, and PPS sample cell material (from SP Wilmad-Labglass Technical Note)

Property @ 20 °C	water	Pyrex glass	PPS
χ (10^{-6}) (Volume susceptibility in SI units)	-9.04	-10.6	-9.17
Wide line NMR Backgrounds		Si, B, Al, Na	H, C, S
H_2O absorption %		0.01	0.03
Density (g/cm^3)	1.0	2.5	1.35
Thermal Conductivity (W/m/K))	0.60	1.14	0.29 – 0.32

The dimensions of the sample cell are calibrated with microCT at room temperature, as shown in Fig. 14(b), which in turn is calibrated by using a 3.000 mm ± 0.0025 mm alumina sphere. The uncertainty of the dimensions obtained from the microCT, as determined from repeated measurements of the calibration sphere, is < 1 %. The measured cylinder diameter and height, for the cell shown in Fig. 14, are 3.00 mm ± 0.03 mm and 3.00 mm ± 0.05 mm respectively. The microCT measurements are confirmed with optical microscopy, which measures the cylinder diameter of the open cell to be 3.00 mm ± 0.03 mm. There are small deviations of the sample cell from an ideal cylinder due to a small chamfer on the top surface of the cell, as seen in Fig. 14(b). The chamfer allows easy assembly of the cell but it introduces a small artifact that can be seen in the 1D magnetic resonance images.

A fiber optic thermometer is embedded in the PPS rod 8.5 mm above the center of the sample cell. The sample is positioned so it is centered in the RF and gradient coils by setting the distance of the spinner base to the bottom of the cell to be 103.5 mm, which makes the center of the sample cell 80 mm below the base of the spinner. The sample is not spun and remains stationary during the measurement and is secured to ensure that the spinner remains seated in the spinner receptacle while the thermal control gas flows around the cell. A set of four lower sample cells are used with four different top sealing rods, each with a different calibrated thermometer.

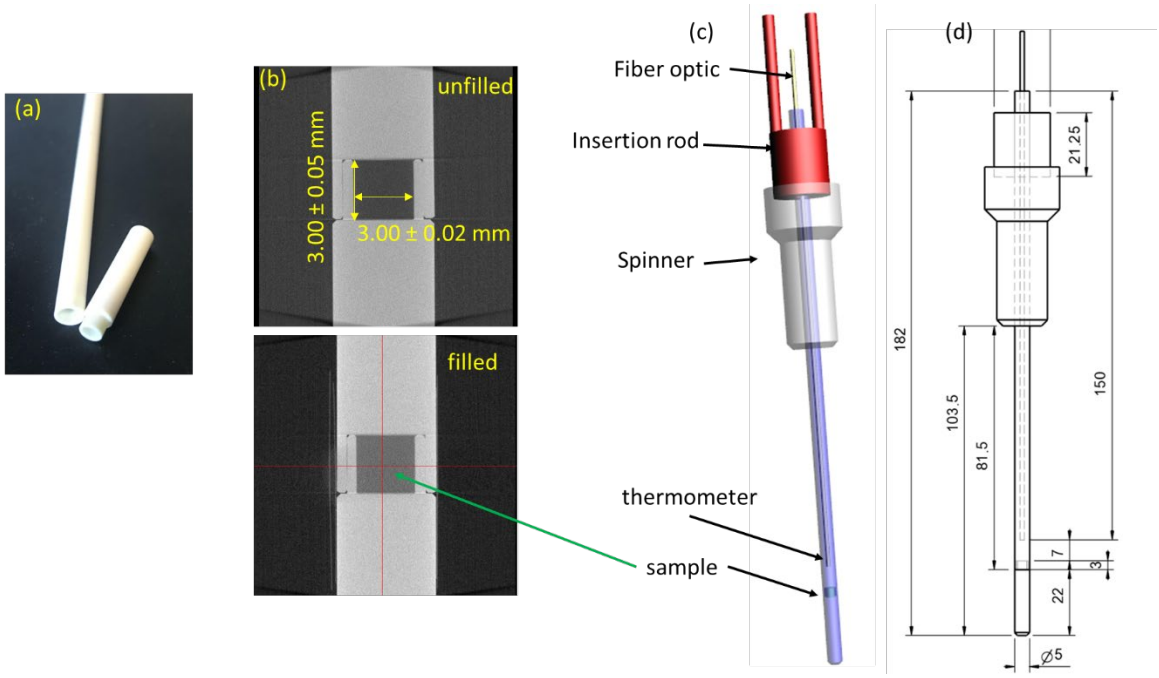

Fig. 14. (a) Photograph of the 2-part NMR sample cell for diffusion measurements. (b) microCT of the sample space with voxel dimension of 13.7 µm, filled and unfilled. (c) Model of the sample insert with the sample cell, spinner, insertion rod, and thermometer installed. (d) drawings of the sample inset with dimensions listed in mm.

The lower cell is filled with sample and a piece of polytetrafluoroethylene (PTFE) sealant tape is put over the sample and the two sections are connected. Measurement of the cell filled with water shows less than 1 mg mass loss over 7 days. All sample measurements are done within 7 days of sample preparation, to ensure that the sample has not changed due to water

evaporation. Any loss of sample due to evaporation readily shows up as an increase in the NMR line width and the presence of a bubble or inhomogeneity is seen in the 1D MR images (Fig. 15). If this occurs, the run is stopped, and a new sample is prepared. The unfilled sample cell shows an NMR signal from protons on the PPS (Fig. 16). These protons have a very short T_2 relaxation time resulting in a very broad peak with a width of 4 kHz. The magnitude of the error due to the sample cell signal is < 0.2 %.

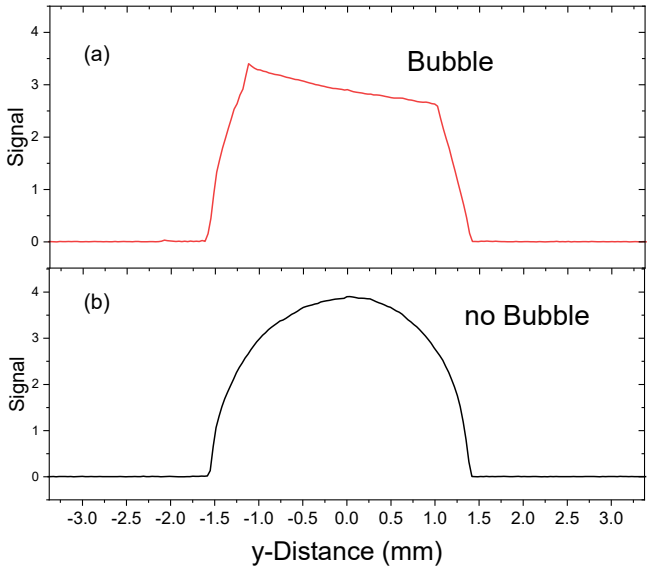

Fig. 15. 1D magnetic resonance image of sample cell with water and (a) a bubble and (b) a well filled sample with no observable bubble.

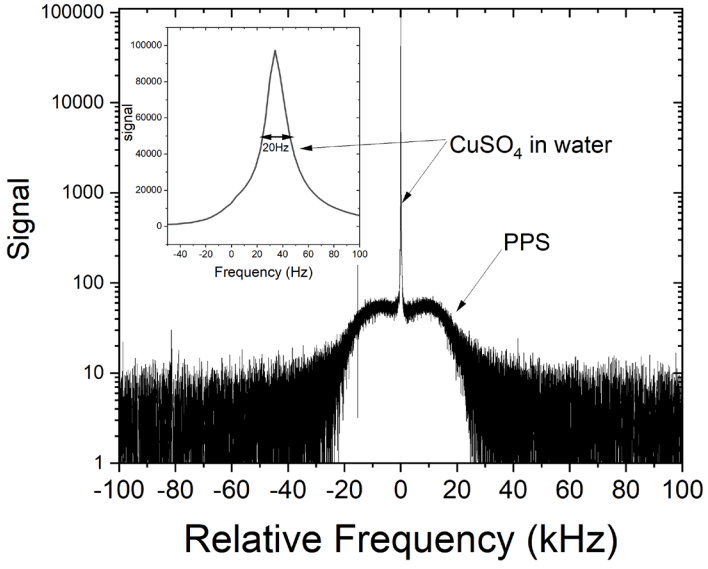

Fig. 16. NMR spectra showing the background signal from protons in the PPS sample holder along with the sharp water proton resonance in a $CuSO_4$ solution.

4.3 Fiber optic temperature probe and temperature control system

The temperature control system, shown in Fig. 17, consists of six computer-controlled components: 1) a fiber optic thermometer to measure sample temperature, 2) N_2 gas system, which flows gas around the sample cell to adjust the sample temperature, 3) a heat exchanger to lower the N_2 gas temperature to a base temperature below the desired sample temperature, 4) a heater to bring the gas temperature up close to the desired sample temperature, 5) a gradient water flow circuit to control the surrounding gradient and probe temperature, and 6) several thermometers to monitor temperatures throughout the probe. The temperature control protocol is to set the probe temperature close to the desired sample temperature using the gradient flow loop, set the incoming N_2 gas temperature to ~10 °C below the desired sample temperature, and set the N_2 flow sufficiently high to ensure enough cooling power to obtain the sample temperature setpoint and to minimize thermal gradients. The N_2 flow rate cannot be increased too high since it is possible to induce sample vibrations. A typical N_2 flow rate, set by a mass flow controller, is 20 SLM. With the N_2 flow fixed, the computer adjusts the heater power to obtain the desired temperature.

The thermal gradients are measured with a sample cell modified to contain two matched platinum resistance thermometers, 14 mm apart. The longitudinal thermal gradients, along the magnet axis, vary linearly and go through zero near the ambient temperature of the probe (~20 °C). The thermal gradients depend on sample cell type, N_2 flow rate, N_2 temperature, and gradient temperature. These parameters are adjusted to ensure a maximum longitudinal temperature gradient of 0.2 °C/cm. This procedure minimizes temperature gradients which reduces the uncertainty in the temperature measurement and reduces thermal effects such as convection. Since the magnetic field gradients are calibrated for each measurement, small changes in geometry of the probe due to thermal variations are taken into account.

The non-magnetic non-conducting fiberoptic temperature probe uses white light interferometry and a small 3 mm birefringent sensor crystal. The fiber optic probe, inserted into the sample cell as shown in Fig. 14, is calibrated against two NIST-calibrated platinum resistance thermometers in a variable temperature water bath over the range of temperatures required for the diffusion measurements. Three gauge factors are determined from a fit of the measured of the fiber optic path difference as a function of calibrated temperature. The gauge factors are input into the fiberoptic sensor controller, and the calibration is verified by a second comparison with the NIST calibrated thermometers. The thermometer calibration is done in zero magnetic field. No trend of the apparent temperature was observed with field, when varied from -7 T to 7 T, with the standard deviations of the measured temperature being 79 mK and 11 mK, at 288 K and 298 K, respectively. Typical optical thermometer calibration uncertainties, given thermometer drift, field dependence, and dispersion about the calibration curve is 0.1 °C.

The sample and fiber optic probe are lowered into the NMR bore and the spindle is locked on the top of the NMR probe. The temperature is controlled by a proportional-integral-derivative (PID) control system that adjusts the heater current and gas flow, as shown in Fig. 5, to maintain the sample temperature as determined by the fiber optic probe. A screen shot of the measured sample temperature during a typical sample run is shown in Fig. 17. The maximum temperature deviation for this run was 50 mK.

Temperature scans are taken from low to high temperature, with the shimming recommended at each temperature. Measurements begin at low temperatures to minimize effects due to evaporation and distillation. The diffusion sample cell can expand in the z-direction to accommodate thermal expansion of the sample and prevents large pressure changes due to thermal cycling.

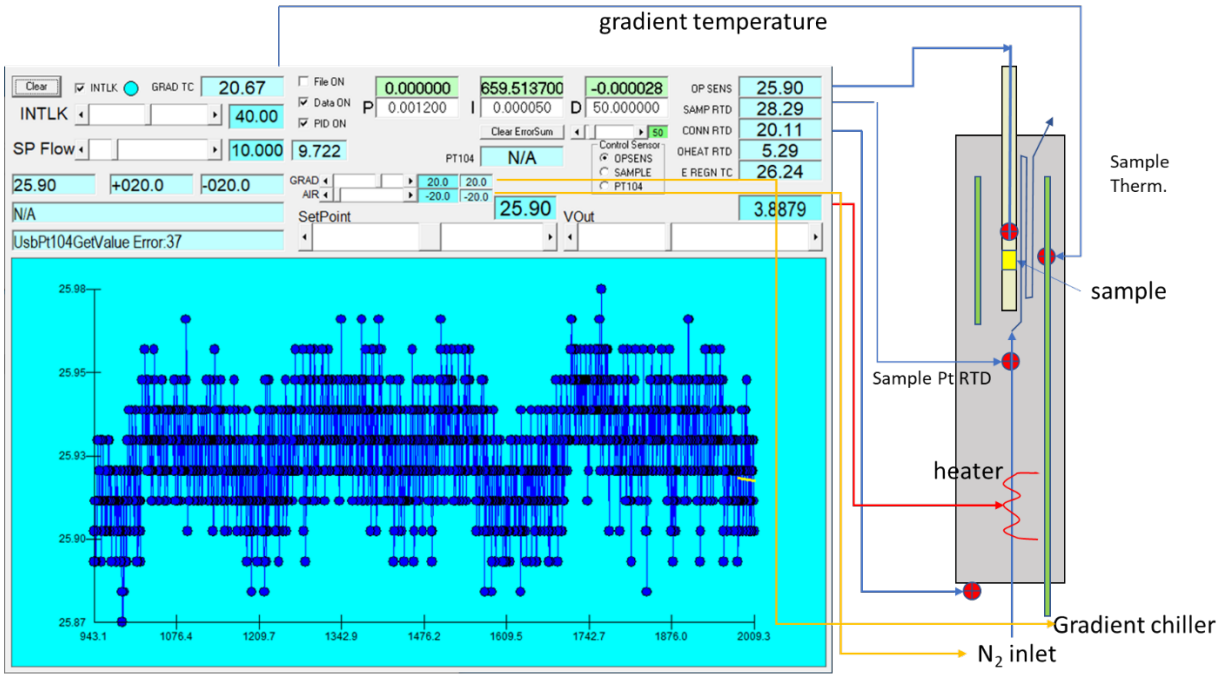

Fig. 17. Screen shot of sample temperature control software with the temperature monitored for 20 min.

An example of temperature dependence of the diffusion coefficient of a polyvinyl pyrrolidone sample is shown in Fig. 18. The measured temperature coefficients are used, along with temperature uncertainty, in the overall uncertainty calculation. Given the large temperature dependence of the diffusion coefficient, the temperature uncertainty constitutes a large fraction of the overall uncertainty of the measured diffusion coefficient.

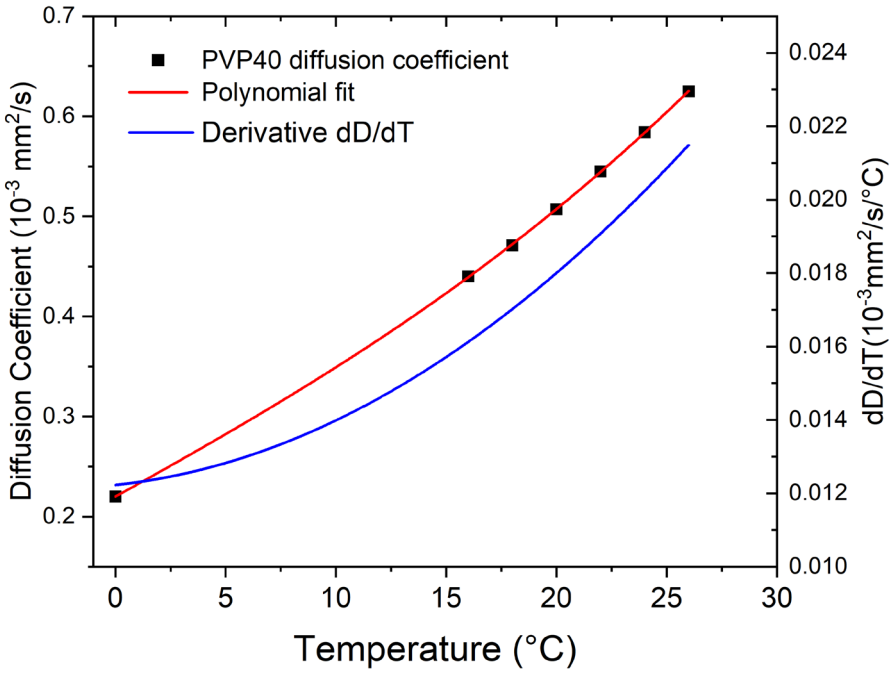

Fig. 18. Water diffusion coefficient (red) in a 40 % by weight polyvinyl pyrrolidone solution as a function of temperature along with its derivative (blue) which gives the diffusion temperature coefficient.

4.4 Gradient Calibrations

Gradient calibrations are done using the precisely machined cylindrical sample cell with dimensions determined by microCT. The traceability path is shown schematically in Fig. 19. The microCT is calibrated with an alumina sphere with a NIST-traceable diameter of 3.0000 mm ± 0.0025 mm. The reported diffusion coefficient is the average of the diffusion coefficient measured along the transverse (x, y) directions, which corresponds to the diameter of the sample cylinder. The height of the sample cylinder is less precisely defined due to the presence of a PTFE sealing film and the need for sample cell compliance to accommodate thermal expansion and contraction. Calibration in the z-direction is done using an isotropic calibrant such as water and the transverse gradient calibrations. This direction is usually not included in the diffusion measurements since the gradient calibration is less precise and more time consuming.

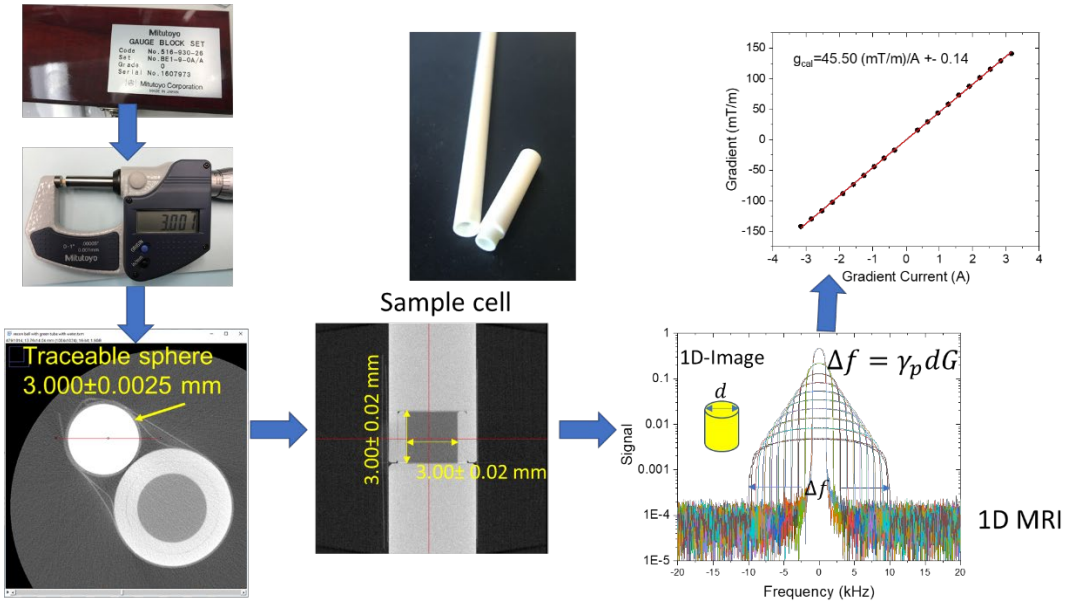

Fig. 19. Gradient calibration traceability chain.

A set of 20 1D spin echo images are obtained by varying the gradient output current, ranging from approximately -5 A to 5 A. Voltage traces from the differential gradient amplifier output monitors are recorded and converted into current using the prescribed 2.5 V/A conversion factor. The current traces are shown in Fig. 20, along with the acquired spin echoes. The spin echoes are Fourier transformed to obtain the 1D images, as shown in Fig. 21(a). The frequency width Δf for each image is determined by fitting the observed image signal S with a 1D model of the cross section of an ideal cylinder parallel to the cylinder axis

$$S = S_0 \sqrt{1 - \frac{4(f - f_0)^2}{\Delta f^2}} \; for \; |f - f_0| < \frac{\Delta f}{2}$$

$$= 0 \; for \; |f - f_0| > \frac{\Delta f}{2} \tag{24}$$

Where S_0, Δf, and f_0 are model parameters. A typical fit is shown in Fig. 22. The frequency width is converted into a gradient strength using

$$G_i = \frac{2\pi\Delta f}{\gamma d_i} \tag{25}$$

where d_i is the dimension of the cell along the ith axis. For most samples without any defects, the estimated standard error from the estimated covariance matrix in the parameter values are quite small, less than 0.1 % (see Fig. 22), and the uncertainty in the gradient calibrations are dominated by systematic uncertainties such as uncertainty in the cell dimensions. For nonuniform samples and samples with defects such as bubbles, the fit uncertainty can increase substantially. For these samples, the gradient calibration is taken from reference samples just prior to the gradient measurements.

The measured gradient is plotted against the average gradient current during the gradient current pulses (Fig. 21(b)). The gradient current calibration, g_{ical}, is then obtained by fitting a line to the gradient vs. current data and obtaining the slope. Note, while the gradient calibration is reported as mT/m/A, the calibration used is the gradient strength per DAC

count. Measuring the precise current is not needed, it is just a convenient and intuitive method of reporting the calibration. All that is required is that the monitor output is consistently related to the DAC output. Figure 23 shows the measured average current versus DAC count during the gradient pulses along with the calibration factor I_{max}, which gives the output current at a DAC output of 500,000. The gradient calibration only uses the quantity $I_{max}g_{ical}$.

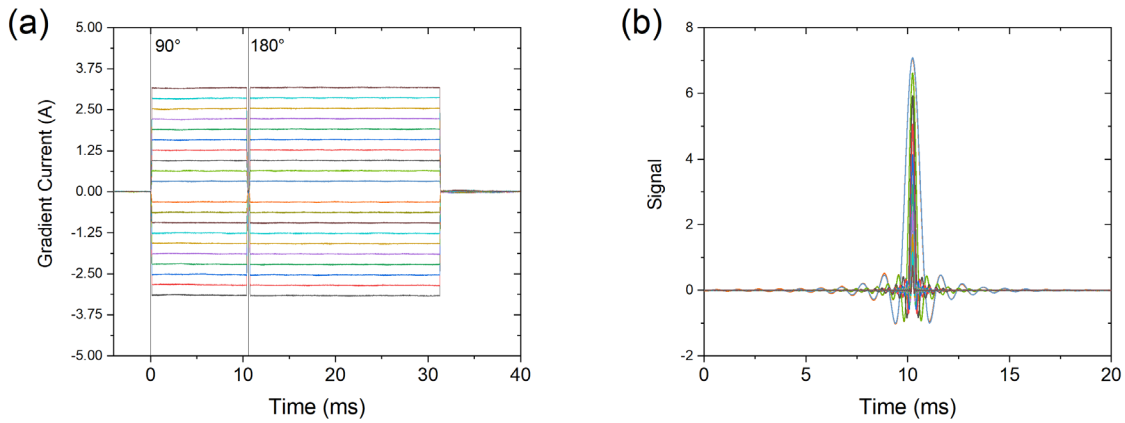

Fig. 20. (a) 1D spin echo image sequence showing gradient pulses, 90° and 180° RF pulses, and schematic spin echo. (b) Acquired spin echoes for different gradient pulse amplitudes.

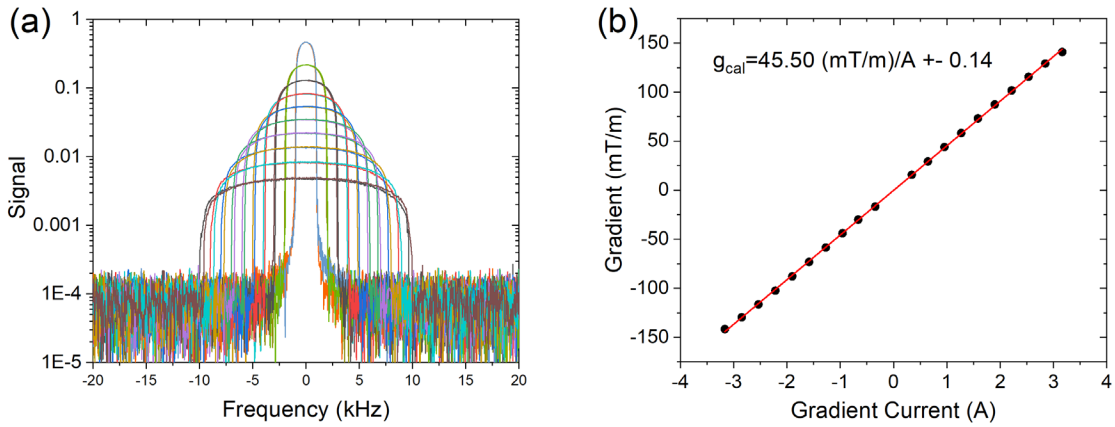

Fig. 21. (a) 1D images of the sample cell. (b) measured gradient versus gradient current.

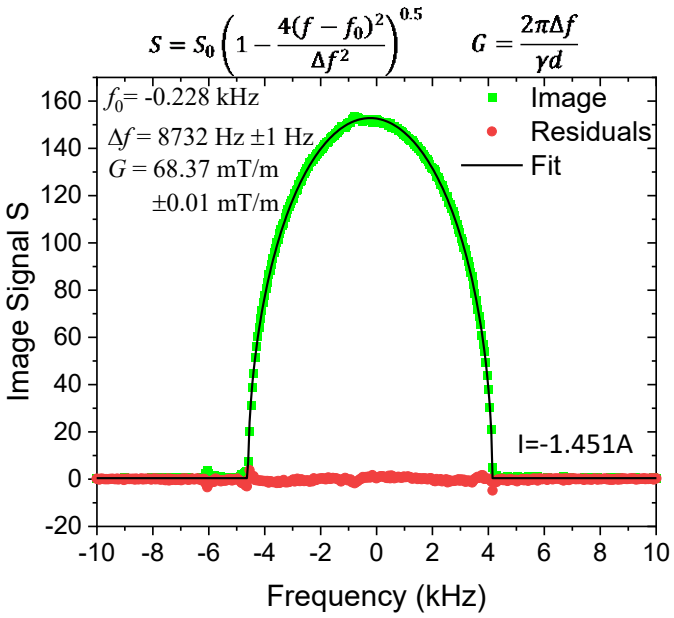

Fig. 22. 1D image of cylindrical sample cell filled with a 30 % PVP solution taken with 1.451 A maximum current applied to the y-gradient coil along with the fit to an ideal cylinder (equations shown on top of the plot) and the associated residuals.

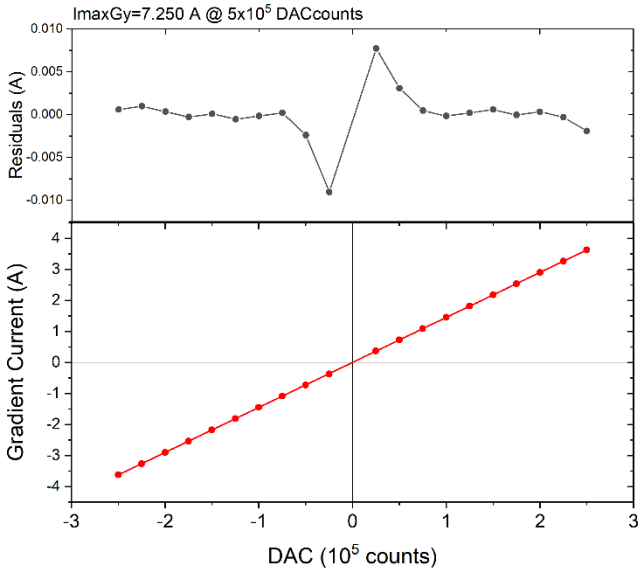

Fig. 23. Average gradient current measured during the peak of a trapezoidal pulse versus the prescribed DAC count. A linear fit and its residuals are shown to indicate a high degree of linearity.

4.5 PGSE Robustness Tests

Several tests are required to determine the uncertainty in the diffusion coefficient measured by a PGSE sequence. The tests are listed below.

4.5.1 Gradient recovery and eddy current compensation

After application of a gradient pulse there can be ringing or overshoot that has not been eliminated by the gradient pre-emphasis settings, and there can be eddy currents set up in the surrounding probe structures, room temperature shim stack, superconducting coil, and shims. The effects can be characterized using a modified PGSE sequence that is identical to the one shown in Fig. 1, except the 90° excitation pulse is moved after the application of the gradients. Ideally, the application of the gradients, when there is no transverse magnetization, will have no effect on the polarization when the RF pulse is applied and the signal, both magnitude and phase, derived from the FIDs should be independent of gradient size. However, when eddy currents are present, the FID will show both a phase shift and a decrease in amplitude, as seen in Fig. 24, as the current induced fields cause phase variation and dephasing of the spin packets across the sample.

The phase shifts are accommodated in the analysis by setting the phase for each FID independently so eddy current phase shifts are accounted for. The decrease in signal magnitude, given well set gradient and B_0 compensation parameters, is small (< 10 %), compared with the large decrease in signal due to diffusion, which for water at 20 °C is a factor of 45000. A correction is applied to account for the eddy current induced loss of signal by fitting the signal loss to an exponential model and subtracting this non-diffusion related component from the measured diffusion coefficient. Fig. 24 shows worst case corrections with the x, y corrections being 0.022 x 10^{-3} mm^2/s and 0.016 x 10^{-3} mm^2/s, respectively. Typical eddy current corrections are between 0.001 x 10^{-3} mm^2/s and 0.01 x 10^{-3} mm^2/s. Uncertainty in the eddy current correction contributes significantly to the overall uncertainty in the diffusion coefficient, when the diffusion coefficient is below ~0.2 x 10^{-3} mm^2/s.

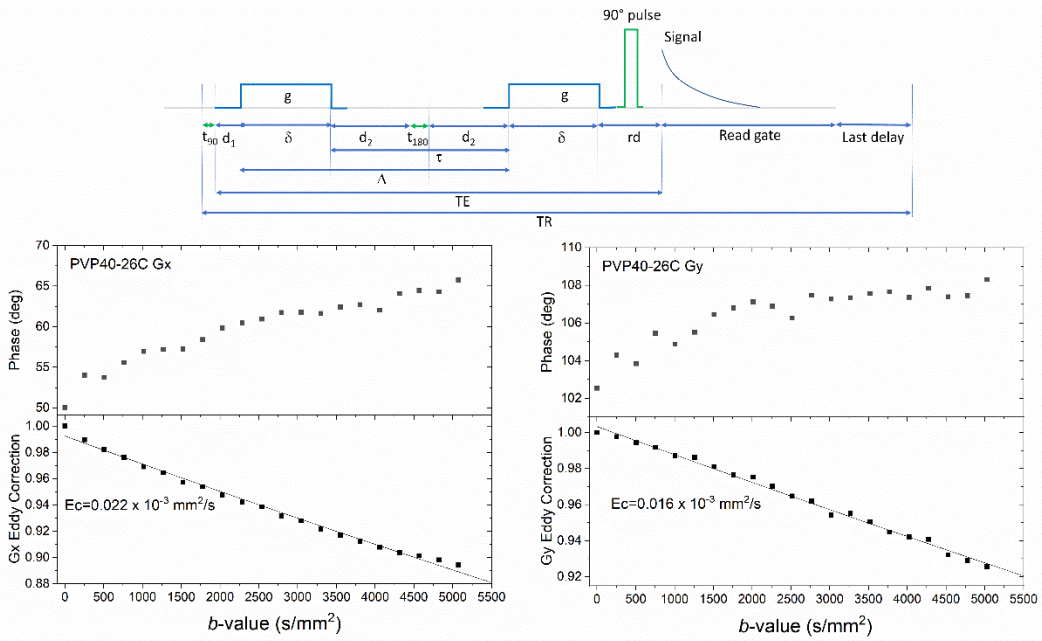

Fig. 24. Eddy current induced phase shift and signal loss for a series of modified PGSE sequences for x (left) and y (right) gradients.

4.5.2 Gradient pulse shape and spacing

There is a lot of latitude in choosing the gradient pulse shape, polarity, and spacing. The current measurement service uses trapezoidal positive-polarity gradient pulses with duration of 7 ms, plus a 0.1 ms rise time and fall time. The amplitude of the gradients is varied to obtain maximum *b*-values between 2000 s/mm^2 and 15000 s/mm^2, depending on the sample and the customer requests. The pulse duration, δ, and gradient pulse delay, τ, can also be varied to give different *q*-space trajectories. The *q*-space trajectory can be characterized by the maximum gradient strength, g_{max}, maximum *q* vector, q_{max}, and maximum *b*-value, b_{max}. For Gaussian diffusion the signal is only dependent on the *b*-value, while for diffusion in more complex materials, the signal will depend on all details of the *q*-space trajectory. Commonly used gradient profiles are shown in Table 4.

Table 4. Gradient scan profile parameters (see Figs. 1,2 and Eq. 8 for definitions). The exact values, for each spatial direction, are determined at scan time and are dependent on the power and gradient calibrations for a particular run.

Gradient ID	b_{max} $\left(\frac{s}{mm^2}\right)$	G_{max} $\left(\frac{mT}{m}\right)$	q_{max} $\left(\frac{1}{mm}\right)$	δ (ms)	τ (ms)
Standard scan	5200	210	400	7	28
Standard scan, high b	15000	350	400	4.3	91
Low q_{max}	5200	100	300	5.0	127
High q_{max}	5200	350	800	8.5	2.4
Half sine	5800	350	650	7	28

For Gaussian diffusion any choice of gradient pulse configuration must give the same diffusion coefficient within the respective uncertainties. The uncertainties for different gradient geometries will vary since eddy currents and deviations from the ideal waveforms depend on gradient geometry. Figure 25 shows the NMR signal of a 50 % polyvinyl pyrrolidone in water sample versus *b*-value with x-axis gradient pulses applied for the standard sequence along with other gradient pulse configurations. These configurations include inverted gradients, larger gradient amplitudes, half sine-wave gradients, and gradients with duration extended to 12 ms. Also shown is the distribution of measured diffusion coefficients along with the reported uncertainty from the Monte Carlo simulations. While all gradient pulse configurations cannot be tested, it is important to sample a variety of gradient geometries to ensure that the reported uncertainty encompasses all possible configurations.

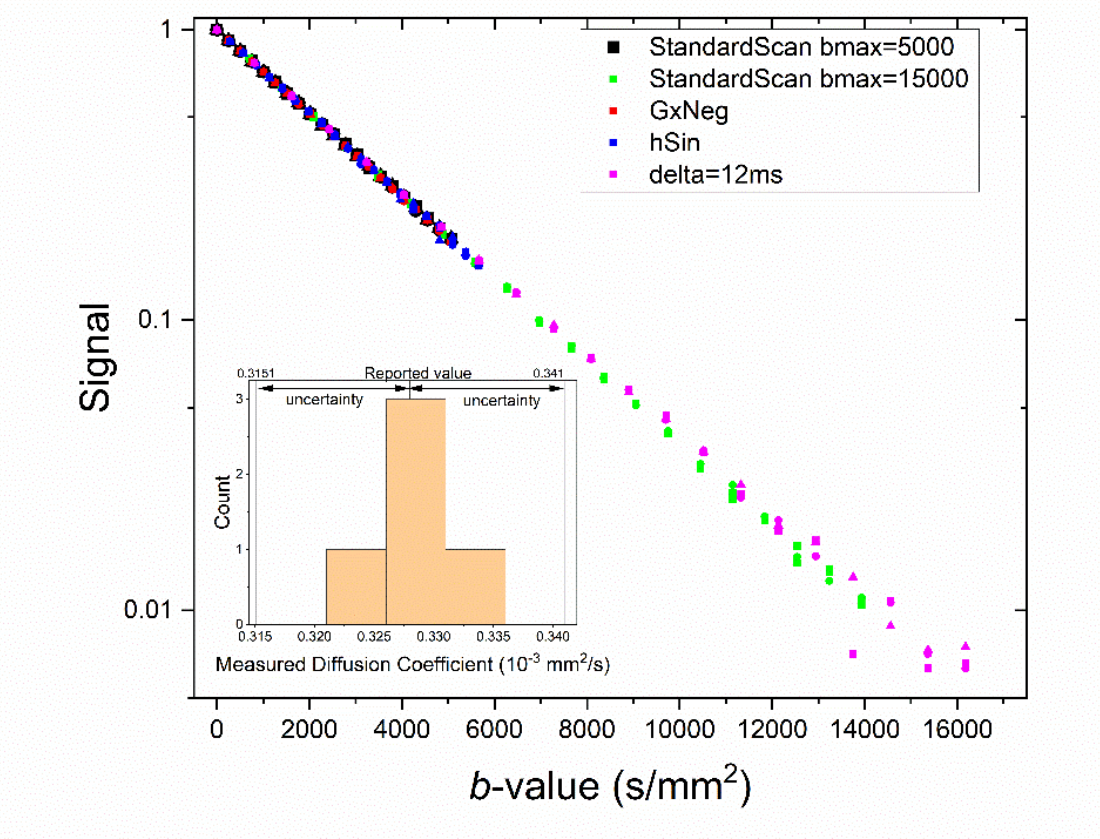

Fig. 25. NMR signal of 50 % polyvinyl pyrrolidone/water solution doped with paramagnetic salts at 3 T, 20 °C versus *b*-value for the standard scans (StandardScan bmax = 5000 s/mm^2 and StandardScan bmax = 15000 s/mm^2), negative polarity gradient pulses (GxNeg), half sine gradient pulses (hSin), trapezoidal pulses with 12 ms duration. Three consecutive measurements for each configuration are shown, demarked by symbols of different shapes, but same color. The inset shows a histogram of the derived diffusion coefficients for the gradient configurations shown along with the reported value and typical uncertainty.

Non-Gaussian water diffusion is common in complex materials, such as tissue and tissue mimics, which have water-confining structures on many different length scales. Figure 26 shows an example of a multicompartment tissue mimic(16) with a complex diffusion behavior with the signal being a function of the *q*-space trajectory, not just the *b*-value. This material cannot be described with a well-defined diffusion coefficient and detailed modeling and parameters measurements are not covered in this document.

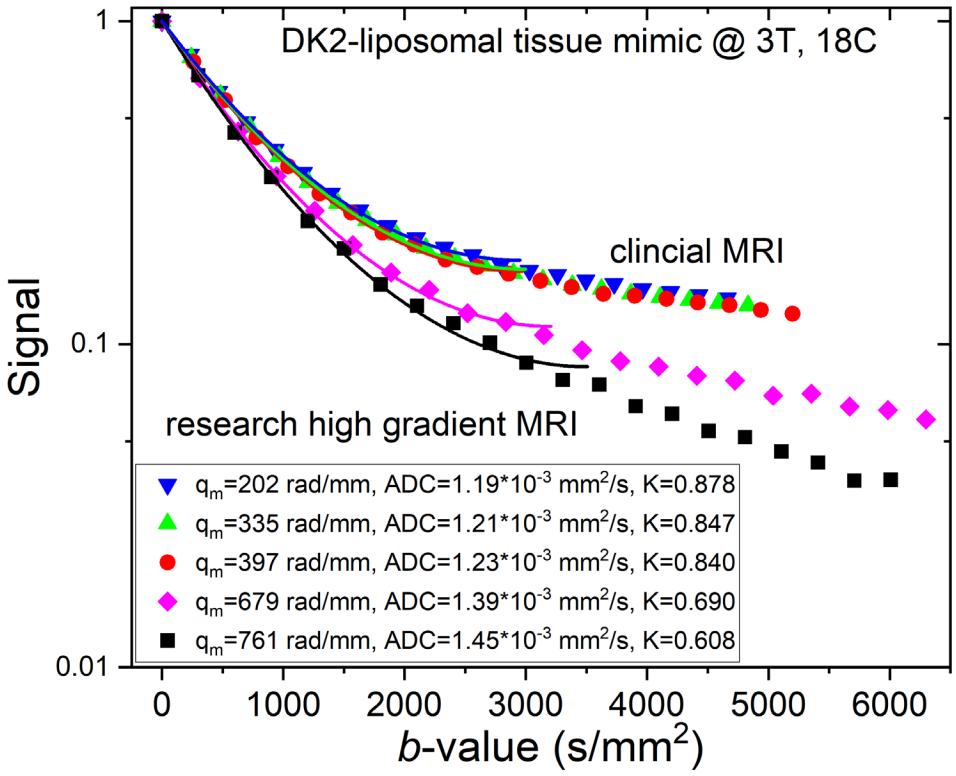

Fig. 26. Signal from a set of PGSE pulse sequences similar to those listed in Table 4 for a liposomal tissue mimic.

4.5.3 Computed vs. measured *b*-values

The accuracy of the computed *b*-values is dependent on the gradient calibrations and the accuracy of the gradient waveform. The *b*-values can be computed analytically if the waveforms are assumed to have a precise form. Figure 27 shows a typical set of trapezoidal gradient pulses along with the spin modulation *q*-vector given by integrating the gradient waveform, considering the reversal of the wave vectors due to the 180° pulse. Alternatively, the *b*-values can be calculated numerically by integrating q^2 over the *q*-space trajectory. Results from both methods are shown in Fig. 28. The methods agree to within ~ 0.5 %.
If the gradient waveforms are simple, the slew rates are not too large, and the gradient pre-emphasis is set correctly, the analytical calculations are simpler and more robust. The numerical calculation of the *b*-value has errors associated with noise in the waveform acquisition and proper baseline subtraction. In the combined uncertainty calculation done by the Monte Carlo simulation, an additional random error, *bValueUn*, is applied to the *b*-value calculation, beyond the gradient calibration error, to account for errors extracting the *b*-value from the gradient waveform.

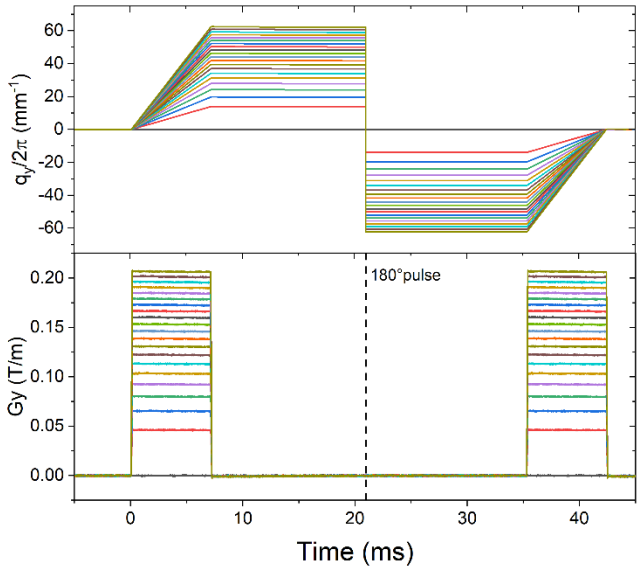

Fig. 27. Measured PGSE gradient pulses and associated spin modulation wavevectors.

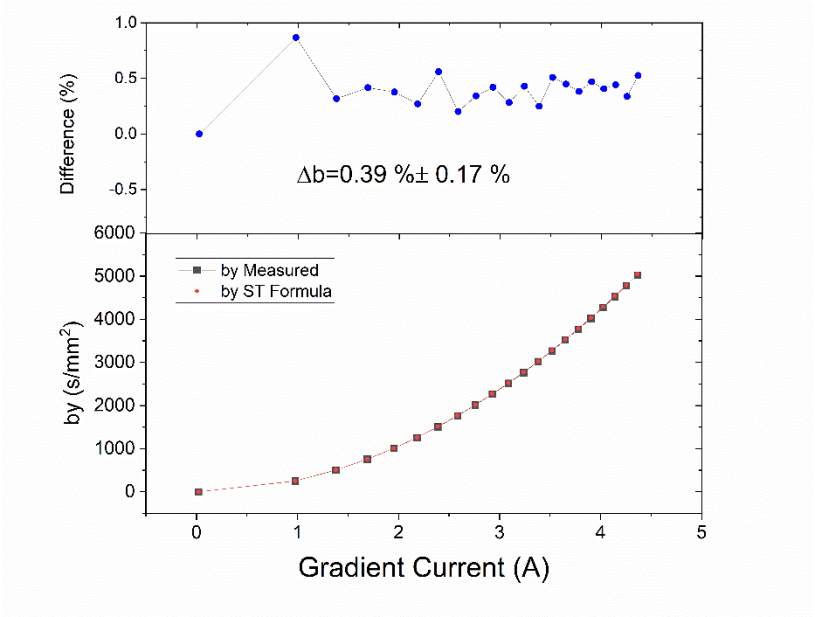

Fig. 28. Lower plot: *b*-values determine from analytical formula for trapezoidal pulses and numerically integrating the measured waveforms. Upper plot: the difference between these calculation methods.

4.5.4 t_{180} Test

Imperfect 180° pulses in the PGSE sequence will lead to errors in the measured diffusion coefficient as seen in Fig. 29. The accuracy of t_{180}, the time duration required for a 180° pulse, is typically less than 0.5 μs and the corresponding uncertainty in the diffusion coefficient is small. It is accounted for in the uncertainty Monte Carlo calculations since the

inversion pulse width is varied about the ideal value with a distribution given by the t_{180} calibration uncertainty.

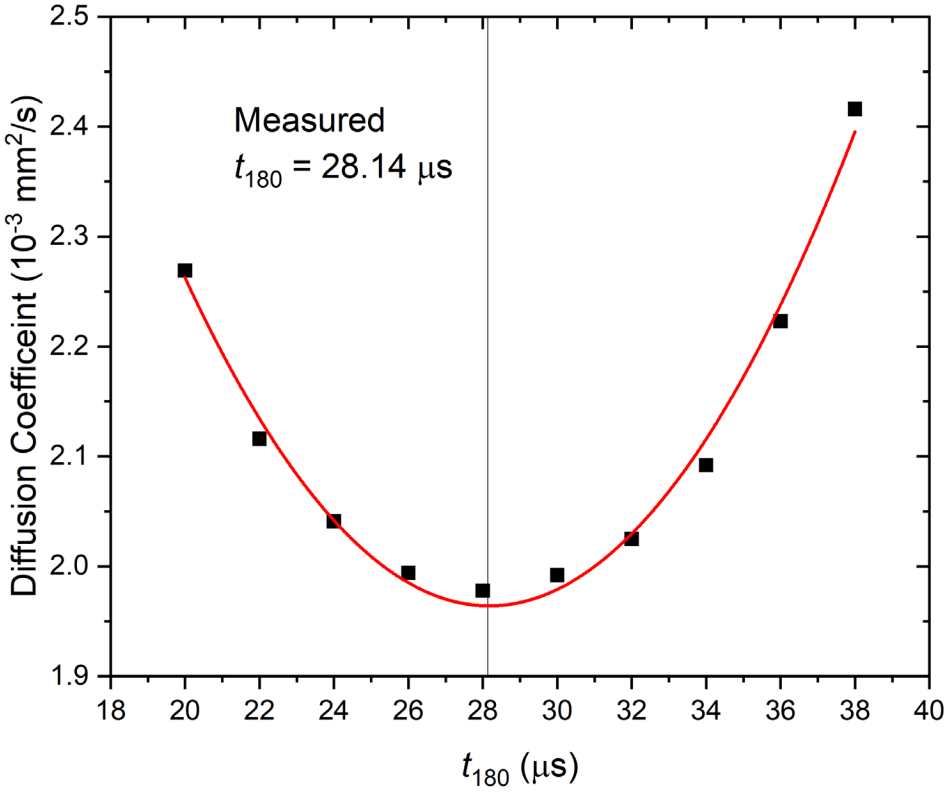

Fig. 29. Measured water diffusion coefficient as a function of the 180° RF pulse duration. The calibrated value for the 180°-pulse duration is 28.12 ms.

4.5.5 Water calibration

Water self-diffusion is often taken as a de facto standard. Holz has published a comparison of NMR diffusion measurements on high purity water along with comparisons to older tracer-based methods (9). The recommended literature-consensus value for the self-diffusion coefficient of high purity water, over a temperature range of 0 °C to 100 °C, is given by:

$$D_{water} = D_0 \left[\left(\frac{T}{T_s} \right) - 1 \right]^{\gamma} \tag{26}$$

$$D_0 = 1.635 \times 10^{-8} \pm 2.242 \times 10^{-11} \frac{\mathrm{m}^2}{\mathrm{s}}$$

$$T_s = 215.05K \pm 1.20K$$

$$\gamma = 2.063 \pm 0.051$$

with a deviation from measured values of < 1 % for the full temperature range except at 0 °C, where the deviation is +2.7 %. A plot of the literature-consensus water-diffusion values

given by Eq. 26 and the deviations of our water diffusion measurements from the literature consensus over a range of temperature from 0 °C to 26 °C are shown in Fig. 30. At present, our average measured values fall within 1.7 % of the consensus values, where the maximum deviation occurs at 0 °C. Our observed positive deviation of the measured water diffusivity at 0° C from the Eq. 26 is consistent with Ref. (9) , however, we are not able currently to resolve this disagreement.

Within our current uncertainty for water diffusivity over this temperature range, $\frac{U_2}{D} \leq 2.6$ %, we have found difference in diffusivity between pure water and water with low doping of Cu^{++} and Ni^{++} ions to be within our stated uncertainty. There may be some systematic difference in the measured diffusivities of pure and doped water, however it is likely to come from the effects of the large differences in the relaxation and measurement times, rather than differences in diffusivity. Given the shorter T_1 and T_2 of the doped water samples, they are quicker to run and we use these as an initial system check during pre-calibration of the measurement system.

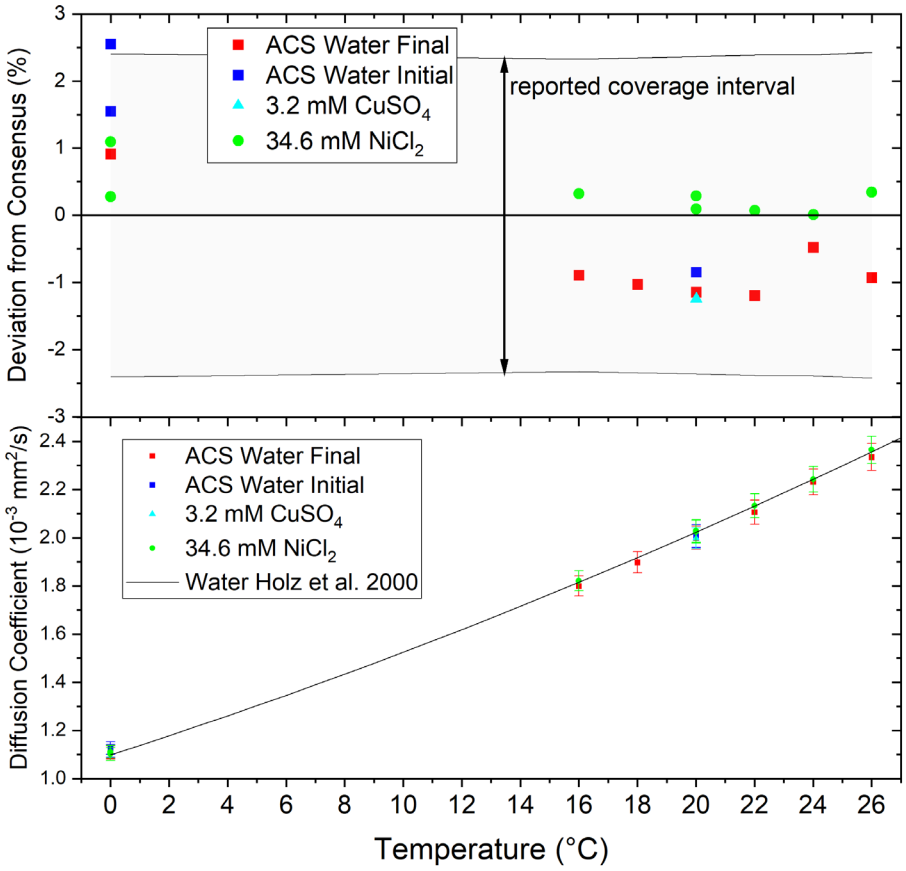

Fig. 30. Lower plot: Literature consensus values for the high-purity water diffusion coefficient and NIST traceable values for American Chemical Society (ACS) regent grade water, Cu^{++}-doped water, and Ni^{++}doped water. Upper plot: Deviation between NIST measurements and literature consensus values. The shaded area shows the reported k=2 coverage intervals.

5. Standard Operating Procedures

5.1 Diffusion Measurement Protocol

The measurement protocol, shown in Fig. 31, has 5 main components: 1) system startup and calibration, 2) sample preparation, 3) pre-run calibrations, 4) data acquisition, and 5) data analysis. Each component will be discussed in the following sections. The measurement protocol is color coded to indicate which steps are taken at the beginning of the run (green), for the first sample in the run (red), for all samples in the run (blue). In addition to customer samples, an additional sample of high purity water and/or a 3.2 mM $CuSO_4$ solution is included as a calibration verification sample. At present, we do not have sufficient resolution to identify any systematic difference in the water diffusion values for pure water versus the $CuSO_4$ solution, as seen in Fig. 30.

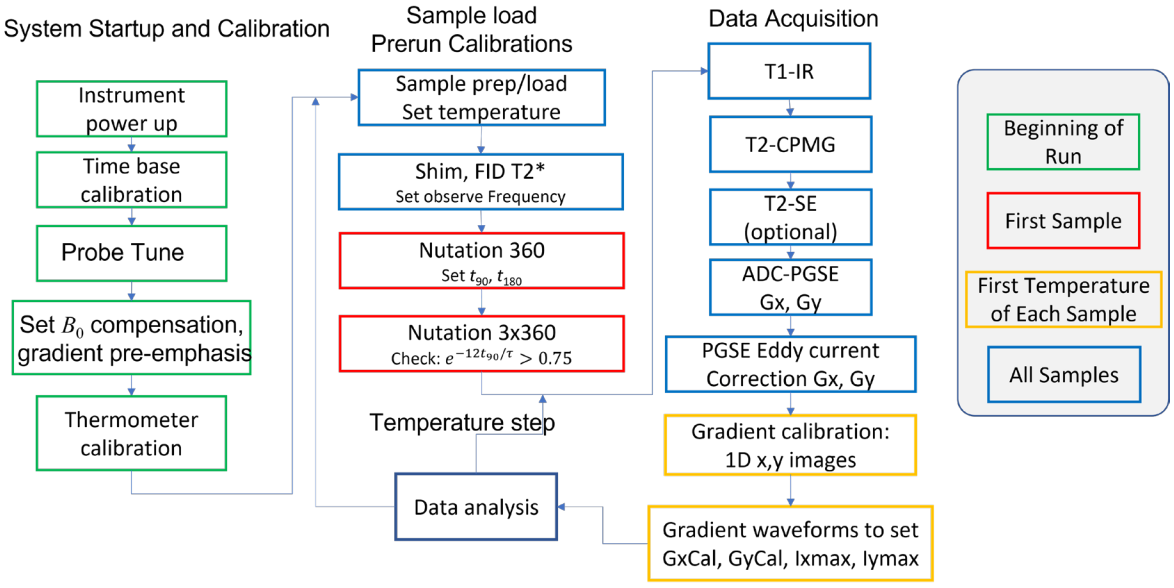

Fig. 31. Diffusion measurement protocol.

5.2 System Startup and Calibration

All electronics and other support systems are powered on at least 24 h prior to the start of a measurement. All test equipment is allowed to equilibrate with room temperature. The superconducting magnet and superconducting shims are allowed to stabilize for at least 24 h after ramping currents. Stabilization is particularly important for the quartz crystal oscillator time base and RF amplifier.

The system time base is calibrated, the sample cell thermometer is calibrated, and the probe is tuned, as detailed in Sec. 4.1.

5.2 NMR Sample Preparation and Setting Temperature

Approximately 25 µl of the sample is transferred, using a clean syringe, into the lower PPS sample cell. The excess can be scraped off using a plastic razor blade. Care is taken so there are no voids or bubbles. A piece of 12.5 mm wide, 0.076 mm thick PTFE sealant tape is placed over the top of the cell, and the bottom part of the cell is inserted into the top part. The excess sealant tape is trimmed off. The sample cell, with the embedded fiberoptic

thermometer is inserted into the sample rod and spinner, using a gauge to ensure the correct insertion depth shown in Fig. 14. The sample is inserted into the NMR and the fiber optic connected to the temperature monitor, with gauge factors set to the fiber optic sensor used. The desired sample temperature, gradient temperature is set along with gas flow as described in Sec. 4.3. Samples are shimmed using an automated Berger-Braun shimming method prior to collecting data (p. 8 in reference (15)).[f]

5.3 Prerun calibrations

Nutation experiments are performed to obtain RF pulse durations t_{90}, t_{180}, for 90° and 180° spin rotations. RF uniformity is tested as described in the NMR RF power calibration section. The measured values for t_{90}, t_{180} are inserted into all subsequent pulse sequences.

5.4 Data Acquisition

***T*₁, *T*₂, *T*₂*:** The T_1, T_2 T_2* measurement procedures are described in Ref (2). T_1 and T_2 values for each sample are required to perform traceable diffusion measurements. The repetition time, TR, for the diffusion sequence must satisfy $TR > 5T_1$. The inhomogeneous broadening ΔB_0, determines the spread in B_0 values experienced by the sample and is used in the uncertainty calculation, must satisfy $\frac{\gamma_p}{2\pi}\Delta B_0 < 10\ Hz$. The inhomogeneous broadening is calculated using $\gamma_p \Delta B_0 = \frac{1}{T_2^*} - \frac{1}{T_2}$.

Diffusion: Eight data sets are acquired for each diffusion measurement: x and y current waveforms for the 1D images, x and y 1D calibration images, x and y eddy current correction data, x and y PGSE diffusion weighted FIDs. The gradient current waveforms are acquired on a digital oscilloscope for the same pulse sequence used to acquire the 1D images, with the exception that only 1 average is used. The 1D images are acquired using 32 or 64 averages for each of the 20 gradient values sampled, 10 negative and 10 positive. The diffusion weighted PGSE are acquired using 8 averages for 20 different gradients and resulting *b*-values. The gradient strengths are chosen to increase linearly starting from 0 to a value b_{max} . b_{max} is adjusted to give approximately 2-3 decades of signal response for the samples being measured. The diffusion coefficient can vary substantially from sample to sample and over the measurement temperature range and it is difficult to a priori determine an optimal set of *b*-values and it is undesirable to have a constantly varying set of *b*-values. Hence, for a given set of samples, a standard set of *b*-values (listed in Table 4) are chosen to match the typical sample type and temperature range and the measured diffusion coefficient is accepted if the observed signal decrease is between 1 to 4 decades, otherwise the gradient strengths are increased (if possible) or decreased for a particular measurement to put the observed signal decrease in the desired range of 2 to 3 decades.

All averaging is done with phase cycling with the protocol shown in Table 5.

[f] The automated shimming procedure uses a simple FID pulse sequence and varies 2 or 3 shim currents at a time, in the order given in reference [15], and maximizes the integral of the FID magnitude for each sequential set of shims.

Table 5. Phase cycling scheme for the PGSE sequence showing the eight measurements that are averaged to get the FID that is analyzed to obtain a diffusion weighted signal. The table entries refer the phase of the applied RF field and detected RF field with x, y,-x,-y respectively corresponding to 0°, 90°, 180°, and 270° phase shift relative to the reference clock.

RF 90°	RF 180°	Receiver
x	y	x
x	-y	x
-x	y	-x
-x	-y	-x
y	x	y
y	-x	y
-y	x	-y
-y	-x	-y

The gradient traces are stored as ASCII data, while the NMR data is stored in a binary format used by the NMR console manufacturer. The NMR data files (.tnt) have raw time domain data along with all pulse sequence information. The embedded pulse sequence information is decoded during analysis to extract pertinent parameters such as time decays, RF pulse amplitudes, gradient amplitudes, and looping parameters. Environmental parameters, such as temperature, as well as protocol identification are not stored within the file and must be included in the file name. The stored NMR data files are executable and allow the rerunning of the same sequence at a later date.

5.5 Data Analysis

The data are analyzed with automated Python scripts contained in the pyNMRms code base. A copy of the Python code and environment are archived along with the calibration data to allow reanalysis with identical protocols as well as with newer protocols contained in upgraded analysis packages. The current code runs Python=3.6.0 installed with Anaconda 4.3.1 (64-bit) numeric packages and uses PyQT and pyqtgraph for the graphics interfaces. The analysis package outputs a comprehensive report, and an example report is contained in Appendix B. Data analysis for T_1 and T_2 measurements are contained in Ref (2). Here, we only describe the diffusion analysis used for this measurement service.

Pulsed Gradient Spin Echo (PGSE) for Diffusion Coefficient measurement:

a) **Gradient calibration:** The script opens the x-axis gradient calibration voltage traces from the 1D image pulse sequence, converts the voltage traces to current using the calibration factor of 2.5 A/V, and calculates the average current during the gradient pulses. A calibration constant, I_{maxGx} , which is the nominal maximum current output the x-gradient amplifier can output with its current gain setting, is calculated. $\frac{I_{maxGx}}{500000}$ specifies the x-gradient output current versus the digital-to-analog converter (DAC) count. The DAC output is the primary parameter determining the gradient strength. The current values are a convenient reference, but their absolute accuracy does not affect the calibration.

The gradient strength, maximum q value, and the b-value are also calculated using the stored reference gradient calibration value. The script then opens the raw time-domain 1D gradient-echo images, subtracts a baseline, then uses a shifted fast Fourier transform to convert to real space images. The real space images are signal intensity versus frequency f, which is proportional to the x-coordinate. The images are inspected to identify any gross defects, such as the presence of a bubble. The images are fit with an ideal cylinder model to find the image width Δf. The gradient is then calculated for each current using $G_x = \frac{\Delta f}{\gamma d_x}$,where d_x is the input cylinder diameter, which is 3.00 mm for the cells currently being used. The gradient calibration parameter, G_{xcal}, the gradient strength per ampere of current flowing through the coil, is determined from data based on a linear model.

The gradient calibration has a weak dependence on probe and sample temperature with an approximate linear increase in the calibration constant with a rate of 0.006 mT/m/A/°C. The gradient calibrations are typically within 1 % of the stored nominal value if no changes to the gradient amplifier gains have been made. Any observed large change in the gradient calibration compared to the historical average must be investigated before accepting data. This process is then repeated for gradients in the y-direction.

b) **Eddy current correction:** The script then opens the x-axis eddy current correction data and fits the data in an identical manner to real diffusion data, as described below. The data is fit to an exponential model to obtain an eddy current correction factor, which describes the loss of signal due to eddy currents.

c) **Diffusion coefficient:** The x-axis diffusion data file is opened. The PGSE gradient amplitude table is read in and converted into a set of gradient strengths using the newly calibrated gradient calibration: $G_x = \frac{GrAmp}{100} * \frac{GradAmpTable}{100} * G_{xcal} * I_{maxGx}$. The b-values are calculated for each of the gradient profiles from the formulas given in Table 1 using the timing parameters embedded in the pulse sequence information. For the standard trapezoidal pulse this includes pulse risetime, duration, and spacing.

A baseline is calculated and subtracted from the FID data. This data is fast Fourier transformed to get spectral data. The major peak in the spectra is identified along with is peak width. A course phasing procedure for each spectrum is used which multiplies by a phase factor to make the imaginary component of the major peak to be equal to zero, maximizing the real value of the major peak. Next a fine phasing procedure is used, which maximizes the amplitude of the integrated signal of the major peak within a window of typically ±10 linewidths. For complex spectra with many closely spaced peaks, smaller integration windows need to be chosen.

The main peaks of the real part of the spectra are integrated within a window of typically ±10 linewidths, to get the signal for each gradient profile which are characterized by their b-value. The signal versus b-value is fit using nonlinear least

squares fit to an exponential decay to extract the apparent diffusion coefficient D_x. The eddy current correction is subtracted to get corrected diffusion coefficients D_{Cx}.

d) **Reported data:** The steps above are repeated for the y-axis data. A reported diffusion is calculated as the average corrected diffusion coefficient $\widehat{D} = (D_{Cx} + D_{Cy})/2$.

6. Uncertainty Evaluation

6.1 Introduction

Measurement uncertainty is a "parameter, associated with the result of a measurement, that characterizes the dispersion of the values that could reasonably be attributed to the measurand" (the unknown true value) (17, 18). Often, this parameter is a standard deviation. Here, we estimate the standard uncertainty (u_c) of the measured diffusion coefficient, $\widetilde{D}$, as the standard deviation of simulated values of measured diffusion coefficients given by a physics-based Monte Carlo code that emulates our measurement apparatus and analysis protocol. Given u_c, the expanded uncertainty is $U = ku_c$ where k is an adjustable coverage factor. Given U, the coverage interval is $(\widetilde{D} - U, \widetilde{D} + U)$ (often expressed as $\widetilde{D} \pm U$) where it is confidently believed that the interval includes the true value D (18). Typically, k is in the range 2 to 3. When the normal distribution applies and u_c has negligible uncertainty, the choices of k = 1, 2 and 3 define intervals having levels of confidence of approximately 68 %, approximately 95 % and approximately 99.7 %, respectively.[g] For this measurement service, we report a k = 2 coverage interval where U is typically determined from the sample standard deviation of approximately N = 60 simulated measurements of D. We expect that the distribution of the measured values of D about the true value is similar to, but more confined than the distribution of simulated diffusion measurements about the assumed theoretical value in the Monte Carlo simulation, given that worst case estimates of several uncertainties are used in the calculation.

---

[g] To better understand these intervals, suppose that a very large number of statistically similar experiments were performed, and a 95 % interval was computed for each experiment. Ideally, approximately 95 % of the resulting intervals would include the true value of interest. As a technical aside, one cannot state that the coverage interval constructed from observed data includes the true value with probability of approximately 95 % because the true value is either covered or not covered by the interval. That is, the probability that the true value falls in the coverage interval is either 0 or 1 – not approximately 95 %. [a,b]

a. NIST. Confidence Limits for the Mean, https://www.itl.nist.gov/div898/handbook/eda/section3/eda352.htm

b. Neyman J, Outline of a Theory of Statistical Estimation Based on the Classical Theory of Probability. Philosophical Transactions of the Royal Society of London Series A, Mathematical and Physical Sciences. 1937;236(767):333-80. https://doi.org/10.1098/rsta.1937.0005

Note that for our Monte Carlo replicates described in the next section, the normality assumption may well approximate some cases but not all cases. Additionally, the standard uncertainty determined from Monte Carlo realizations of measured $\widetilde{D}$ has non-negligible uncertainty because of the low number of simulated values and because of effects due to assuming worst case distributions in the Monte Carlo, since we don't know how close the "worst case distributions" are to the unknown theoretical distributions. For these reasons, the true levels of confidence will likely differ from what we report, as stated in NIST Technical Note 1297.

Any particular measurement can be decomposed as the sum of the unobserved true value, a random error (with expected value 0) and a systematic error (bias). The bias is the difference between the expected measured value and the unknown true value. The goal of the measurement service is to account for all sources of bias, through careful measurement and SI-traceability, and minimize the uncertainty associated with these bias corrections so that the uncertainty and associated coverage interval will be predominantly due to random errors.

An example of bias correction for the diffusion measurement protocol is the use of an eddy current correction. The presence of gradient-induced eddy currents, which are difficult to measure and model, will give rise to the loss of signal not directly related to water diffusion. This leads to a systematic error where the measurement will consistently overestimate the diffusion coefficient. The implementation of the eddy current correction accounts for this bias but contributes to the variability in the measurement due to the uncertainties in the correction value.

Practical measurements, particularly those involving in-vivo measurements in patients, may be constrained by other factors such as time, cost, and safety. These measurements may introduce an unknown bias, which is the motivation for the measurement service to be able provide reference samples where the reported uncertainty for the measured value of D for each sample accounts for both random and systematic effects. The variance of a clinical measurement, which is only part of the uncertainty, may still be useful in guiding decision making if the bias is constant and consistent over a given set of measurements.

The individual uncertainty components for the NIST NMR measurements, shown schematically in Fig. 32, are estimated following guidelines given in NIST Technical Note 1297 (18). The uncertainty components are separated into Type A uncertainty evaluations, obtained statistically from a series of measurements, and Type B uncertainty evaluations, determined by subjective judgment or other non-statistical methods. Unlike older methods for combining uncertainties, this measurement service uses a physical model of the measurement system and measurement process, which reports an uncertainty in measured D due to all known random and systematic effects with a Monte Carlo method. The physics model can identify systematic effects that contribute to measurement error and accounts for correlated effects that are not considered in the traditional method of combining uncertainties listed below.

For Type A uncertainty evaluations, we assume that measurements are independent and normally distributed. For example, the standard uncertainty, $u_{Type\ A}$, associated with a single measurement of a component (assuming there are no other sources of uncertainty associated with the component) is:

$$u_{Type\ A} = \sqrt{\frac{1}{N-1}\sum_{h=1}^{N}(x_h - \bar{x})^2}\ , \tag{27}$$

where x_h represents the individual measurements of a value, $\bar{x}$ is the average of the measurements, and N is the number of measurements made.

For Type B uncertainty evaluations, we typically assume that the value of a model parameter is uniformly distributed in an interval between a and b where $b - a = 2\delta$. The standard uncertainty, $u_{Type\ B}$, is equated to the standard deviation of this distribution and is given by:

$$u_{Type\ B} = \frac{\delta}{\sqrt{3}}. \tag{28}$$

Some uncertainty sources arise from both Type A and Type B uncertainty evaluations. The combined standard uncertainty, u_c, for an analytical measurement equation is given by summing the standard uncertainty associated with the input parameters in quadrature, weighted by sensitivity coefficients as specified in (18).

In summary, we do not have an analytic measurement equation, so instead uncertainty for the measurand, water diffusivity, is calculated via a Monte Carlo method using the Bloch-Torrey model. The inputs are worst-case determinations of experimental and calibration uncertainties that go into the measurement process. The physics-based Monte Carlo simulations propagate the input uncertainties to give an uncertainty in the output measurand. We report a $k = 2$ coverage interval. The physics-based code identifies and accounts for many, but not all, systematic effects on measured D.

6.2 Overview of Measurement System Uncertainties

The sources of uncertainty for diffusion measurements are indicated schematically in Fig. 32 and can be categorized by where they occur in the measurement chain and whether they are type A or B. The traceable calibrations (TC) include calibration of the system time base and the sample temperature probe. The major source of uncertainty comes from non-idealities of the pulse sequences (NPS) due to hardware limitations and to local environment (LE) factors that cause non-uniformities in B_0, B_1, and temperature. There will be uncertainties due to non-ideal material properties (NM) such as lack of stability and lack of Bloch model applicability. While these material uncertainties are described here, they are the responsibility of the customer. Finally, there are uncertainties due to data analysis (DA) methods including procedures such as baseline subtraction, integration range, phasing of the complex signals.

The individual uncertainty components are described below. The combined uncertainty is calculated by a Monte Carlo method, described in Sec. 7, in which *worst-case distributions* of the relevant parameters are fed into a Bloch simulator that performs a simulated measurement using the same pulse sequence and analysis used in the physical measurement. The distributions of diffusion coefficients from the simulated measurements are calculated and used to generate the expanded combined uncertainty reported to the customer. A worst-case distribution is defined for each parameter based on observable properties of the

measurement system and measured data. For example, the B_0 uncertainty is taken from the measured inhomogeneous linewidth, described in Sec 6.4, and a worst-case distribution is defined as a Gaussian distribution with a standard deviation of 0.125 μT. Measured diffusivity distributions on standard samples are used to directly compare the uncertainty in measured data sets with calculated uncertainties to validate the Monte Carlo model.

A typical set of uncertainties for diffusion measurements are given in Table 6. These uncertainties are evaluated for each measurement and will vary depending on the condition of the measurement equipment and customer sample properties.

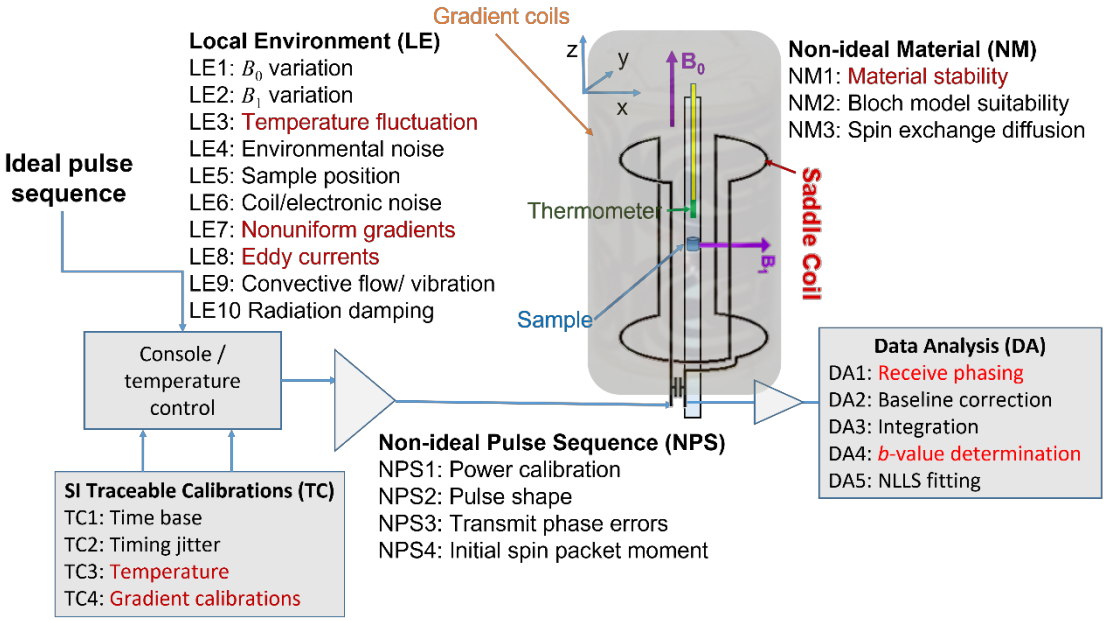

Fig. 32. NMR system schematic with labeled sources of uncertainty. The uncertainties highlighted in red are the major sources of uncertainty in the current measurement of diffusion coefficients.

Time base (TC1) and time jitter (TC2)

Proton relaxation times are based on measuring the time dependence of the sample magnetization decay. The measurement of time intervals is based on a complex programmable logic device counting cycles of a 50 MHz frequency reference produced by a 10 MHz temperature-stabilized quartz crystal oscillator. The oscillator is calibrated against a NIST frequency reference yearly to ensure the frequency standard uncertainty is less than 5 Hz. Other sources of timing errors come from jitter in the NMR time base and digitization in the programmable logic devices controlling the system. The maximum measured jitter in the NMR time base, over the time intervals used in these measurements has a Gaussian distribution with a standard deviation of 60 ps. The error in a measured time interval Δt, is the sum of two components, an error given by the calibration of the time base, E_{tbc}, and a timing jitter E_{tj}. The error due to time base calibration is given by

$$E_{tbc} = R * TimeBaseError * \Delta t \tag{29}$$

where R is a random variable taken from a continuous uniform distribution from −1 to 1, $TimeBaseError$ is a measure of the uncertainty in the NMR time base (typically equal to 0.5 x 10^{-6}. E_{tj} is a Gaussian distributed random variable with a standard deviation of 60 ps. For short times, such as RF pulse durations, which are typically 30 μs, the 60 ps jitter dominates the uncertainty. For longer times the uncertainty of the time base dominates. The timing jitter is stochastically varied every timing event, and the calibration uncertainty is stochastically varied after each complete measurement. In general, timing uncertainty given proper calibration and maintenance of the NMR system, is not a major contributor to the total uncertainty.

The accuracy of the transmit frequency is not relevant for these measurements since the transmit frequency is calibrated using the material under measurement. However, the transmit phase accuracy and phase stability are critical since variations in the transmit phase will lead to variations in the observed FIDs and hence errors in the relaxation time measurements. The primary transmit phase reference is the phase of the RF field during the spin excitation event. This phase sets the phase of the proton precession. As long as the transmit path and probe tuning do not change during the pulse sequence, subsequent RF pulses will be properly referenced to the initial excitation pulse apart from variation due to phase noise. The uncertainty due to phase noise is determined by applying a distribution to the nominal applied transmit phase given from a measured phase noise spectrum.

Temperature calibration/transfer (TC3):
The uncertainty in the sample temperature arises from errors in the sample thermometer calibration and from potential temperature differences between the sample and the nearby sample thermometer. The sample thermometer is calibrated relative to two NIST-calibrated platinum resistance thermometers with errors bounded by ±0.010 °C. The errors in the sample temperature, T_s, due to miscalibration of the sample thermometer, are bounded by ±0.150 °C, which corresponds to the maximum drift between calibration intervals. From experiments with changing the thermal coupling between the sample and sample thermometer, e.g., changing the coupling media from air to a high thermal conductivity fluid, the maximum temperature difference is less than ±0.1 °C. For Monte Carlo simulations, we assume that the temperature error is given by the sum of two random variables, ΔT_t and ΔT_{cal}, where ΔT_t is uniformly distributed over ±0.1 °C and ΔT_{cal} is uniformly distributed over an interval of ±0.15 °C. The temperature contribution to the error in the diffusion coefficient, D, is given by:

$$\Delta D_T = (\Delta T_t + \Delta T_{cal}) \frac{\partial D}{\partial T_s} \tag{30}$$

Typical values of the change in diffusion coefficients with temperature (Fig. 18) are $\frac{1}{D}\frac{\partial D}{\partial T_s} = 4\ \%/°\mathrm{C}$. However, these coefficients vary considerably with field and temperature, as well as with the type of material being tested. While we have chosen to use worst-case uniform distributions of temperature error, more realistic distributions can easily be substituted in the simulations. Uncertainty in sample temperature is a major source of uncertainty in the measured relaxation times.

Gradient calibrations (TC4)
The gradient calibrations are described in Sec. 4.4. The uncertainties in the calibration are primarily derived from the uncertainty in the cell diameter *d,* which has a maximum relative uncertainty of 1 %. This value is used in the gradient uncertainty calculations. There is an associated uncertainty in calculating *b*-values from the gradients (DA5), which involves multiple integrations over the gradient waveforms. We assume that the *b*-value calculation errors and gradient calibration errors are uncorrelated.

6.3 Non-Ideal Pulse Sequence (NPS)

RF power calibration (NPS1):
The RF field amplitude is calibrated by a nutation experiment described in Sec. 4.1. The magnitude of the error in the RF field amplitude, determined from the fit, is no greater than ±5 %. This is taken into account in the uncertainty calculation by modeling RF power amplitudes as Gaussian random variables with a worst-case standard deviation of 5 %. The fit to the nutation data also provides a check that the nonuniformity of the RF field is within the worst-case profile used in the uncertainty calculation.

RF pulse shape (NPS2):
The RF pulse shapes used for these measurements are all rectangular. There was no significant change in the pulse shape when monitoring the RF transmit pulses except for timing jitter, which is accounted for in TC2.

RF transmit phase error (NPS3):
The RF transmit phase is self-referenced, so the phase difference of the main clock to the transmit signal is not relevant. However, phase noise will be present and will cause the transmit phase to vary. This is taken into account by including Gaussian phase noise with a standard deviation of 1°, applied to each RF pulse. This is consistent with phase noise values measured by a spectrum analyzer at an offset frequency commensurate with the typical RF pulse duration.

Initial spin packet moment (NPS4):
The initial spin packet magnetization vector may not be given by its thermal equilibrium value due to insufficient wait time or due to noise being picked up and transmitted by the resonant transmit/receive coil. The wait times for all sequences are a minimum of $5T_1$ from excitation to re-excitation, ensuring that the magnetization is within 0.67 % of the equilibrium value. This incomplete recovery time is taken into account in the Bloch simulator calculation of uncertainties. Additional fluctuations may arise due to noise, particularly if the transmit gate is open before the excitation. These effects can be included in the uncertainty calculation by adding RF noise during the pre-transmit period.

6.4 Local Environment Variation (LE)

B_0 variation: Nonuniformity of the DC magnetic field (LE1):
The uniformity of the DC magnetic field is accomplished using superconducting and room temperature shims. Maximum inhomogeneous linewidths are on the order of 10 Hz (see Fig. 6). These are included in the uncertainty calculation using a Gaussian B_0 distribution with a

standard deviation in the range of 0.125 μT to 0.50 μT depending on the obtainable quality of the shimming for a particular set of samples.

Nonuniformity of the RF field amplitude (LE2):
For a given RF pulse applied to the RF coil with a specified amplitude, frequency, phase, and shape, there will be a distribution of RF field amplitudes experienced by the sample determined by the RF transmit coil design and the sample loading. The RF field amplitude was measured along the *z*-axis to obtain a B_1 field variation that is used in the Monte Carlo simulation of uncertainty. Since the same coil is used for both transmit and receive, the variation in the RF transmit field also corresponds to a variation in the receive sensitivity. The parameters in the model B_1 variation are required to be consistent with the damping time determined from the nonlinear least squares fit of the nutation data using Eq. 19.

Temperature fluctuation (LE3):
The temperature is set by a closed loop system that controls a heater and cooled gas flow system and feeds back on a fiber optic thermometer placed next to the sample. The measured thermal fluctuations of the sample thermometer are approximately Gaussian with a standard deviation < 0.050 °C. The measurement uncertainties from temperature fluctuations are included in the Monte Carlo error estimate by incorporating a Gaussian-distributed worst-case temperature error at the beginning of each pulse sequence.

Environmental noise (LE4):
Environmental noise is due to RF radiation or low frequency magnetic field fluctuations coming from the vicinity of the NMR scanner. Care is taken to locate the scanner in a low noise environment and environmental noise is monitored by taking repeated scans with the same sample and configuration. If deviations occur in the integrated signal by more than 0.2 % in the sets of three identical repeat measurements, the measurements are halted, and noise issues are fixed before proceeding. *We, therefore, do not take environmental noise into account in the uncertainty analysis.*

Sample position (LE5):
Slight variations in the sample position and orientation of the capillary and fiber optic thermometer may alter both B_0 and B_1 distortions. To determine the error due to sample positioning, a test/retest protocol is used where the sample is removed from the NMR system, the thermometer insertion is redone, the sample is reinserted and measured. For short samples < 10 mm, the sample is centered within the RF coil to ±1 mm and verified by monitoring the nutation curve and inversion recovery parameters. The Monte Carlo calculations will vary the sample position by ±1 mm.

Coil noise/electronics noise (LE6):
Coil noise and electronic noise are measured from the spectrometer during an interval when no signal is present. To determine uncertainty, a Gaussian noise term, similar to the measured noise spectra, is added to the simulated signal before the analysis. Typical signal-to-noise ratio (SNR) values are between 2000 and 20000. A typical worst-case SNR is between 2000 to 5000, depending on the data set. This is then used to determine the Gaussian noise standard deviation, which is given by the maximum observed signal divided by the worst-case SNR.

Nonuniform gradients and gradient offsets (LE7)
As shown in Fig. 9b, the gradient strength will vary slightly over the 3 mm sample volume. The spatial variation of the magnetization, described by the *q*-vector and the derived *b*-value, will also vary over the sample. The variation of the gradient amplitudes is taken into account in the Monte Carlo calculations by each spin packet having a gradient amplitude given by its position and spatial gradient variation given by Eqs. 23a,b,c.

If there is a gradient offset $\vec{g}_0$, a nonzero component of the gradient when the gradient signals are off, there will be an additional contribution to the observed signal decay b_t given by(19)

$$b_t = b + b_0 = \gamma^2\delta^2 g^2\left(\Delta - \frac{1}{3}\delta\right) + \vec{g}\cdot\vec{g}_0\delta(d_1^2 + rd^2 + \delta(d_1 + rd) + \frac{2}{3}\delta^2 - 2TE^2) \quad (31)$$

where the pulse sequence parameters are defined in Fig. 1. The b_0 correction, due to the interference of the background gradient with the applied gradient, can lead to positive or negative deviations of the signal from simple exponential fits when plotted as a function of b. The maximum value of $\vec{g}_0$ can be set by the amount of maximum allowed inhomogeneous broadening after shimming $\frac{\gamma_p}{2\pi}\Delta B_0 = 10$ Hz and the sample size, which gives maximum value of $|\vec{g}_0|$ of $g_{0\max} = 12.4 \times 10^{-6}$ T/m. This offset gradient, using our standard pulse sequences and Eq. 31, will give a maximum offset gradient error in the reported diffusion coefficient of ±0.2 %, where the sign is determined by the angle between the offset and applied gradients. Typical measurements of the diffusivity with the gradients applied in +x, +y and then -x,-y directions, which reverses the sign of the gradient offset error, agree within 0.5 %, which is within the stated uncertainty (an example is shown in Fig. 25)

Sample generated gradients due to susceptibility mismatches can also lead to large field gradients. This is addressed using a sample cell that is approximately susceptibility matched with the uncertainty limits described above being valid. However, if the sample in intrinsically inhomogeneous with large susceptibly variations, there may be errors in the diffusion measurements, which are not accounted for here.

Eddy currents (LE8)
A correction for eddy current induced signal loss, which can mimic diffusional signal loss, is applied by running the same PGSE sequenced used to calculate the diffusivity, except with the RF excitation pulse just after the diffusion gradients, rather than just before the diffusion gradients (see Sec. 4.5.1). Any observed signal loss is due to gradient-induced eddy currents rather than diffusion effects. The eddy-current correction data is collected and fit in the same manner as the diffusion data. The exponential decay constant obtained from the fit is subtracted from the measured diffusivity. This correction accounts for eddy-current diffusion effects that inflate the estimate of the diffusion coefficient. The bias correction is imperfect and the component of uncertainty due to imperfect bias correction is of $5 \times 10^{-6}\,\frac{\text{mm}^2}{\text{s}}$, which corresponds to the maximum observed variation of the eddy current correction. This source of uncertainty is implemented in the Monte Carlo simulations as a random Gaussian error applied to the measured eddy-current correction.

Convective flow and vibrations (LE9)
If thermal gradients are present, there can be convective flow within the measurement cell giving rise to a motion-dependent loss of signal that can incorrectly be ascribed to diffusion (20, 21). To minimize convective effects the sample cell is kept small, the temperature is kept

as uniform as possible by using a multi-pass N_2 flow sample cell and maintaining the probe temperature close to the sample temperature. Convective flow will be worse in low viscosity samples, particularly in organic solvents such as acetone and chloroform. Here, we are mostly measuring tissue mimics where pure water will be the lowest viscosity material of interest. The lack of convection is determined by having no systematic deviations from the water diffusivity consensus values and by performing a flow encoded 2D J-resolved IDOSY sequence to measure maximum velocities(21). If convection is observed, the thermal geometry will be altered until a convection free state is achieved.

If there is sample motion in a nonuniform field, e.g., the gradients, there can be a loss of signal that may be misinterpreted as due to diffusion. Here we ensure a low vibration environment by rigidly inserting the sample in a tight spindle with an insertion rod that presses the spindle on top on the probe housing. The NMR magnet rests on air legs on a low-vibration on-grade floor. The spindle and sample cell cannot rotate or vibrate. A primary source of vibrations is due to the temperature control gas that flows around the sample cell which is typically set to 20 l/m. An upper bound on signal loss due to vibrations can be made by determining the minimum measurable diffusion coefficient using a high signal, low diffusivity sample.

Radiation damping (LE10)
The precessing proton magnetization will generate resonance RF currents in the RF transmit/ receive coil that can damp the precessing magnetization. These radiation damping effects can cause errors in the diffusion measurements (19). These errors show up as a decrease in the amplitude of the large signals obtained at low *b*-values. Here, we minimize radiation damping effects by using a small sample (20 µl), minimizing the time large transverse magnetizations are present (*d1*, *rd* in Fig. 1), and running at low fields commensurate with MRI operation. The time constant associated with radiation damping is given by $T_{rd} = \frac{2}{\mu_0 \gamma M_0 s \eta Q}$,where η is the coil fill factor, M_0 is the equilibrium proton magnetization at the operation field and temperature, and Q is the quality factor of the RF coil. For our system $\eta \cong, 0.02; Q \cong 100$ giving a radiation damping time at a field of 3 T and sample temperature of 20 °C of $T_{rd} > 400$ ms. This time is long compared to TE typically used and the radiation damping effects will be small.

Radiation damping will cause a deviation from ideal exponential behavior and will be identified by the "lack of fit test" (Appendix A.), which does not consistently occur for these measurements. Further, radiation damping affects the spectra with large signal, and it can be identified by the diffusivity being dependent on the choice of points being fit. For our data, the magnitude deviation in diffusivity from using the full set of data, including $b = 0$ s/mm^2, and truncated data where only $b > 500$ s/mm^2 is fit, is typically < 0.3 %. A warning is issued if the full b ≥ 0 s/mm^2 data fit differs from the $b \geq 500$ s/mm^2 by more than 0.3 %.

6.5 Non-ideal material properties (NM)

Stability (NM1):
There are several possible causes for this non-ideality. *The supplied materials may not be stable and may change properties during shipping, transferring into the measurement capillary, or due to insertion into a high magnetic field* environment. The content of

dissolved gases, such as oxygen, which can modify proton spin relaxation, can change over time or during sample handling and measurement, particularly during temperature cycling. Samples can also change during the measurement process due to evaporation/distillation or materials plating out on the sides of the storage or measurement vessels. Care is taken to transfer and seal the samples rapidly to prevent evaporation. For higher temperature measurements, care must be taken so that no distillation occurs, which would leave a more concentrated solution at the bottom relative to the top of the capillary. The standard operating procedure is to start at low temperatures and work up in temperature to minimize possible distillation. To monitor changes in the samples due to changes in dissolved gas content after thermal cycling, a repeat measurement is done at the starting temperature. These changes are noted and recorded. Samples are visually inspected before and after measurement to ensure that the sample looks homogenous. NIST will exercise care both in handling and in selecting the measurement vessels to minimize change of properties. However, *because NIST cannot control or always know the composition and properties of the samples, the uncertainties due to material instability are the responsibility of the customer. Special handling protocols can be established for particular samples as required, including handling in controlled atmospheres.*

Bloch model suitability (NM2):
The materials supplied by the customer may not have-well defined Gaussian diffusion coefficients, which will manifest as poor fits to the Bloch Torrey equation predictions. If this is the case, traceable diffusion coefficients cannot be reported. However, a special measurement result will be provided that includes measured data, multiexponential fit parameters, and measurement procedure. Effective parameters such as apparent diffusivity and kurtosis can be extracted, but since these values are dependent on model and gradient trajectories, they cannot be unambiguously defined.

Spin diffusion via exchange and dipolar coupling (NM3):
Other processes can lead to magnetization diffusion in addition to physical motion of the protons. Spin diffusion due to exchange and dipolar coupling will lead to magnetization diffusion, parameterized by the diffusion coefficient D_e, in the absence of any physical motion. The has been extensively studied in crystals and large molecules. The diffusivity is on the order of magnitude of (3) $D_e = \frac{a^2}{50 \cdot T2} < 10^{-16}\ \mathrm{m}^2/\mathrm{s}$, whereas this measurement service is limited to diffusivities $>10^{-12}\ \mathrm{m}^2/\mathrm{s}$. Hence, the magnitude of corrections due to spin diffusion by exchange and dipolar interactions are less than 0.01 % and are ignored for the samples measured here.

6.6 Data Analysis (DA)

Receive phase (DA1):
The NMR system has timing delays during receive amplification and digitization. While quadrature signals can be measured precisely, the absolute phase information is lost during the signal detection process. A phase shift is applied to complex data to compensate for the phase delay that occurs during signal reception and detection. Since the receive and digitization processes are the same for all FIDs, all spectra will have the same phase shift

resulting in a similar change in signal for all spectra. Uncertainty occurs due to errors in determining the phase shift to be applied. The magnitude of the error in the phase shift was less than 5°. We apply a flat distribution of phase shift errors of ±5° in the Monte Carlo calculation.

Integration/baseline subtraction (DA2):
The spectra are integrated over a range corresponding to ±10 FWHM, where FWHM is the full width at half-maximum of the spectra with the maximum amplitude. There is an uncertainty introduced due to the range of the integration and to the non-zero baseline of the data. The baseline is subtracted before integration by measuring the offset in the last 10 % of the spectra. However, this is imperfect, and the error is simulated in the Monte Carlo calculation by adding a random offset to each data set that has a Gaussian distribution with a width equal to that of the maximum observed distribution in baseline values. This value is typically 5×10^{-5} times the maximum signal.

Nonlinear Least Squares (NLLS) fitting (DA3):
The data is fit with standard NLLS fitting algorithms using the Levenberg-Marquardt method, such as implemented in scipy.optimize. NLLS fitting, when compared to linear fitting of logarithm of the signal, intrinsically weights the large signal points more heavily than the low signal points. The low signal points that are close to the noise limit contribute very little to the calculated diffusion coefficient but are important to validate the simple exponential model.

6.7 Summary of Measurement Uncertainties

The main components giving rise to the diffusion coefficient uncertainty are uncertainties in the sample temperature, gradient calibration, and eddy current corrections. For materials with a diffusivity that has a strong temperature dependence, the uncertainties in temperature will dominate. For materials with very low diffusivities the uncertainty in the eddy current correction will dominate. In most other cases, the error in the gradient calibrations will be the dominant contributor to the uncertainty.

7. Monte Carlo Uncertainty Calculation

A Monte Carlo approach is appropriate for computing measurement uncertainty when the measurand cannot be represented using the traditional propagation-of-errors method (17), which is the case for uncertainties in diffusion measurements. Here, the uncertainty is calculated using a Monte Carlo technique in which distributions of parameters that contribute to the measurement uncertainty, described in Sec. 6, are input into a standard Bloch-solver that integrates the Bloch-Torrey equations for each event in the NMR pulse sequence. The performance of the ordinary differential equation solver was checked against two other independent solvers on several standard problems to establish that the errors in the numerical integrations were considerably less than the errors from the instrument and sample uncertainties listed above. Figure 33 is a diagram of the calculation, which consists of three loops. The first/inner loop integrates over a large ensemble of spin packets, typically ~10^4, where B_0 and B_1 are determined from a random spin packet position within the sample.

Figure 34 shows typical spin packet distributions for the 3 mm cylindrical sample, color coded for local field and gradient nonuniformity. The second loop (parameter loop) is over the desired pulse sequence parameter list, gradient strength or b-value, with typically 20 values, and includes uncertainties due to timing jitter, phase noise, and thermal fluctuations. The output from these calculations is then fed into a data processing pipeline identical to the one used for real data. Additional noise and receive phase errors are added in this stage before a nonlinear least squares fit is done to obtain the reported diffusion coefficient. Figure 35 shows the signal versus b-value for real data and five simulation runs along with fits that determine the diffusion coefficient. The third/outer loop (measurement loop) then iterates this process with different values of measurement conditions to build a distribution of simulated diffusion measurements, from which we can calculate the uncertainty. The outer loop includes uncertainties due to sample position, thermometer calibration, gradient calibrations, and time base calibrations. The mean values of these distributions are compared with the assumed value of D in the Monte Carlo simulation to determine the measurement bias, the difference between average of simulated values of D and input diffusion coefficient. The estimated standard deviations $\tilde{\sigma}$ of the distributions are used to determine an expanded uncertainty interval as discussed below.

Figs. 36 and 37 show example outputs from the Monte Carlo calculations when all non-idealities are included. The simulation shown in Fig. 36 is for a 40 % PVP solution at 3 T, 20 °C. The mean value, $D_m = 0.5078 \times 10^{-3} \frac{\mathrm{mm}^2}{\mathrm{s}}$ is close to the input prescribed value $D_{in} = 0.5070 \times 10^{-3} \frac{\mathrm{mm}^2}{\mathrm{s}}$ indicating little bias. Table 6 shows the experimental uncertainties used in the Monte Carlo Bloch simulations shown in Fig. 36. The simulation shown in Fig. 37 is for a 20 % PVP solution at 3 T, 20 °C and also shows the important primary input-value distributions for the simulation.

The distribution of Monte Carlo realizations of measured diffusivity values cannot always be well approximated as a Gaussian distribution (see sample distributions in Fig. 38). However, we can construct k = 2 coverage intervals, $\widetilde{D} \pm 2\tilde{\sigma}$, where $\tilde{\sigma}$ is the measured standard deviation of the distribution output by the Monte Carlo. Due to the finite number of simulated measurements, $\tilde{\sigma}$ will only approximate the standard deviation, σ, of the underlying distribution of simulated measurements. Fig. 38 shows two examples of simulated diffusivity measurements for a water calibrant along with the input value of the diffusivity and the reported uncertainty intervals $U = 2\tilde{\sigma}$. Fig. 39 shows the deviation of the diffusivity from the literature consensus values for water calibrants along with the independently calculated coverage interval from the simulations. The physics-based Monte Carlo calculations show that the simulated measurements fall within the reported coverage interval, centered on the theoretical input value, approximately 95% of the time. This is consistent with measurements on water calibrant samples using consensus values as the true values.

Most uncertainty simulations are restricted to 40 to 100 trials for each sample, at a given temperature and field value, due to limited computational resources. For a full set of correlated measurements, such as those done on a particular sample as a function of temperature, the uncertainties can be better defined by plotting the uncertainties versus sample parameters and doing an analytical fit to the observed trends, as shown in Fig. 40. Here, each measurement at a different temperature is modeled with 56 to 64 trials in the Monte Carlo code. The expanded $U = 2\tilde{\sigma}$ uncertainty is well fit with a low-order

polynomial. The uncertainty for the full set of measurements, 12 temperatures in this case, can be taken from the fit. This allows us to leverage all of the Monte Carlo repeats taken for a particular sample when calculating uncertainties (292 in the example shown in Fig. 39), partially alleviating potential issues from such a small Monte Carlo sample size at an individual temperature and allowing us to extrapolate to other temperatures where there are no Monte Carlo samples.

For standard diffusion measurements, the bias, the difference of the mean simulated diffusivity from the prescribed diffusivity, is small compared to the standard deviation, as expected since all known sources of bias are accounted for in the measurement methodology or in the analysis. An example of accounting for bias in the measurement methodology includes the use of a small sample volume to ensure the inhomogeneities in the RF and gradient fields are small. An example of accounting for bias in the analysis process includes the use of an eddy current correction that accounts for the systematic increase in apparent diffusivity when eddy currents are present. In cases where measurement bias cannot be avoided, as for example when a larger sample must be measured, that extends beyond the homogeneous regions of the gradients, the Monte Carlo estimate of bias will be subtracted from the measured value, bringing the bias back close to zero. The empirical evidence that all major effects that produce systematic error are accounted for, when the methodology documented in this paper is used, is the agreement, within the stated uncertainty of our measurements of pure water diffusivity to consensus data that use both isotopic and spin tagging techniques. There is no evidence that the published diffusivity consensus data of pure water is more accurate than the data presented here.

The bias and uncertainty calculation methods are detailed in the Monte Carlo code, which is archived with each measurement series, the input files detailing the measurement parameter error distributions and pulse sequences, and the Monte Carlo output file that contains output distributions for the diffusivity along with sampled measurement parameter distributions. The uncertainty calculations are summarized in the calibration reports along with the measurements uncertainties that exist at the time of the measurements.

Table 6. Input uncertainties used in the Monte Carlo Bloch simulations shown in Figs. 35, 36. Type A evaluations of uncertainty are based on the statistical analysis of repeated measurements. Type B evaluations are derived via other means, such as manufacturer specifications or expert opinion. In this context, Type A refers to measured uncertainties where mostly Gaussian distributions, characterized by a standard deviation σ, are assumed and Type B refers to estimated uncertainties where mostly worst-case uniform distributions, specified by their uncertainty intervals, are used.

Uncertainty Source	Type	Distribution	Standard deviation (Type A) or interval (Type B)
TC1: Time base calibration	B	Uniform	±0.5 ppm
TC2: Time base jitter	A	Gaussian	σ = 60 ps
TC3: Temperature calibration transfer	B B	Uniform Uniform	±0.15 °C ±0.10 °C
TC4: Gradient calibration	B	Uniform	±1.0 %
NPS1: Power calibration, B_1 amplitude	B	Uniform	±5 %
NPS3: Transmit phase errors	B	Gaussian	σ = 0.05°
LE1: B_0 nonuniformity δB_0	A	Gaussian	σ = 0.125 μT
LE3: Temperature fluctuation	A	Gaussian	σ = 0.05 °C
LE5: Sample position z	B	Uniform	±1.0 mm
LE6: Coil/electronic noise MaxSig /SNR	A	Gaussian	σ = 0.001
LE8: Eddy current correction error	A	Gaussian	$5x10^{-6}\,\mathrm{mm}^2/s$
DA1: Receiver phase error	B	Uniform	±4°
DA2,3: Integration/ base line error	B	Gaussian	σ = 0.00005
DA4: b-value determination	B	Uniform	±0.5 %

Table 7. Components of uncertainty arising from systematic effects.

Nonideality	Distribution	parameters
LE2: B1 nonuniformity	Quartic	a = b = c = 9.1 mm
LE7: Nonuniform gradient δg	Quadratic	$A, B, C = 2x10^{-3}\,\frac{\%}{\mathrm{mm}^2}$

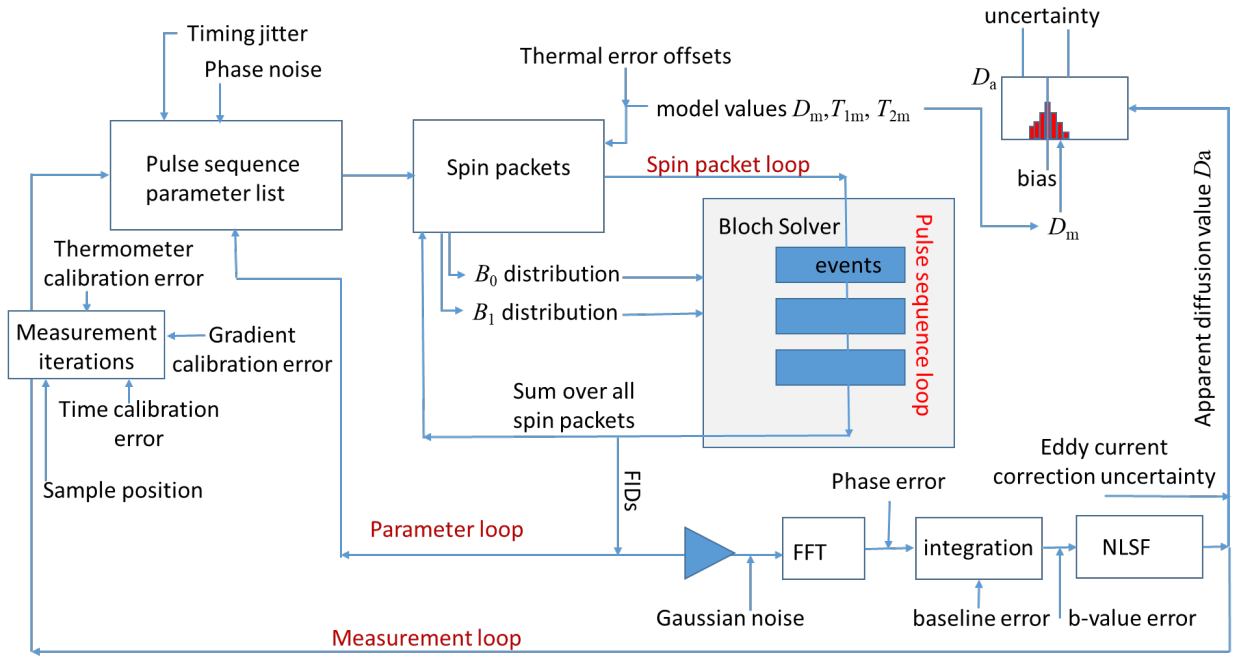

Fig. 33. Schematic of Monte Carlo calculation showing conversion of uncertainties in input parameters into uncertainty in diffusion coefficients.

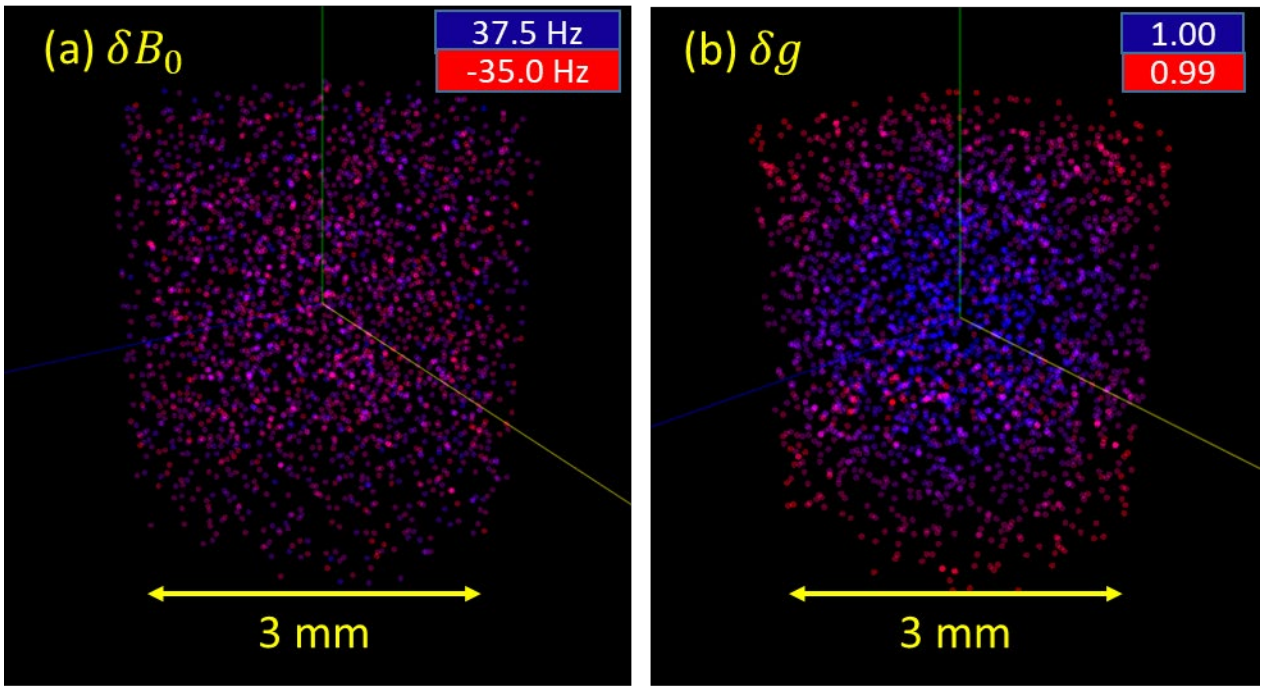

Fig. 34. Point clouds showing typical spin packet positions color coded to show (a) local fields and (b) gradient nonuniformity.

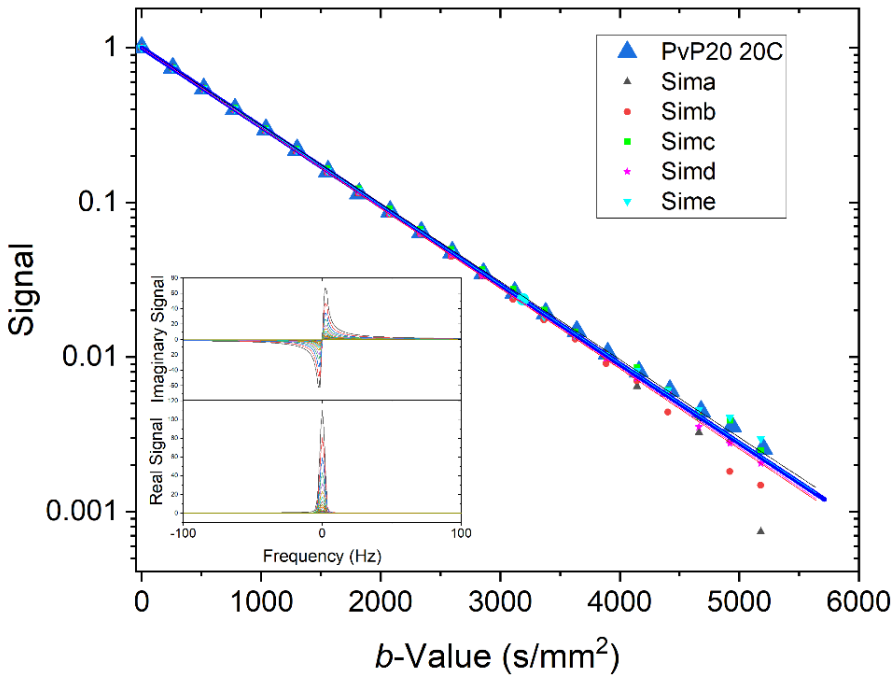

Fig. 35. Signal versus *b*-values for a 20 % PVP solution at 3 T, 20 °C including data and simulated data along with diffusion fits. The inset shows a set of simulated spectra from which the simulated signal is calculated.

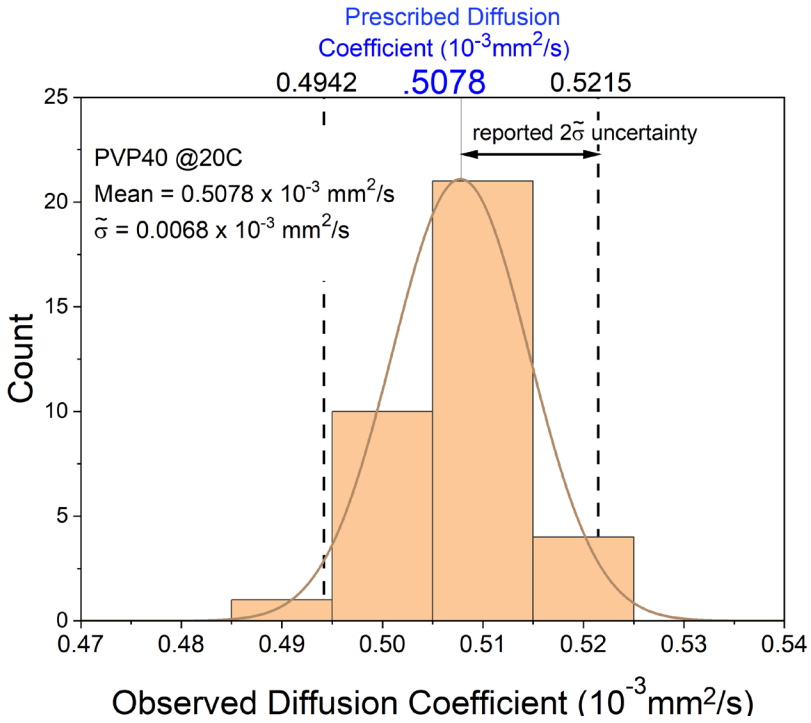

Fig. 36. Water diffusion coefficient distribution from Monte Carlo calculations varying all parameters for N = 36 trials. The input material parameters are for a 40 % PVP solution in water at 20 °C. The reported expanded uncertainty is $2\tilde{\sigma} = 0.014 \times 10^{-3} \frac{\mathrm{mm}^2}{\mathrm{s}}$.

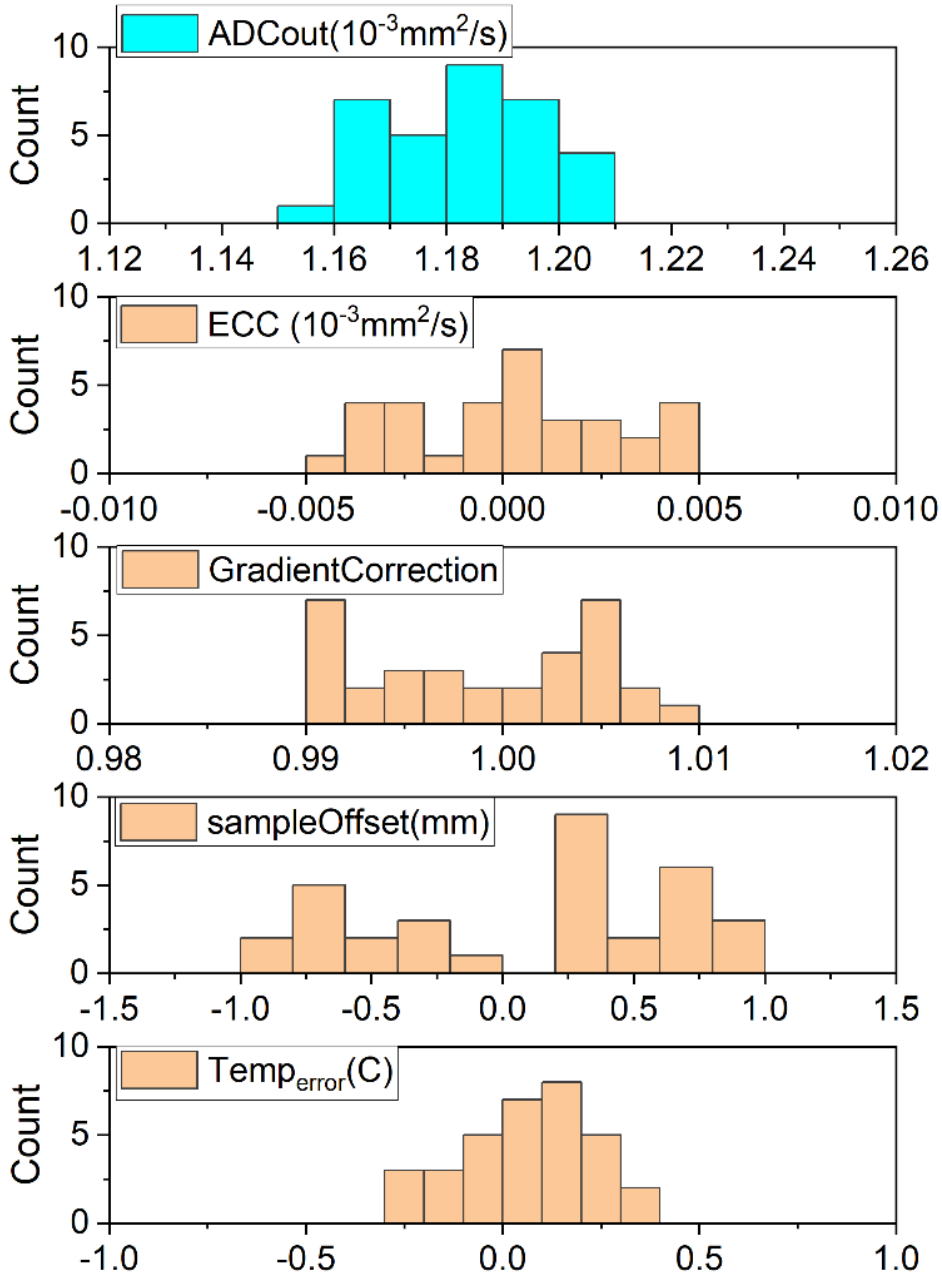

Fig. 37. Empirical distributions from a Monte Carlo simulation of a 20 % PVP sample at 20 °C, 3 T. Distribution of important input values are shown in orange, while the output distribution for the diffusion coefficient is shown in cyan.

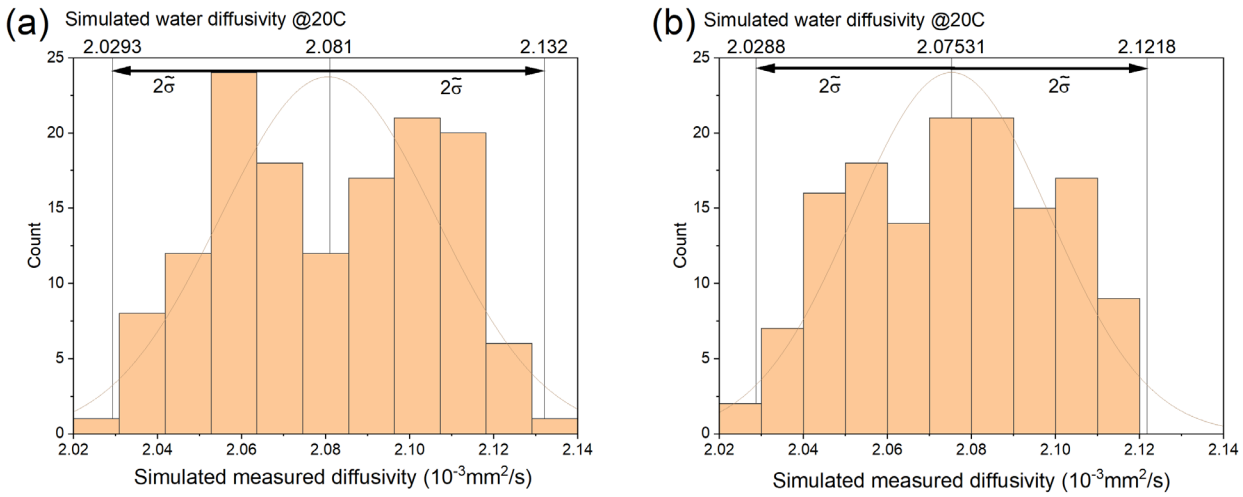

Fig. 38. Two sets of simulated measurements of diffusivity on the identical sample of pure water at 20 °C with coverage intervals determined using $U = 2\tilde{\sigma}$, where $\tilde{\sigma}$ is the calculated standard deviation of each distribution.

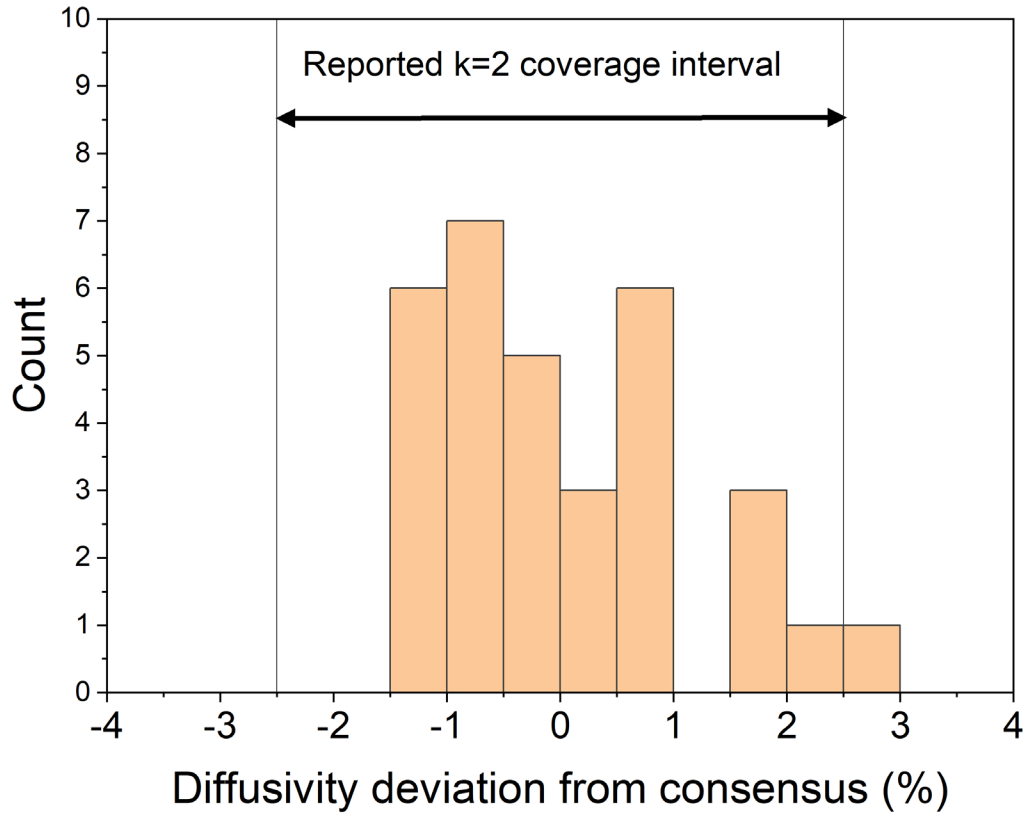

Fig. 39. Deviation in diffusivity of water calibrants from literature consensus values. Also shown is the reported k = 2 coverage interval determined by Monte Carlo simulation.

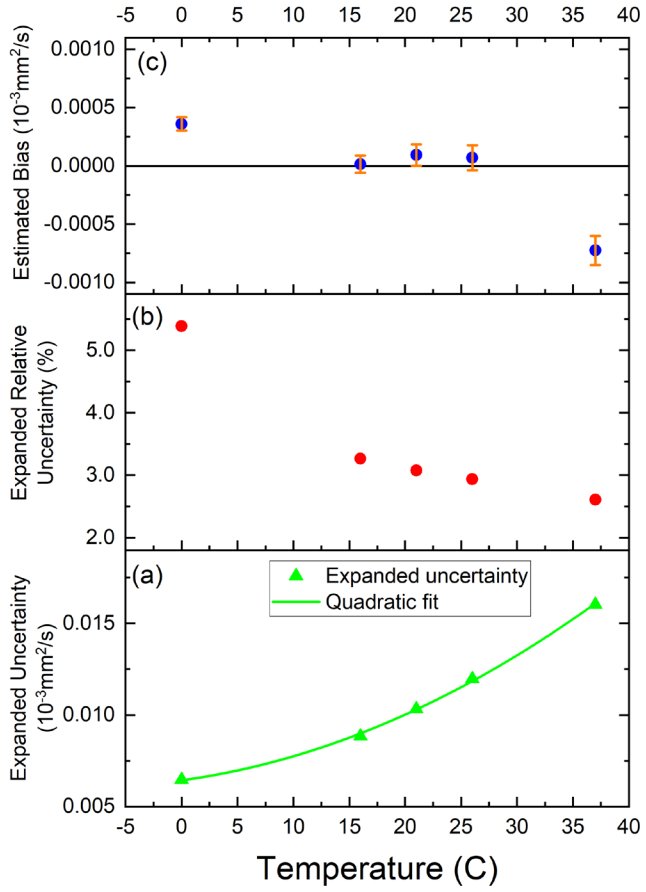

Fig. 40. The combined expanded $U = 2\tilde{\sigma}$ uncertainty (a), combined expanded relative uncertainty(b), and estimated bias in diffusivity (c) for a water sample with 50 % by weight PVP at various temperatures. Each point represents 56 to 64 trials. The green line is a quadratic fit to the uncertainty and is used to generate uncertainties for a series of temperature dependent measurements. The estimated bias is quite small compared to the reported expanded uncertainty and is ignored for this particular set of measurements. The half-width of each error bar in (c) corresponds to the component of uncertainty due to finite sampling effects.

8. Quality Control

NIST's measurement services make use of quality assurance practices to ensure the validity of measurement results and their uncertainties. Such practices include:

- Repeated measurements/calibrations compared over many time intervals.
- Comparison of previous results obtained using multiple measurement methods, if available.
- Routine, periodic measurements with different methods.

For this service, we assess the reproducibility of the NMR measurements prior to each measurement series using pure water and comparing the measured diffusion coefficient with both NIST and literature values. We calibrate the fiber optic temperature before each

measurement series at 0 °C (ice-point) and with traceable platinum resistance thermometers at several temperatures. The quality control plan for NMR measurements, software version control, and data storage are documented in MRI Biomarker Calibration Service Quality Manual III.

A set of quality control tests are done during data analysis (see Appendix A). These include:

1. The recovery times for all experiments are greater than $5T_1$.
2. The lack of fit test yields p-value > 0.003 or the standard deviation of the residuals from the normalized signal is $\sigma_{res} < 0.003$.
3. The inhomogeneous line width (FWHM) after shimming is less than 10.4 Hz.
4. The inversion efficiency in the T_1 inversion recovery fit, which is a measure of RF homogeneity, must be greater than 0.97 for this short sample.

If any of these conditions are not satisfied, the problem will be corrected, and the measurement repeated.

Historic data from previous measurements of the NMR apparatus shall be placed into the test folder by the Measurement Services Coordinator after the preparation of the calibration report. The Calibration Leader and the Group Leader shall review the data before signing the calibration reports. If a significant variance from previous results is noted, the Group Leader may require another measurement of the calibration item as a test of measurement system conformance.

9. Summary

NIST provides a measurement service to determine the water diffusion coefficient of solutions used in phantoms (calibration artifacts) at a specified field strength and temperature. In this document, we have summarized the basic measurement equations, the measurement procedure, and described the quantities that contribute to the standard uncertainty.

10. Acknowledgements

We wish to thank from the Yuxi Pang, Dariya Malyarenko, Thomas Chenevert from the University of Michigan, and Prof. William Price from Western Sydney University for critical reading of the manuscript and providing their expertise on magnetic-resonance-based diffusion measurements.

References

1. Kessler LG, Barnhart HX, Buckler AJ, Choudhury KR, Kondratovich MV, Toledano A, Guimaraes AR, Filice R, Zhang Z, Sullivan DC, Group QTW. The emerging science of quantitative imaging biomarkers terminology and definitions for scientific studies and regulatory submissions. Statistical methods in medical research. 2015;24(1):9-26. Epub 2014/06/13. doi: https://doi.org/10.1177/0962280214537333. PubMed PMID: 24919826.
2. Boss MA, Dienstfrey AM, Gimbutas Z, Keenan KE, Splett JD, Stupic KF, Russek SE. Magnetic Resonance Imaging Biomarker Calibration Service: Proton Spin Relaxation Times2018;Special Publication (NIST SP) - 250-97.
3. Torrey HC. Bloch Equations with Diffusion Terms. Physical Review. 1956;104(3):563-5. doi: https://doi.org/10.1103/PhysRev.104.563.
4. Tiesinga E, Mohr PJ, Newell DB, Taylor BN. CODATA recommended values of the fundamental physical constants: 2018. Reviews of Modern Physics. 2021;93(2). doi: https://doi.org/10.1103/RevModPhys.93.025010.
5. Callaghan PT, Le Gros MA, Pinder DN. The measurement of diffusion using deuterium pulsed field gradient nuclear magnetic resonance. The Journal of Chemical Physics. 1983;79(12):6372-81. doi: https://doi.org/10.1063/1.445745.
6. Holz M, Weingartner H. Calibration in accurate spin-echo self-diffusion measurements using 1H and less-common nuclei. Journal of Magnetic Resonance (1969). 1991;92(1):115-25. doi: https://doi.org/10.1016/0022-2364(91)90252-O.
7. Price WS. Pulsed-field gradient nuclear magnetic resonance as a tool for studying translational diffusion: Part 1. Basic theory. Concepts in Magnetic Resonance. 1997;9(5):299-336. doi: https://doi.org/10.1002/(SICI)1099-0534(1997)9:5<299::AID-CMR2>3.0.CO;2-U.
8. Price WS. Pulsed-field gradient nuclear magnetic resonance as a tool for studying translational diffusion: Part II. Experimental aspects. Concepts in Magnetic Resonance. 1998;10(4):197-237. doi: https://doi.org/10.1002/(Sici)1099-0534(1998)10:4<197::Aid-Cmr1>3.0.Co;2-S. PubMed PMID: WOS:000074178400001.
9. Holz M, Heil SR, Sacco A. Temperature-dependent self-diffusion coefficients of water and six selected molecular liquids for calibration in accurate 1H NMR PFG measurements. Physical Chemistry Chemical Physics. 2000;2(20):4740-2. doi: https://doi.org/10.1039/b005319h.
10. Price WS. NMR Studies of Translational Motion: Principles and Applications. Cambridge: Cambridge University Press; 2009.
11. Kuperman V. Magnetic Resonance Imaging: Physical Principles and Applications: Elsevier Science; 2000.
12. Stejskal EO, Tanner JE. Spin Diffusion Measurements: Spin Echoes in the Presence of a Time-Dependent Field Gradient. The Journal of Chemical Physics. 1965;42(1):288-92. doi: https://doi.org/10.1063/1.1695690.
13. Mattiello J, Basser PJ, Lebihan D. Analytical Expressions for the b Matrix in NMR Diffusion Imaging and Spectroscopy. Journal of Magnetic Resonance, Series A. 1994;108(2):131-41. doi: https://doi.org/10.1006/jmra.1994.1103.
14. Sinnaeve D. The Stejskal-Tanner equation generalized for any gradient shape-an overview of most pulse sequences measuring free diffusion. Concepts in Magnetic Resonance Part A. 2012;40A(2):39-65. doi: https://doi.org/10.1002/cmr.a.21223.
15. Berger S, Braun S. 200 and more NMR experiments : a practical course. 3rd rev. and expanded ed. Weinheim: Wiley-VCH; 2004. xv, 838 p. p.

16. Malyarenko DI, Swanson SD, Konar AS, LoCastro E, Paudyal R, Liu MZ, Jambawalikar SR, Schwartz LH, Shukla-Dave A, Chenevert TL. Multicenter Repeatability Study of a Novel Quantitative Diffusion Kurtosis Imaging Phantom. Tomography. 2019;5(1):36-43. Epub 2019/03/12. doi: https://doi.org/10.18383/j.tom.2018.00030. PubMed PMID: 30854440; PMCID: PMC6403043.
17. BIPM. Evaluation of measurement data – Supplement 1 to the "Guide to the expression of uncertainty in measurement" – Propagation of distributions using a Monte Carlo method. Joint Committee for Guides in Metrology. 2008;101.
18. Taylor BN, Kuyatt CE. Guidelines for Evaluating and Expressing the Uncertainty of NIST Measurement Results. NIST Technical Note 12971994.
19. Price WS, Stilbs P, Jönsson B, Söderman O. Macroscopic Background Gradient and Radiation Damping Effects on High-Field PGSE NMR Diffusion Measurements. Journal of Magnetic Resonance. 2001;150(1):49-56. doi: https://doi.org/10.1006/jmre.2001.2316.
20. Chung K-C, Yu H-Y, Ahn S-D. Convection Effects on PGSE-NMR Self-Diffusion Measurements at Low Temperature: Investigation into Sources of Induced Convective Flows. Bulletin of the Korean Chemical Society. 2011;32(6):1970-4. doi: https://doi.org/10.5012/bkcs.2011.32.6.1970.
21. Swan I, Reid M, Howe PW, Connell MA, Nilsson M, Moore MA, Morris GA. Sample convection in liquid-state NMR: why it is always with us, and what we can do about it. J Magn Reson. 2015;252:120-9. Epub 2015/02/15. doi: https://doi.org/10.1016/j.jmr.2014.12.006. PubMed PMID: 25681799.

Appendix A. Lack of Fit Tests

An *F*-statistic is calculated from a ratio of the sum-of-squares due to lack of fit (SSLF) to the sum-of-squares due to pure error (SSPE). Several identical measurements are required, typically the minimum n = 3 is used. The deviation from the model fit summed over n measurements and M *b*-values, SSLF, is compared to the deviation seen between the identical measurements, SSPE. Two input matrices, of dimension (M,n), are required, the measured signal , S_{ij}, and the values predicted by the model, $\hat{S}_{ij}$. For the predicted values we use the fit to the entire set of measured data, hence $\hat{S}_{ij}$ is independent of j.

The sums of squares are computed as:

$$\mathrm{SSLF} = \sum_{i=1}^{M}\sum_{j=1}^{n_i}\left(\bar{S}_i - \hat{S}_{ij}\right)^2 \qquad \text{(A1.1)}$$

$$\mathrm{SSPE} = \sum_{i=1}^{M}\sum_{j=1}^{n_i}\left(S_{ij} - \bar{S}_i\right)^2$$

where $\bar{S}_i$ is the average response for the i^{th} *b*-value and the j subscript indicates the j^{th} repeat measurement.

The *F*-statistic is calculated as:

$$\mathrm{Fstat} = \frac{\mathrm{SSLF}/(M-d)}{\mathrm{SSPE}/(N-M)}, \qquad \text{(A1.2)}$$

where N = n*M is total number of data points, M = number of distinct b-values (typically 20), d = number of parameters to be estimated (d = 2 for Gaussian diffusivity). The p-value, which ranges from 0 to 1,

corresponds to the upper tail of the F distribution: p-value =1- $F.cdf$(F-statistic, M-d, N-M), where $F.cdf$ is the F-cumulative distribution[h] calculated using the Python SciPy library scipy.stats.

If the p-value associated with the test statistic is smaller than the significance level, α, then we reject the null hypothesis and conclude that the assumed model is not reasonable. The significance level is a pre-selected small number, and we adopt $\alpha = 0.001$. If the p-value is greater than α, then we conclude that there is insufficient evidence to claim that the assumed model is not reasonable, and the model data is accepted. A second test, comparison of the standard deviation of the residuals, σ_r, is performed, If $\sigma_r < 0.003$, which indicates that the average deviation of the normalized measured data from the model is less than 0.3 %, the model data is accepted even if p-value < α. In summary, a diffusivity derived from a mono-exponential model is reported if p-value > α or $\sigma_r < 0.003$

If the mono-exponential model is rejected, then a bi-exponential model will be used. If the p-value > α or $\sigma_r < 0.003$ the bi-exponential diffusion coefficients will be reported. If neither model is accepted, no diffusion constants will be reported, although raw data and best fits will be given.

Figs. A1, A2 show examples where the mono-exponential model data is accepted and rejected, respectively. For the data in Fig. A2, we would report bi-exponential diffusivity values since these fits satisfy (p-value > α or $\sigma_r < 0.003$).

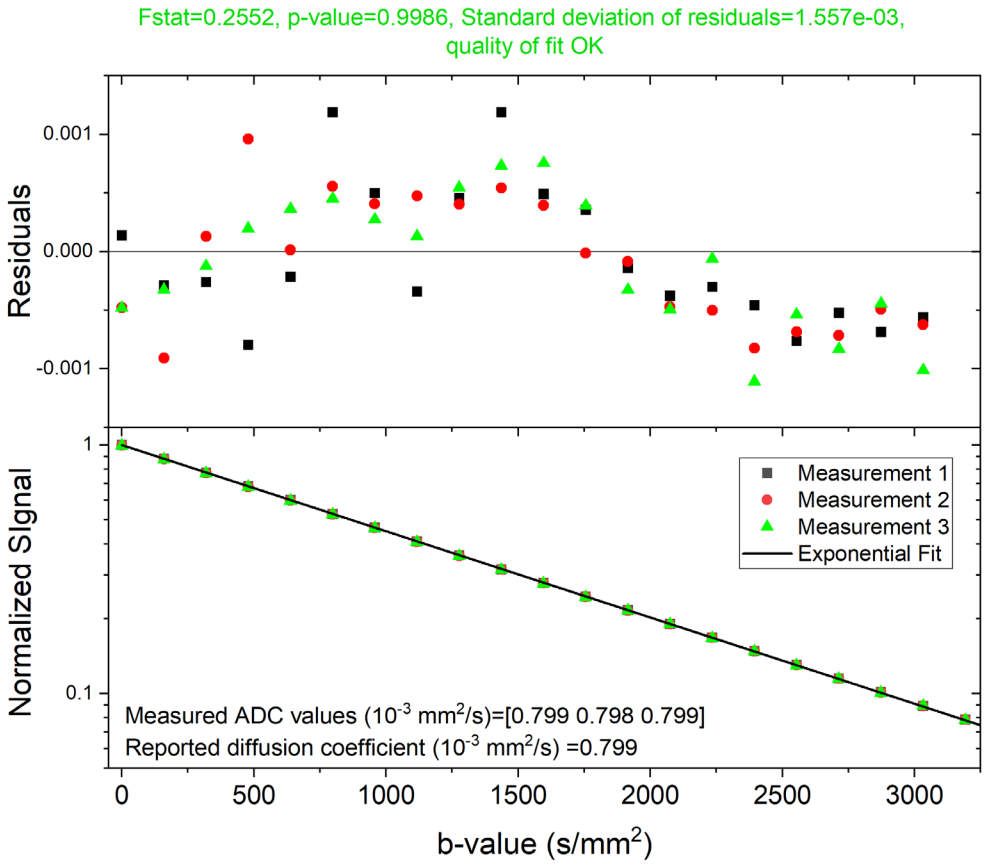

Fig. A1. Accepted diffusivity measurement satifying p-value and residual standard deviation tests. The text at the top of the figure, in green, is the acceptance message given by the analysis software for the mono-exponential fit.

[h] https://www.itl.nist.gov/div898/handbook/eda/section3/eda3665.htm

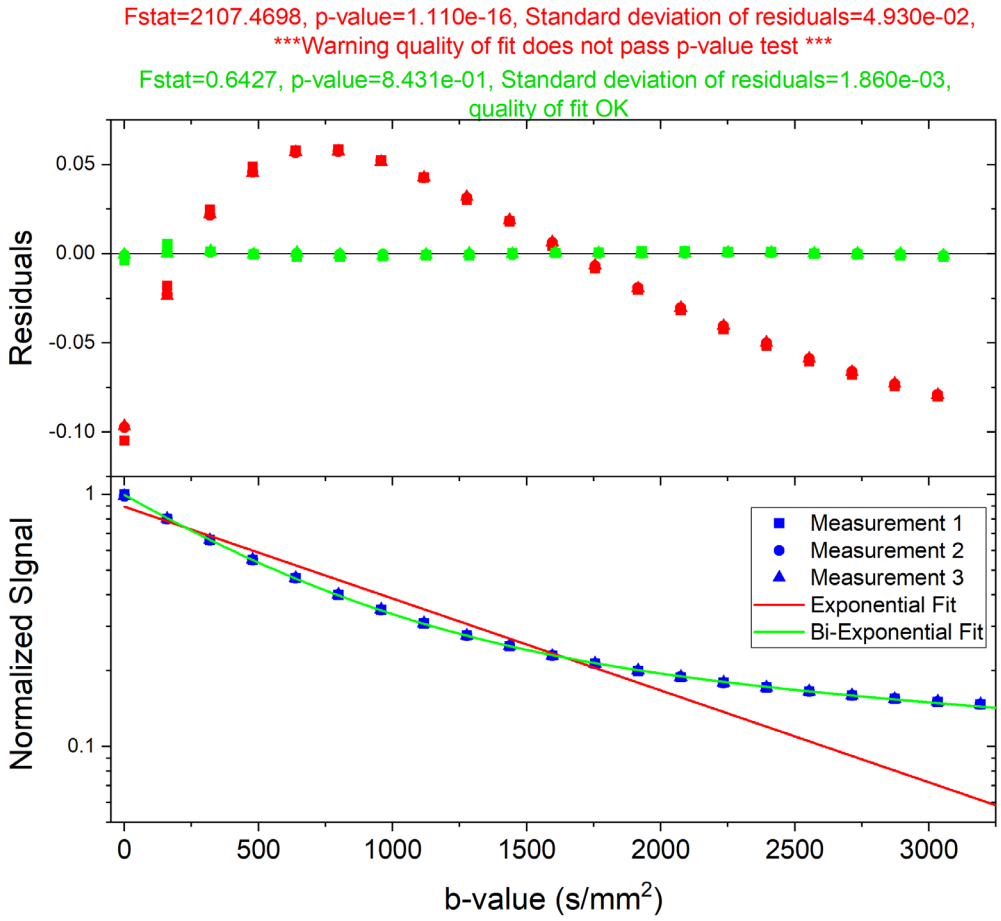

Fig. A2. Diffusivity measurement which cannot be well fit with a single exponential model but can be well fit with a bi-exponential model. The text at the top of the figure, in red and green, are the warning and acceptance messages given by the analysis software for the mono and bi-exponential fits, respectively.

Appendix B. Computer Generate Analysis Report

NIST National Institute of Standards and Technology U.S. Department of Commerce

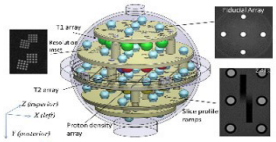

MRI BioMarker Measurement Service
NIST, 325 Broadway, Boulder CO, 80027

https://www.nist.gov/programs-projects/magnetic-resonance-imaging-mri-biomarker-measurement-service

NIST MRI Biomarker Calibration Service: software pyNMRms V4-12-2022; Date of analysis: 2022-04-12 11:12 **Python=**3.6.0 |Anaconda 4.3.1 (64-bit)| (default, Dec 23 2016, 11:57:41) [MSC v.1900 64 bit (AMD64)]; **PyQt=**5.6**Using gyromagnetic ratio =** 2.675153 10^8 rad/s/T,42.576385 MHz/s/T

********Diffusion Processing********

Input Gradient Current Traces: X-direction

Input current traces: //68608nmr/data/BreastPhantomCal/PVP25_07-20-2021/PVP25p_20C/DifSetup/GxCal_tflip=10.6ms_DACmax=50_20C/GxCal_tflip=10.6ms_DACmax=50_20C_01.csv

Gradient monitor(A/V)=2.50, Gcal(mT/m/A)=49.05I(A), ave Gradient(mT/m), q/2□(1/mm), b(s/mm^2)Flipping q after 10.6ms -3.535 -173.38 -76.34 5513.30

-3.182 -156.09 -68.72 4468.24
-2.828 -138.72 -61.07 3529.60
-2.474 -121.36 -53.42 2701.73
-2.121 -104.05 -45.81 1984.86
-1.769 -86.75 -38.20 1380.68
-1.414 -69.37 -30.54 881.92
-1.061 -52.03 -22.89 496.20
-0.711 -34.89 -15.27 220.52
-0.369 -18.11 -7.65 55.28
0.363 17.82 7.61 54.71
0.711 34.88 15.28 220.51
1.061 52.06 22.91 496.02
1.414 69.34 30.52 881.72
1.767 86.65 38.15 1376.25
2.122 104.06 45.83 1985.59
2.475 121.38 53.45 2701.60
2.827 138.68 61.06 3525.46
3.181 156.01 68.69 4463.30
3.534 173.34 76.33 5508.35
Reset Gx Imax=7.068A

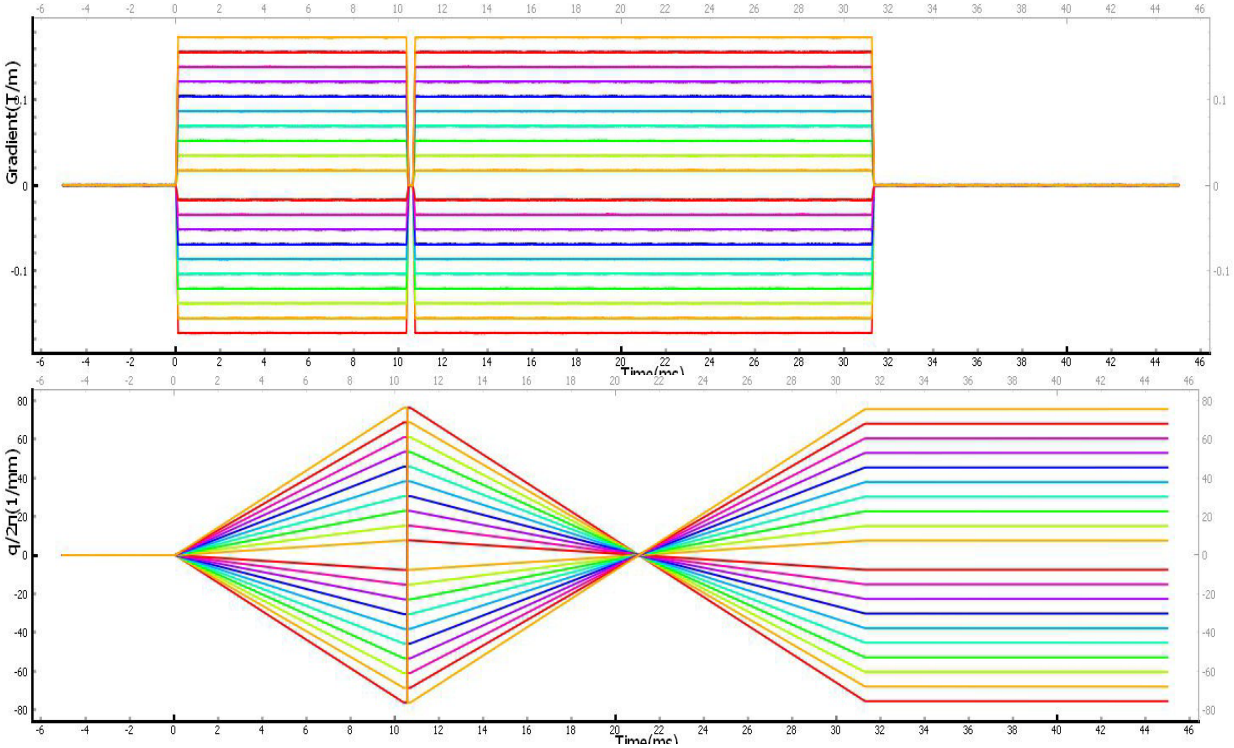

Calculate Image Widths: X-direction

Open 1D Image for Gradient Calibration X-direction

****

File= DifSetup\5_1DImage_PGSE_GxCal_20C_20210723_183446.tntData type= Diffusion
Field(T)=3.006715, **Obs. Frequency(MHz)**=128.015044, **Temperature(C)=**20
Data Acquisition time (UTC): start= 2021-07-23T23:14:32, finish= 2021-07-24T00:34:46
Data shape: Number of data points=2048, parameters=20, repeats=1
T90(μs)= 14.00; **T180(μs)**= 28.00; **tau(ms)**= 0.00
GrAmp= 50.00 : Igr=Imax*GrAmp*GrDAC/1E4
CPMG loop table: [8. 16. 24. 32. 40. 48. 56. 64. 72. 80. 88. 96. 104. 112. 120. 128. 136. 144. 152. 160.]
PGSE grad amplitude table: [-100. -90. -80. -70. -60. -50. -40. -30. -20. -10. 10. 20. 30. 40. 50. 60. 70. 80. 90. 100.],
PGSE gradient pulse type: trap
gradient strength (mT/m)=[-173.33676708 -156.00309038 -138.66941367 -121.33573696 -104.00206025 -86.66838354 -69.33470683 -52.00103013 -34.66735342 -17.33367671 17.33367671 34.66735342 52.00103013 69.33470683 86.66838354 104.00206025 121.33573696 138.66941367 156.00309038 173.33676708]
b-values (s/mm^2)= [10000., 8100., 6400., 4900., 3600., 2500., 1600., 900., 400., 100., 100., 400., 900., 1600., 2500., 3600., 4900., 6400., 8100., 10000.]
Dwell time(s)=1e-05, **Recovery time(s)=**7.52048
Subtract background;[330.77 +375.56j, -1.01 +225.15j, 360.93 +926.69j, -64.65 -841.07j, 8.90+1030.3j , -11.31 +898.4j , -384.21 -19.j , -121.87 +265.08j, 303.45 +75.07j, 2082.66-3609.72j,-1205.14+2984.56j, 29.05 -411.5j , -407.97 +115.32j, 314.27 -402.48j, 475.06 -267.86j, -787.81 +126.92j, -87.69 -281.66j, 238.15 +912.29j, -244.16 -84.31j, 651.49 +490.95j]
Cell diameter: X-direction d(mm)=3.000
Igrad(A), Smax, f0(Hz), df(Hz), bg, G(mT/m), Gerr(mT/m), ferr (Hz), DAC
-3.535 1.7e+07 2483.0 21968.3 403108.0 -171.99 0.09 5.64 -250000

-3.182 2.5e+07 2270.5 19823.8 415764.1 -155.20 0.08 5.00 -225000
-2.828 3.6e+07 2027.7 17578.8 420194.1 -137.63 0.06 3.86 -200000
-2.474 5.3e+07 1790.2 15404.1 425926.6 -120.60 0.04 2.29 -175000
-2.121 7.5e+07 1556.5 13213.3 419262.8 -103.45 0.03 2.19 -150000
-1.769 1.1e+08 1318.7 11042.8 406609.1 -86.45 0.02 1.14 -125000
-1.414 1.6e+08 1048.2 8779.0 453223.5 -68.73 0.02 1.55 -100000
-1.061 2.3e+08 792.1 6570.4 470328.6 -51.44 0.02 0.96 -75000
-0.711 3.8e+08 534.9 4370.1 504953.7 -34.21 0.02 1.15 -50000
-0.369 8.0e+08 292.0 2186.7 508469.6 -17.12 0.01 0.45 -25000
0.363 8.0e+08 -206.7 2176.9 525937.7 17.04 0.01 0.35 25000
0.711 3.8e+08 -466.9 4366.2 460900.8 34.18 0.01 0.61 50000
1.061 2.3e+08 -726.0 6571.1 434099.8 51.45 0.02 1.02 75000
1.414 1.6e+08 -968.5 8744.5 433783.4 68.46 0.03 1.69 100000
1.767 1.1e+08 -1227.6 10951.2 426937.2 85.74 0.02 1.19 125000
2.122 7.6e+07 -1476.0 13112.5 420019.6 102.66 0.03 1.87 150000
2.475 5.3e+07 -1749.8 15361.4 402897.8 120.27 0.04 2.59 175000
2.827 3.7e+07 -2004.7 17583.5 401508.1 137.66 0.06 3.53 200000
3.181 2.5e+07 -2236.4 19708.3 405063.3 154.30 0.05 3.45 225000
3.534 1.7e+07 -2471.4 21881.9 405937.8 171.31 0.11 6.80 250000
Set: gradient direction=X, Gcal(mT/m/A)= 48.606, Imax(A)= 7.069

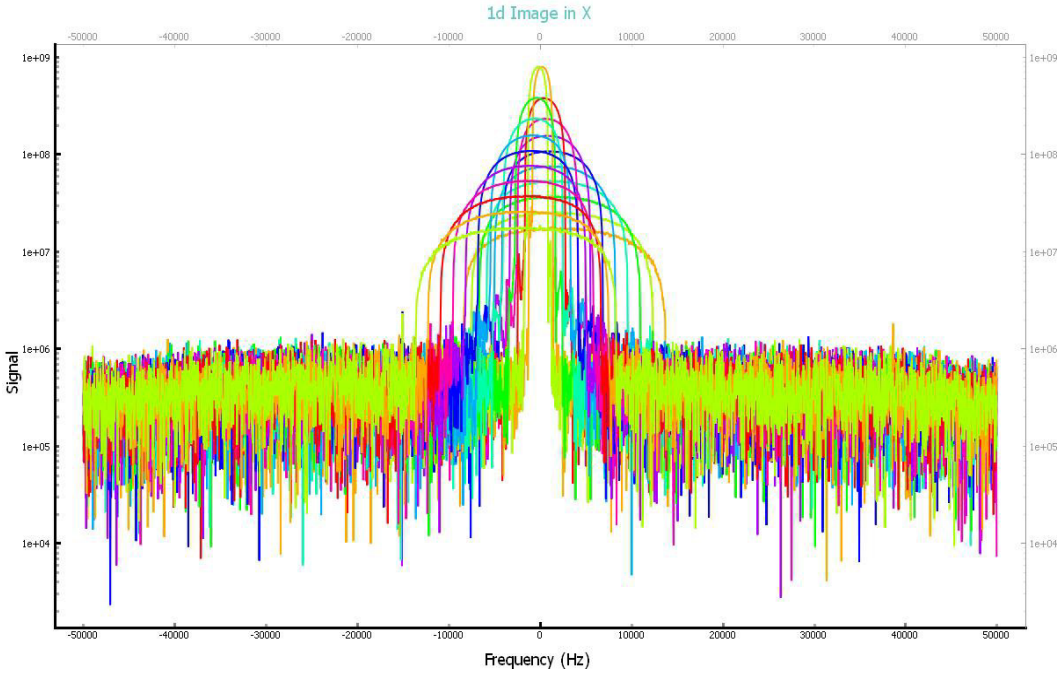

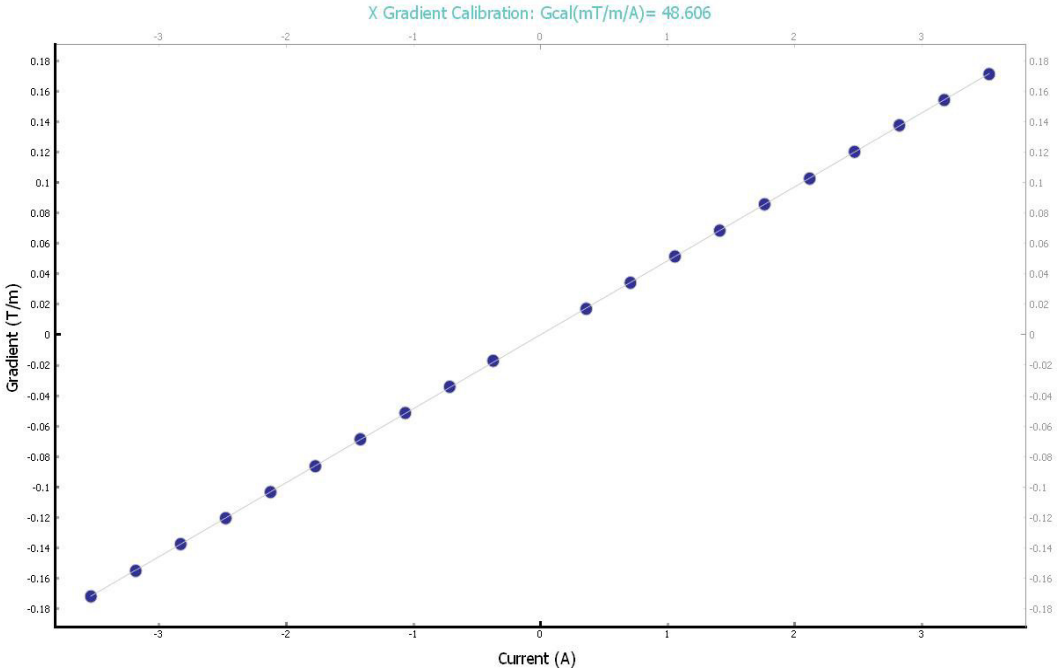

Open Eddy Current Correction PGSE File, Gradient direction= X

****

File= EddyTests\eddytest_PGSE_trap_Gx_delta=14ms_grad=7ms_rd=1ms_GrAmp=100_20210723_164854.tntData type= Diffusion
Field(T)=3.006715, **Obs. Frequency(MHz)=**128.015044, **Temperature(C)**=20
Data Acquisition time (UTC): start= 2021-07-23T22:23:22, finish= 2021-07-23T22:48:54
Data shape: Number of data points=4096, parameters=21, repeats=1
T90(μs)= 14.00; **T180(μs)=** 28.00; **tau(ms)=** 0.00
GrAmp= 100.00 : Igr=Imax*GrAmp*GrDAC/1E4
CPMG loop table: [8. 16. 24. 32. 40. 48. 56. 64. 72. 80. 88. 96. 104. 112. 120. 128. 136. 144. 152. 160.]
PGSE grad amplitude table: [0. 13.41641 18.97367 23.2379 26.83282 30. 32.86335 35.49648 37.94733 40.24922 42.42641 44.49719 46.4758 48.37355 50.1996 51.96152 53.66563 55.31727 56.921 58.48077 60.], **PGSE gradient pulse type:** trap
gradient strength (mT/m)=[0. 46.0993246 65.19429357 79.84635943 92.1986492 103.08120712 112.91979293 121.96733356 130.38855278 138.29793944 145.77885189 152.89413529 159.69271886 166.21346422 172.4878455 178.54187351 184.39726404 190.07236554 195.58284635 200.94227883 206.16241424]
b-Value calculated using ST formula: trap pulse, risetime(ms)=0.1000, duration(ms)=7.2000, pulsespacing(ms)35.3470
qmax (1/mm)= 397.092
b-values (s/mm^2)= [0. , 252.85, 505.69, 758.54, 1011.38, 1264.23, 1517.07, 1769.92, 2022.76, 2275.61, 2528.45, 2781.3 , 3034.14, 3286.99, 3539.83, 3792.68, 4045.53, 4298.37, 4551.22, 4804.06, 5056.91]
Dwell time(s)=0.001, **Recovery time(s)**=9.096
Subtract background;[4.70+12.83j, 29.52+39.11j, 26.07 +6.19j, 18.02+14.22j, 36.92+34.25j, 14.21-12.15j, -0.89+18.43j, 11.02+19.9j , 12.80+14.14j, 2.64 +6.48j, 5.73+30.47j,-10.74+15.32j, 44.70 -9.3j , 27.21+11.13j,38.10+44.16j, -21.48+41.97j, 18.91+22.87j,-11.05 +6.j , -5.44+13.99j,-15.65+43.03j, 3.51 +5.35j]
Phase angles=[-28.933,-23.227,-17.96 ,-14.541,-11.964,-10.629, -8.757, -6.808, -6.965, -6.801, -6.022, -2.438, 2.187, 1.611, 0.815, 0.287, 1.701, 2.515, 13.718, 1.786, 0.18]
Integration: from spectra=0, peak found at 1857,f0=46.5088Hz, approx FWHM=1.709Hz, Smax=4.014e-08,T2*(ms)=186.25676

Integrate n linewidths, **Integration width (Hz)**=34.17969
Fine phase adjust 0: Phase angles=[-20.933 -15.227 -11.96 -9.541 -7.964 -5.629 -3.757 -2.808 -1.965 -0.801 0.978 1.562 2.187 3.611 3.815 4.287 5.701 6.515 7.718 7.786 8.18]

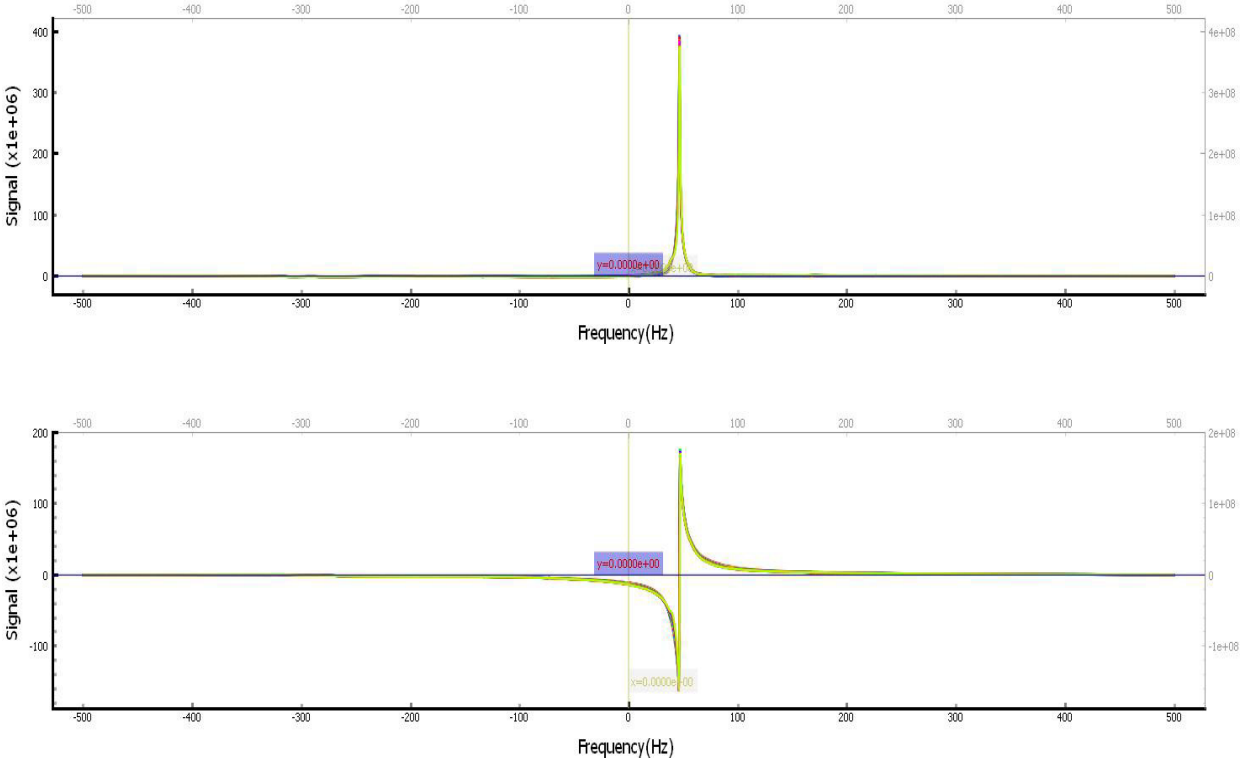

Integrating real part of Diffusion data from 1787 to 1927, from 29.42Hz to 63.60Hz, **Phase adj**(degree)=0.0**Diffusion-PGSE fit repeat=**0: bValue(s)
[[Variables]] ADC: 9.7856e-06 +/- 2.93e-07 (2.99%) (init= 0.0003954987) K: 0 (fixed) Si: 1.00368804 +/- 0.000858 (0.09%) (init= 1) ADC2: 7.909974e-05 (fixed) Si2: 0 (fixed) B: 0 (fixed) [[Correlations]] (unreported correlations are <0.100) C(ADC, Si) = 0.851
Ave of fits, ADC mean and sd (10^-3 mm^2/s)= 0.0098, 0.0000
Diffusion-PGSE fit repeat=all: bValue(s)
[[Variables]] ADC: 9.7856e-06 +/- 2.93e-07 (2.99%) (init= 0.0003954987) K: 0 (fixed) Si: 1.00368804 +/- 0.000858 (0.09%) (init= 1) ADC2: 7.909974e-05 (fixed) Si2: 0 (fixed) B: 0 (fixed) [[Correlations]] (unreported correlations are <0.100) C(ADC, Si) = 0.851
Fitting All, ADCall (10^-3 mm^2/s)=0.010
Fstat=nan, p-value=nan, Standard deviation of residuals=1.9149e-03, *****Warning quality of fit does not passp-value test *****
Measured ADC values (10^-3 mm^2/s)=[0.01]
Reported diffusion coefficient (10^-3 mm^2/s) =0.010
Eddy corrected X-diffusion coefficient(10^-3 mm^2/s) = 0.010, ECC=0.000

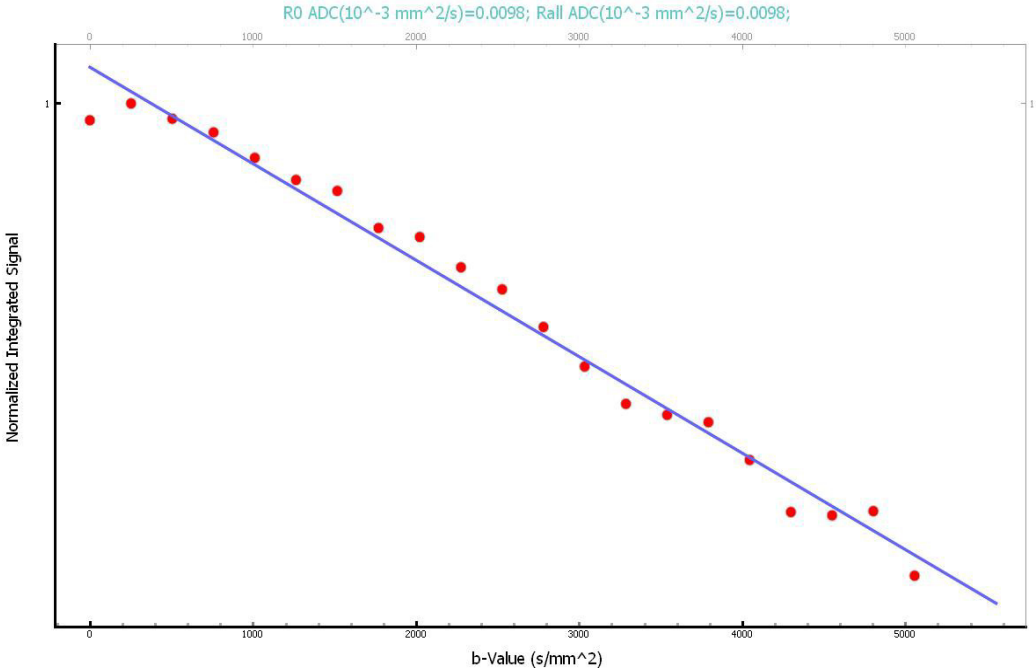

Open Diffusion PGSE File, Gradient direction= X

****

File= DifMeasure\e_PGSE_trap_Gx_delta=14ms_grad=7ms_rd=1ms_GrAmp=100_20210723_155744.tntData type= Diffusion
Field(T)=3.006715**, Obs. Frequency(MHz)**=128.015044, **Temperature(C)**=20
Data Acquisition time (UTC): start= 2021-07-23T21:32:11, finish= 2021-07-23T21:57:44
Data shape: Number of data points=4096, parameters=21, repeats=1
T90(μs)= 14.00; **T180(μs)=** 28.00; **tau(ms)=** 0.00
GrAmp= 100.00 : Igr=Imax*GrAmp*GrDAC/1E4
CPMG loop table: [8. 16. 24. 32. 40. 48. 56. 64. 72. 80. 88. 96. 104. 112. 120. 128. 136. 144. 152. 160.]
PGSE grad amplitude table: [0. 13.41641 18.97367 23.2379 26.83282 30. 32.86335 35.49648 37.94733 40.24922 42.42641 44.49719 46.4758 48.37355 50.1996 51.96152 53.66563 55.31727 56.921 58.48077 60.], **PGSE gradient pulse type:** trap
gradient strength (mT/m)=[0. 46.0993246 65.19429357 79.84635943 92.1986492 103.08120712 112.91979293 121.96733356 130.38855278 138.29793944 145.77885189 152.89413529 159.69271886 166.21346422 172.4878455 178.54187351 184.39726404 190.07236554 195.58284635 200.94227883 206.16241424]
b-Value calculated using ST formula: trap pulse, risetime(ms)=0.1000, duration(ms)=7.2000, pulsespacing(ms)35.3470
qmax (1/mm)= 397.092
b-values (s/mm^2)= [0. , 252.85, 505.69, 758.54, 1011.38, 1264.23, 1517.07, 1769.92, 2022.76, 2275.61, 2528.45, 2781.3 , 3034.14, 3286.99, 3539.83, 3792.68, 4045.53, 4298.37, 4551.22, 4804.06, 5056.91]
Dwell time(s)=0.001, **Recovery time(s)=**9.096
Subtract background;[34.16+13.86j, 26.53+10.1j , 12.77-15.08j, -9.96 -1.38j, 41.50+71.52j, 28.61+25.79j, 38.49+35.99j, 6.53 +8.66j, 22.90+34.81j, 11.97+38.43j, 23.13+21.22j, 16.50+11.07j, 1.79+24.8j , 38.35 +5.22j, 4.25+20.87j, 23.98 -1.8j , 4.37 -2.99j, 15.25+28.67j, 0.94+23.08j, 50.60 +4.59j, 65.44+12.46j]
Phase angles=[100.503, 102.479, 100.533, 99.156, 103.363, 106.126, 106.299, 108.329, 109.646, 112.673, 114.641, 114.308, 114.916, 115.167, 117.907, 117.073, 116.788, 118.141, 94.373, 116.177, 96.688]
Integration: from spectra=0, peak found at 1856,f0=46.7529Hz, approx FWHM=1.465Hz, Smax=3.441e-08,T2*(ms)=217.29955

Integrate n linewidths, **Integration width (Hz)**=29.29688
Fine phase adjust 0: Phase angles=[109.503 107.479 107.533 107.156 108.363 108.126 107.299 107.329 106.646 108.673 107.641 107.308 106.916 107.167 107.907 107.073 106.788 107.141 107.373 106.177 106.688]

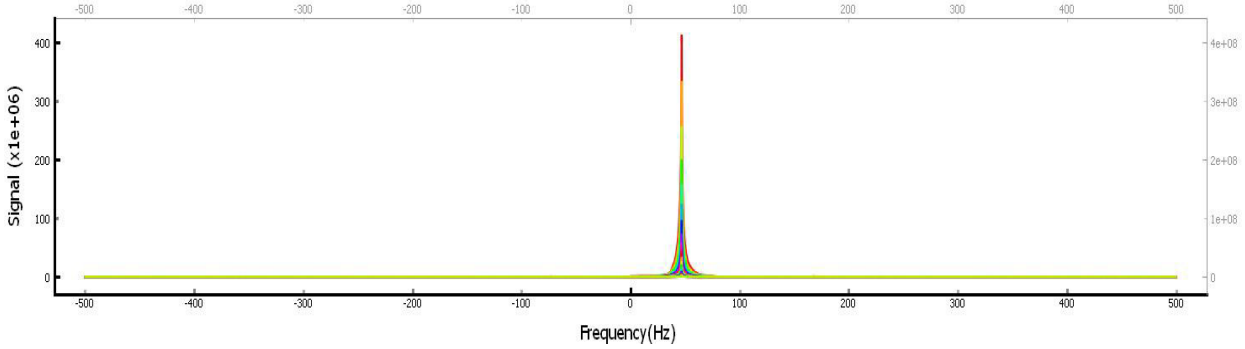

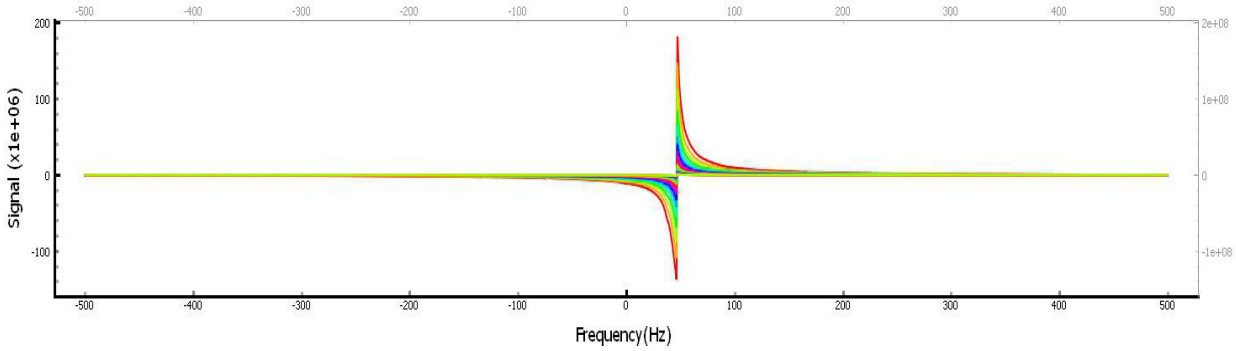

Integrating real part of Diffusion data from 1796 to 1916, from 32.10Hz to 61.40Hz, **Phase adj**(degree)=0.0**Diffusion-PGSE fit repeat=**0: bValue(s)
[[Variables]] ADC: 0.00099561 +/- 2.64e-06 (0.27%) (init= 0.0003954987) K: 0 (fixed) Si: 0.99564626 +/- 0.001654 (0.17%) (init= 1) ADC2: 7.909974e-05 (fixed) Si2: 0 (fixed) B: 0 (fixed) [[Correlations]] (unreported correlations are <0.100) C(ADC, Si) = 0.614
Ave of fits, ADC mean and sd (10^-3 mm^2/s)= 0.9956, 0.0000
Diffusion-PGSE fit repeat=all: bValue(s)
[[Variables]] ADC: 0.00099561 +/- 2.64e-06 (0.27%) (init= 0.0003954987) K: 0 (fixed) Si: 0.99564626 +/- 0.001654 (0.17%) (init= 1) ADC2: 7.909974e-05 (fixed) Si2: 0 (fixed) B: 0 (fixed) [[Correlations]] (unreported correlations are <0.100) C(ADC, Si) = 0.614
Fitting All, ADCall (10^-3 mm^2/s)=0.996
Fstat=nan, p-value=nan, Standard deviation of residuals=1.9683e-03, ***Warning quality of fit does not passp-value test ***
Measured ADC values (10^-3 mm^2/s)=[0.996]
Reported diffusion coefficient (10^-3 mm^2/s) =0.996
Eddy corrected X-diffusion coefficient(10^-3 mm^2/s) = 0.986, ECC=0.010

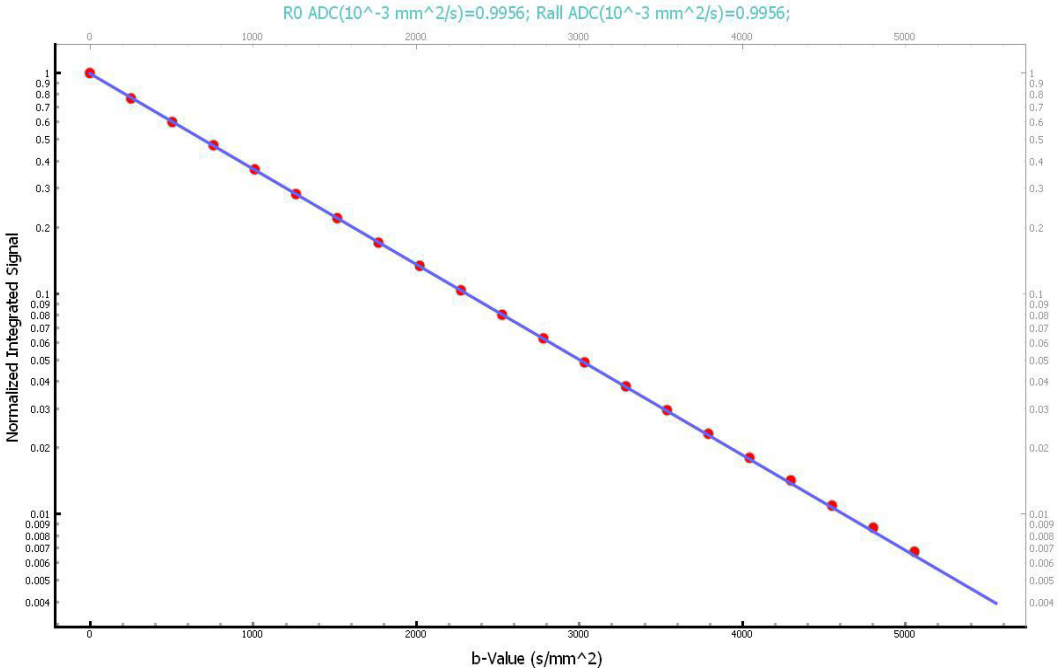

Input Gradient Current Traces: X-direction

Input current traces: //68608nmr/data/BreastPhantomCal/PVP25_07-20-2021/PVP25p_20C/DifSetup/GyCal_tflip=10.6ms_DACmax=50_20C/GyCal_tflip=10.6ms_DACmax=50_20C_01.csv

Gradient monitor(A/V)=2.50, Gcal(mT/m/A)=47.62I(A), ave Gradient(mT/m), q/2□(1/mm), b(s/mm^2)Flipping q after 10.6ms

-3.607 -171.76 -75.71 5387.26
-3.247 -154.62 -68.15 4365.68
-2.887 -137.48 -60.61 3451.09
-2.526 -120.28 -53.03 2642.04
-2.164 -103.05 -45.42 1938.54
-1.804 -85.90 -37.86 1347.81
-1.444 -68.77 -30.32 863.89
-1.083 -51.59 -22.73 485.75
-0.724 -34.49 -15.15 215.82
-0.372 -17.71 -7.55 53.88
0.374 17.81 7.57 53.97
0.726 34.58 15.14 215.62
1.083 51.57 22.72 484.99
1.443 68.73 30.31 862.22
1.805 85.95 37.89 1349.40
2.164 103.04 45.42 1937.80
2.525 120.24 53.00 2639.41
2.887 137.46 60.61 3449.39
3.248 154.63 68.17 4365.68
3.607 171.75 75.71 5385.89

Reset Gy Imax=7.214A

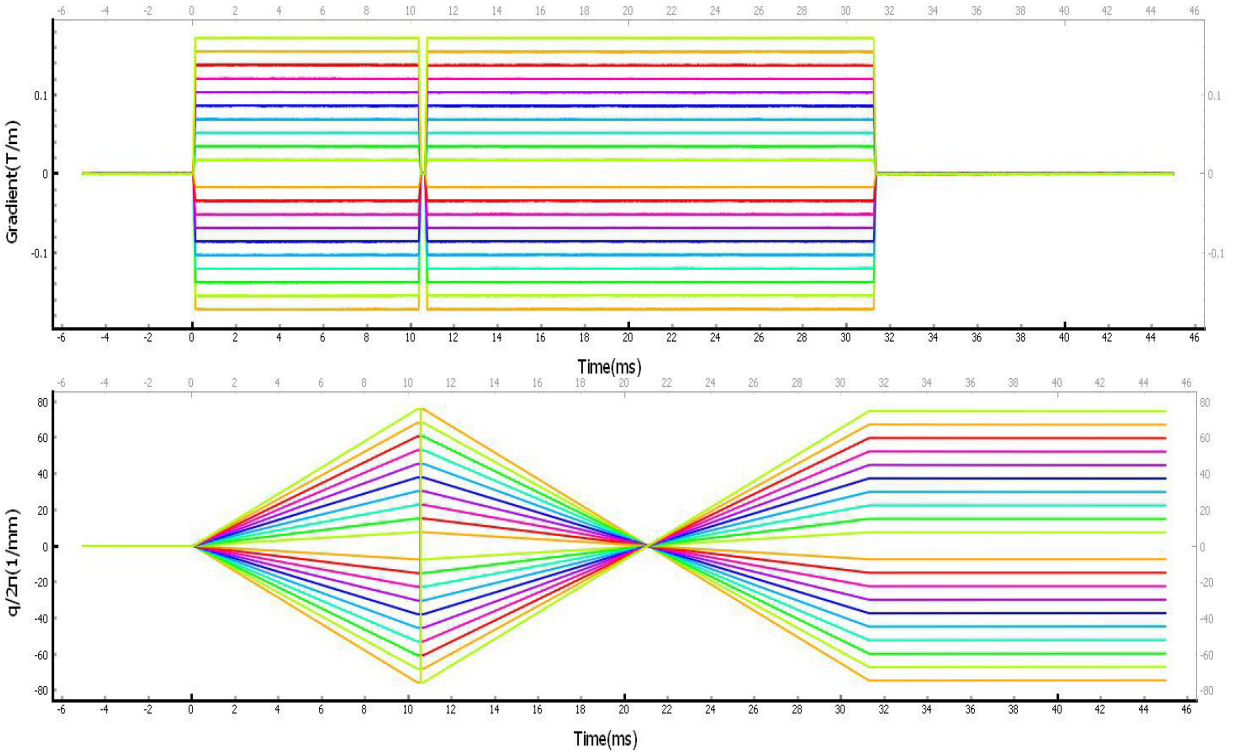

Calculate Image Widths: Y-direction

Open 1D Image for Gradient Calibration Y-direction

****

File= DifSetup\6_1DImage_PGSE_GyCal_20C_20210723_195503.tntData type= Diffusion
Field(T)=3.006715, **Obs. Frequency(MHz)=**128.015044, **Temperature(C)=**20
Data Acquisition time (UTC): start= 2021-07-24T00:34:49, finish= 2021-07-24T01:55:03
Data shape: Number of data points=2048, parameters=20, repeats=1
T90(□s)= 14.00; **T180(□s)**= 28.00; **tau(ms)**= 0.00
GrAmp= 50.00 : Igr=Imax*GrAmp*GrDAC/1E4
CPMG loop table: [8. 16. 24. 32. 40. 48. 56. 64. 72. 80. 88. 96. 104. 112. 120. 128. 136. 144. 152. 160.]
PGSE grad amplitude table: [-100. -90. -80. -70. -60. -50. -40. -30. -20. -10. 10. 20. 30. 40. 50. 60. 70. 80. 90. 100.],
PGSE gradient pulse type: trap
gradient strength (mT/m)=[-171.75282428 -154.57754186 -137.40225943 -120.226977 -103.05169457 -85.87641214 -68.70112971 -51.52584729 -34.35056486 -17.17528243 17.17528243 34.35056486 51.52584729 68.70112971 85.87641214 103.05169457 120.226977 137.40225943 154.57754186 171.75282428]
b-values (s/mm^2)= [10000., 8100., 6400., 4900., 3600., 2500., 1600., 900., 400., 100., 100., 400., 900., 1600., 2500., 3600., 4900., 6400., 8100., 10000.]
Dwell time(s)=1e-05, **Recovery time(s)=**7.52048
Subtract background;[-206.04 +216.14j, -250.16 -486.3j , 547.79 -10.97j, 77.09 +61.41j, -601.61 -42.1j , 922.97 -246.31j, -266.22+1032.15j, 439.26 -531.1j , 17.07 +145.91j, 75.10+2863.25j, 1748.40-1674.34j, 630.47 +832.6j , -491.28 +293.83j, -927.86 +994.5j , -129.42 -665.08j, 307.38 +538.65j, -578.74+1058.19j, -866.80 +447.9j , -359.58 +418.16j, -333.84 +249.17j]
Cell diameter: Y-direction d(mm)=3.000

Igrad(A), Smax, f0(Hz), df(Hz), bg, G(mT/m), Gerr(mT/m), ferr (Hz), DAC
-3.607 1.9e+07 317.7 21786.3 400148.8 -170.57 0.08 5.17 -250000
-3.247 2.7e+07 307.4 19630.7 408786.6 -153.69 0.05 3.51 -225000
-2.887 3.9e+07 282.0 17429.2 405478.7 -136.45 0.04 2.47 -200000
-2.526 5.6e+07 252.1 15252.1 421013.4 -119.41 0.02 1.34 -175000
-2.164 7.8e+07 226.8 13062.1 427477.0 -102.26 0.02 1.31 -150000
-1.804 1.1e+08 195.5 10883.1 444550.7 -85.20 0.02 1.31 -125000
-1.444 1.6e+08 164.1 8709.0 450033.2 -68.18 0.02 1.18 -100000
-1.083 2.4e+08 144.8 6546.9 432622.3 -51.26 0.00 0.32 -75000
-0.724 3.8e+08 104.0 4341.9 480887.3 -33.99 0.01 0.61 -50000
-0.372 8.0e+08 70.9 2175.3 528976.9 -17.03 0.01 0.52 -25000
0.374 8.1e+08 10.8 2164.6 533157.3 16.95 0.01 0.43 25000
0.726 3.8e+08 -24.6 4348.6 446255.3 34.05 0.00 0.16 50000
1.083 2.4e+08 -55.8 6496.3 458203.7 50.86 0.01 0.77 75000
1.443 1.6e+08 -85.5 8671.7 441038.4 67.89 0.01 0.75 100000
1.805 1.1e+08 -120.3 10829.4 771370.3 84.78 0.02 1.48 125000
2.164 7.9e+07 -153.1 13007.3 422923.6 101.83 0.02 1.09 150000
2.525 5.6e+07 -189.9 15173.5 418480.9 118.79 0.03 1.82 175000
2.887 3.9e+07 -223.4 17345.0 414531.0 135.79 0.02 1.54 200000
3.248 2.7e+07 -259.2 19511.6 467625.3 152.76 0.05 3.08 225000
3.607 1.8e+07 -291.4 21550.8 967190.6 168.72 0.21 13.31 250000
Set: gradient direction=Y, Gcal(mT/m/A)= 47.116, Imax(A)= 7.214

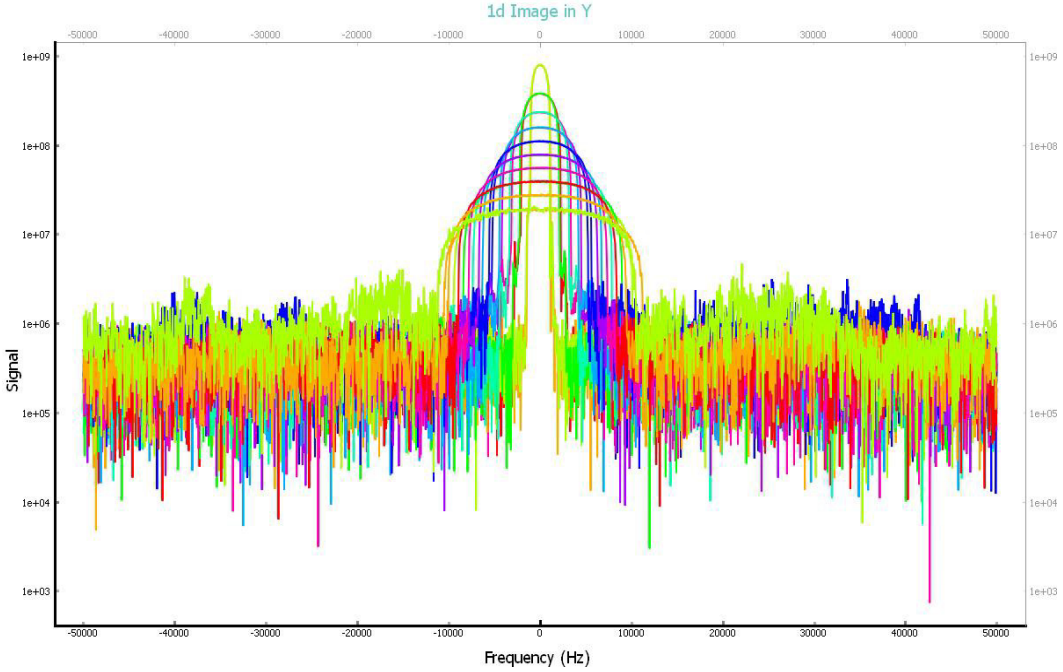

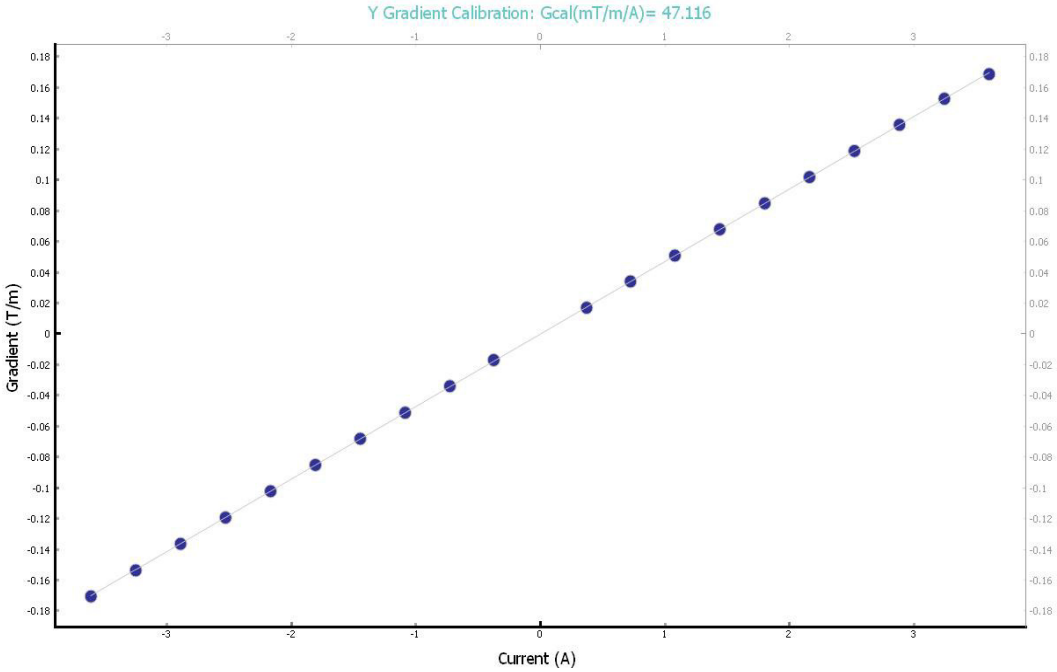

Open Eddy Current Correction PGSE File, Gradient direction= Y

****

File= EddyTests\eddytest_PGSE_trap_Gy_delta=14ms_grad=7ms_rd=1ms_GrAmp=100_20210723_171430.tntData type= Diffusion
Field(T)=3.006715, **Obs. Frequency(MHz)=**128.015044, **Temperature(C)=**20
Data Acquisition time (UTC): start= 2021-07-23T22:48:57, finish= 2021-07-23T23:14:29
Data shape: Number of data points=4096, parameters=21, repeats=1
T90(□s)= 14.00; **T180(□s)**= 28.00; **tau(ms)**= 0.00
GrAmp= 100.00 : Igr=Imax*GrAmp*GrDAC/1E4
CPMG loop table: [8. 16. 24. 32. 40. 48. 56. 64. 72. 80. 88. 96. 104. 112. 120. 128. 136. 144. 152. 160.]
PGSE grad amplitude table: [0. 13.41641 18.97367 23.2379 26.83282 30. 32.86335 35.49648 37.94733 40.24922 42.42641 44.49719 46.4758 48.37355 50.1996 51.96152 53.66563 55.31727 56.921 58.48077 60.], **PGSE gradient pulse type:** trap
gradient strength (mT/m)=[0. 45.6028763 64.49220961 78.98648589 91.20575259 101.97111514 111.70374823 120.65385498 128.98438523 136.8085949 144.20894464 151.24760284 157.97297177 164.42349457 170.63030639 176.61913797 182.4114712 188.02545695 193.47659484 198.77831105 203.94223029]
b-Value calculated using ST formula: trap pulse, risetime(ms)=0.1000, duration(ms)=7.2000, pulsespacing(ms)35.3470
qmax (1/mm)= 392.815
b-values (s/mm^2)= [0. , 247.43, 494.86, 742.29, 989.72, 1237.14, 1484.57, 1732. , 1979.43, 2226.86, 2474.29, 2721.72, 2969.15, 3216.58, 3464. , 3711.43, 3958.86, 4206.29, 4453.72, 4701.15, 4948.58]
Dwell time(s)=0.001, **Recovery time(s)=**9.096
Subtract background;[-0.96-18.93j, 5.33-17.96j, -0.77-18.16j,-18.28+22.68j, -1.90-34.25j, -27.79 -0.31j,-51.30 -3.21j,-16.39-21.11j,-14.92 +1.39j, -7.44-24.52j, 12.17-12.1j ,-44.10-18.19j, 9.44 -2.02j,-33.62 +1.09j, -6.76-12.64j, -29.00-39.23j,-11.41-26.27j, 12.02 -3.15j,-20.59-14.37j, -9.44-31.03j, -24.95-13.52j]
Phase angles=[-8.796, -7.41 , -7.198, -5.399, -6.899, -8.231, -6.651, -4.738, -3.345, -3.846, -2.055, -1.08 , -0.208, 0.978, 0.606, 0.76 , 4.157, 8.798, 11.521, 11.906, 10.492]
Integration: from spectra=0, peak found at 1856,f0=46.7529Hz, approx FWHM=2.197Hz, Smax=5.161e-08,T2*(ms)=144.86637

Integrate n linewidths, **Integration width (Hz)**=43.94531
Fine phase adjust 0: Phase angles=[-3.796 -2.41 -2.198 -1.399 -0.899 -2.231 -1.651 -0.738 -1.345 -0.846 -0.055 -1.08 -0.208 -0.022 -0.394 0.76 1.157 0.798 0.521 0.906 1.492]

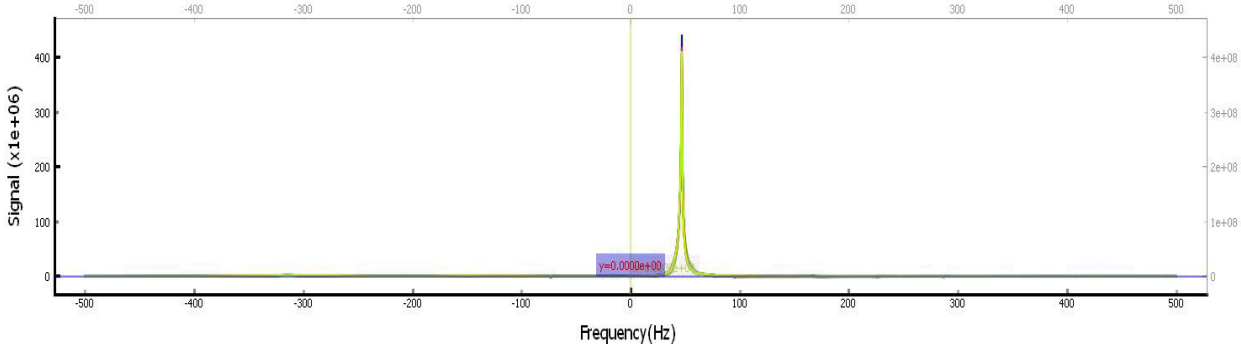

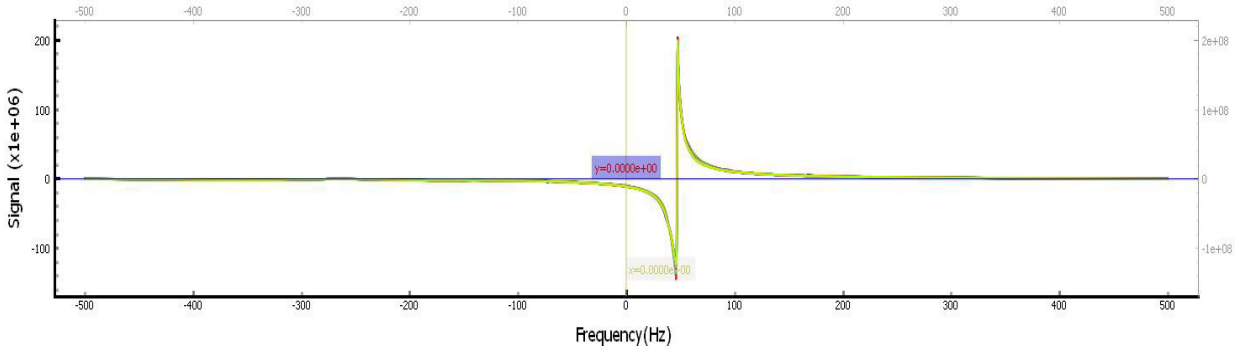

Integrating real part of Diffusion data from 1766 to 1946, from 24.78Hz to 68.73Hz, **Phase adj**(degree)=0.0**Diffusion-PGSE fit repeat=**0: bValue(s)
[[Variables]] ADC: 3.5421e-06 +/- 2.59e-07 (7.30%) (init= 0.0004041566) K: 0 (fixed) Si: 0.99868820 +/- 0.000744 (0.07%) (init= 1) ADC2: 8.083132e-05 (fixed) Si2: 0 (fixed) B: 0 (fixed) [[Correlations]] (unreported correlations are <0.100) C(ADC, Si) = 0.854
Ave of fits, ADC mean and sd (10^-3 mm^2/s)= 0.0035, 0.0000
Diffusion-PGSE fit repeat=all: bValue(s)
[[Variables]] ADC: 3.5421e-06 +/- 2.59e-07 (7.30%) (init= 0.0004041566) K: 0 (fixed) Si: 0.99868820 +/- 0.000744 (0.07%) (init= 1) ADC2: 8.083132e-05 (fixed) Si2: 0 (fixed) B: 0 (fixed) [[Correlations]] (unreported correlations are <0.100) C(ADC, Si) = 0.854
Fitting All, ADCall (10^-3 mm^2/s)=0.004
Fstat=nan, p-value=nan, Standard deviation of residuals=1.6735e-03, *****Warning quality of fit does not passp-value test *****
Measured ADC values (10^-3 mm^2/s)=[0.004]
Reported diffusion coefficient (10^-3 mm^2/s) =0.004
Eddy corrected Y-diffusion coefficient(10^-3 mm^2/s) = -0.006, ECC=0.010

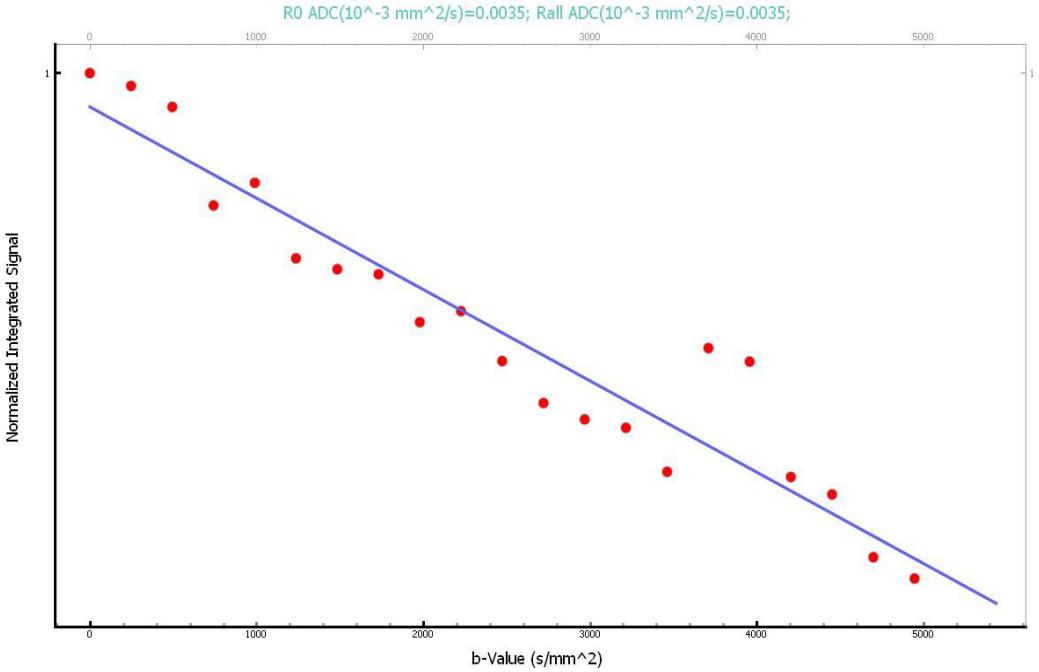

Open Diffusion PGSE File, Gradient direction= Y

****

File= DifMeasure\f_PGSE_trap_Gy_delta=14ms_grad=7ms_rd=1ms_GrAmp=100_20210723_162319.tntData type= Diffusion
Field(T)=3.006715, **Obs. Frequency(MHz)=**128.015044, **Temperature(C)=**20
Data Acquisition time (UTC): start= 2021-07-23T21:57:47, finish= 2021-07-23T22:23:19
Data shape: Number of data points=4096, parameters=21, repeats=1
T90(□s)= 14.00; **T180(□s)**= 28.00; **tau(ms)**= 0.00
GrAmp= 100.00 : Igr=Imax*GrAmp*GrDAC/1E4
CPMG loop table: [8. 16. 24. 32. 40. 48. 56. 64. 72. 80. 88. 96. 104. 112. 120. 128. 136. 144. 152. 160.]
PGSE grad amplitude table: [0. 13.41641 18.97367 23.2379 26.83282 30. 32.86335 35.49648 37.94733 40.24922 42.42641 44.49719 46.4758 48.37355 50.1996 51.96152 53.66563 55.31727 56.921 58.48077 60.], **PGSE gradient pulse type:** trap
gradient strength (mT/m)=[0. 45.6028763 64.49220961 78.98648589 91.20575259 101.97111514 111.70374823 120.65385498 128.98438523 136.8085949 144.20894464 151.24760284 157.97297177 164.42349457 170.63030639 176.61913797 182.4114712 188.02545695 193.47659484 198.77831105 203.94223029]
b-Value calculated using ST formula: trap pulse, risetime(ms)=0.1000, duration(ms)=7.2000, pulsespacing(ms)35.3470
qmax (1/mm)= 392.815
b-values (s/mm^2)= [0. , 247.43, 494.86, 742.29, 989.72, 1237.14, 1484.57, 1732. , 1979.43, 2226.86, 2474.29, 2721.72, 2969.15, 3216.58, 3464. , 3711.43, 3958.86, 4206.29, 4453.72, 4701.15, 4948.58]
Dwell time(s)=0.001, **Recovery time(s)=**9.096
Subtract background;[-16.44-15.8j ,-23.88-19.34j, -3.48-17.59j,-31.48-30.3j , 33.27 -0.96j, -11.66-47.87j,-35.83-25.j ,-32.58-20.03j, 33.04-16.77j,-29.62 +8.18j, -31.69+17.6j , 11.74-23.14j, -2.52-29.52j,-13.57-22.72j,-39.67-14.79j, -0.89-29.8j ,-29.76-38.21j,-11.42-37.52j,-26.56 +5.64j,-39.51 -2.65j, -6.40 -2.59j]
Phase angles=[118.002, 116.355, 119.956, 121.521, 121.834, 122.849, 125.35 , 124.777, 124.369, 123.537, 122.298, 123.61 , 123.001, 123.482, 122.368, 123.204, 118.94 , 120.239, 120.954, 124.091, 123.436]
Integration: from spectra=0, peak found at 1857,f0=46.5088Hz, approx FWHM=1.465Hz, Smax=3.441e-08,T2*(ms)=217.29955

Integrate n linewidths, **Integration width (Hz)**=29.29688
Fine phase adjust 0: Phase angles=[127.002 126.355 128.956 127.521 126.834 127.849 128.35 128.777 128.369 128.537 128.298 127.61 128.001 128.482 128.368 128.204 127.94 128.239 127.954 130.091 126.436]

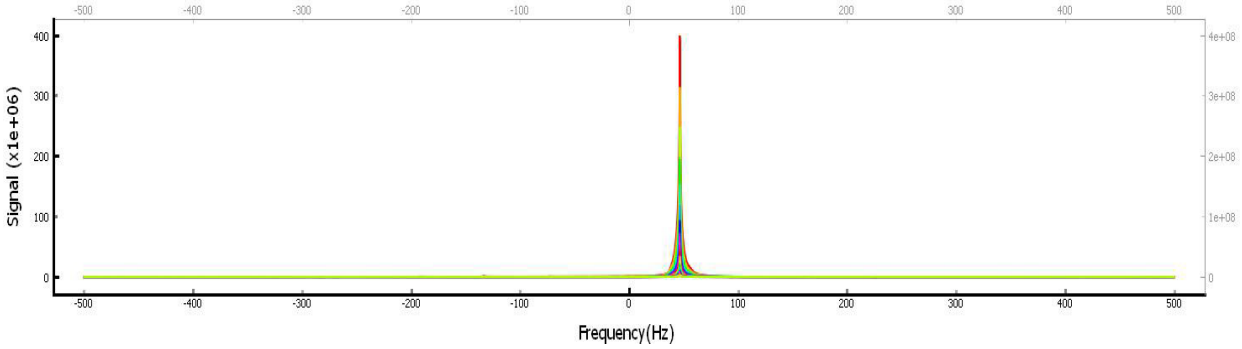

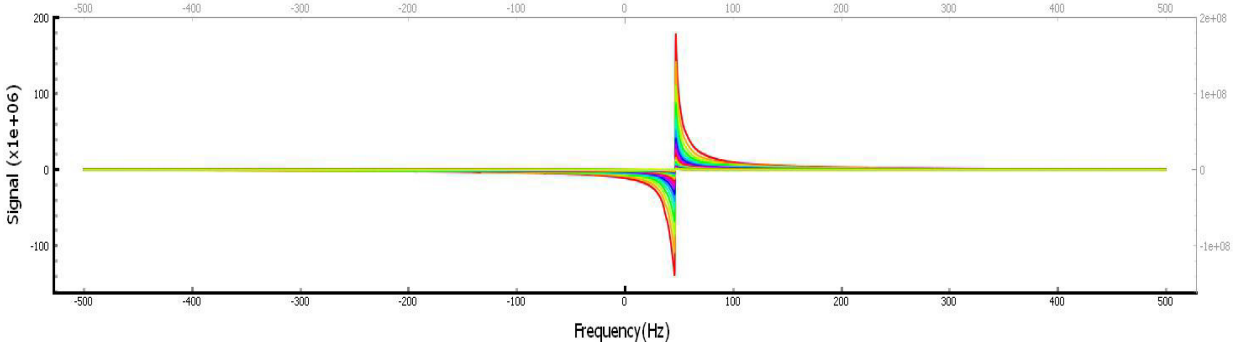

Integrating real part of Diffusion data from 1797 to 1917, from 31.86Hz to 61.16Hz, **Phase adj**(degree)=0.0
Diffusion-PGSE fit repeat=0: bValue(s)
[[Variables]] ADC: 0.00098836 +/- 1.24e-06 (0.13%) (init= 0.0004041566) K: 0 (fixed) Si: 0.99882783 +/- 0.000784 (0.08%) (init= 1) ADC2: 8.083132e-05 (fixed) Si2: 0 (fixed) B: 0 (fixed) [[Correlations]] (unreported correlations are < 0.100) C(ADC, Si) = 0.617
Ave of fits, ADC mean and sd (10^-3 mm^2/s)= 0.9884, 0.0000
Diffusion-PGSE fit repeat=all: bValue(s)
[[Variables]] ADC: 0.00098836 +/- 1.24e-06 (0.13%) (init= 0.0004041566) K: 0 (fixed) Si: 0.99882783 +/- 0.000784 (0.08%) (init= 1) ADC2: 8.083132e-05 (fixed) Si2: 0 (fixed) B: 0 (fixed) [[Correlations]] (unreported correlations are < 0.100) C(ADC, Si) = 0.617
Fitting All, ADCall (10^-3 mm^2/s)=0.988
Fstat=nan, p-value=nan, Standard deviation of residuals=9.3020e-04, **quality of fit OK**
Measured ADC values (10^-3 mm^2/s)=[0.988]
Reported diffusion coefficient (10^-3 mm^2/s) =0.988
Eddy corrected Y-diffusion coefficient(10^-3 mm^2/s) = 0.979, ECC=0.010

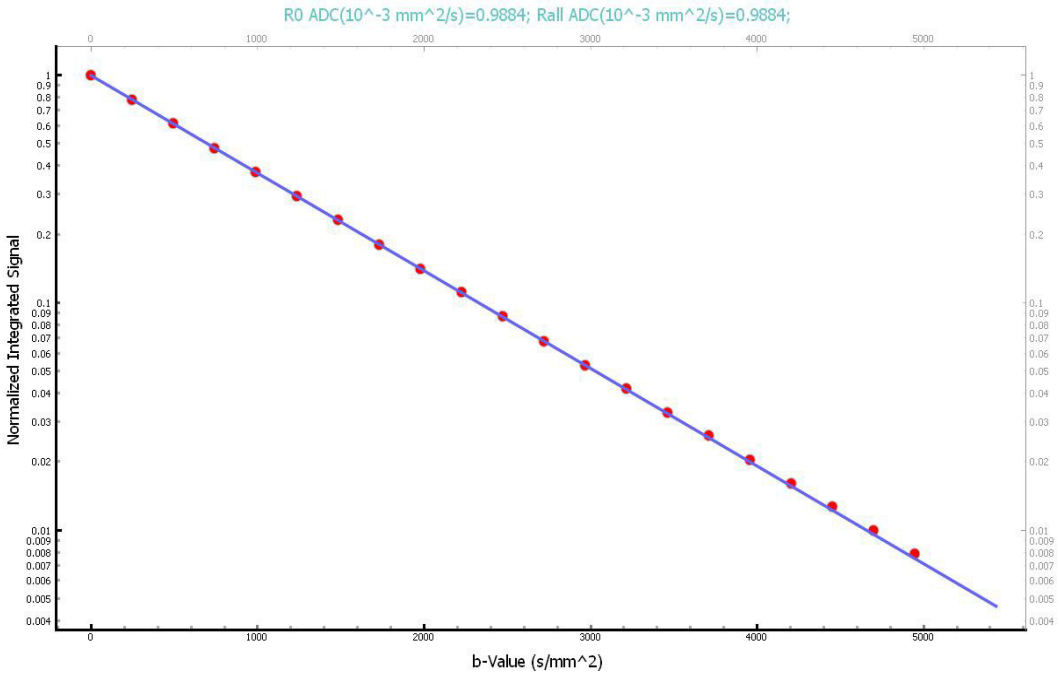

Diffusion Summary
*****Recovery time(s)= 9.096 ?adequate? *****
ImaxGx, ImaxGy(A)=7.069 7.214, Gradient Cal: Gxcal, Gycal(mT/m/A)=48.606 47.116Eddy Current Corrections (ECC): GxECC,GyECC(10^-3 mm^2/s)=0.0098 0.0035 Corrected Diffusion Coefficients: Dx, Dy, Dav(10^-3 mm^2/s)= 0.986 0.979 0.982
Diffusion Summary: Recovery time, ImaxGx, ImaxGy, GxCal, GyCal, ECCx, ECCy, Dx, Dy, Dav
9.096 7.069 7.214 48.606 47.116 0.0098 0.0035 0.986 0.979 0.982

Appendix C. Simulator Input File and Screen Shot

The following input file contains the information to setup the distributions required for the Monte Carlo calculation and the pulse sequence used by the Bloch simulator.

#A-2601-1038 20% Aqueous PVP NiCl2 16 831.1 682.2 1.041 dDdT=0.0324

PulseSequenceFile: 09/30/17 21:39:08 #general pulsed gradient spin echo sequence
PulseSequenceName=PGSE-PVP20-16C
PulseSequenceType=PGSE
B0(T)=3.0
gamma(rad/s/T)=267515317.087
Temperature(C)=16
TR(s)=1.02604049517
TE(s)=0.1
TI(s)=0.1
T1(s)=0.8311
T2(s)=0.6822
T1TempCo(%/C)=1.3
T2TempCo(%/C)=1.3
ADC(mm2/s)=1.041e-3
ADCTempCo(mm2/sC)=0.0324E-3
nSpinPackets=2500

SpinPacketDistribution=RandomCylinder
nIterations=4
SampleLength(mm)=3.0
SampleWidth(mm)=3.0
SampleOffsetMax=1
SampleOffsetType=Random
B1AmpError=0.05
B1NonUniformity=TecMagQuartic
RandomLocalField=Gaussian
LocalFieldWidth(T)=0.04E-6
LocalFieldAve(T)=0.0
ReceivePhaseJitter=5
TimeBaseError=5E-6
TimeBaseJitter(ns)=0.200
TransmitPhaseJitter=1.0
TempUncert(C)=0.10
TempTransferUncert(C)=0.1
TempFluc(C)=0.025
SNRinv=0.001
bValueUn(%)=1
gradCalUn(%)=1
gradientUniformity=Quadratic
EddyCurrentCorrectionUn(mm2/s)=0.005E-3
OutputFile=DataOut
QuietMode=True
AutoSave=True
XpType=Gx(mT/m)
Xp=[0. 46.21 65.36 80.05 92.43 103.34 113.2 122.27 130.71 138.64 146.14 153.27 160.09 166.63 172.92 178.99 184.86 190.55 196.07 201.44 206.68] #gradients in mT/m, usually chosen to increment by square root so b-value increases linearly
ntsteps=400000
Event: Type=RF, Name=excite,tStart(s)=0.0, EventDuration(s)=1.34983898415e-05, EventPropagator=odeint, mPoints=128, PulseShape=Trapezoid, PulseWidth(s)=1.34983898415e-05, RiseTime(s)=0, FallTime(s)=0, PulseAmp(T)=0.000435, RFPhase(deg)=0, FreqOffset(Hz)=0
Event: Type=delay, Name=tau, tStart(s)=1.34983898415e-05, EventDuration(s)=0.001, EventPropagator=odeint, mPoints=1000
Event: Type=Grad, Name=dGrad1,tStart(s)=1.0134983e-03, EventDuration(s)=7.2e-3, EventPropagator=odeint, mPoints=128, gPulseShape=Trapezoid, gPulseWidth(s)=7e-03, gRiseTime(s)=0.1E-3, gFallTime(s)=0.1E-3,Gx(T/m)=0.20
Event: Type=delay, Name=delta, tStart(s)=1.34983898415e-05, EventDuration(s)=0.014, EventPropagator=odeint, mPoints=1000
Event: Type=RF, Name=qflip, tStart(s)=0.00101349838984, EventDuration(s)=2.69967796829e-05, EventPropagator=odeint, mPoints=128, PulseShape=Trapezoid, PulseWidth(s)=2.69967796829e-05, RiseTime(s)=0, FallTime(s)=0, PulseAmp(T)=0.000435, RFPhase(deg)=90, FreqOffset(Hz)=0
Event: Type=delay, Name=delta, tStart(s)=1.34983898415e-05, EventDuration(s)=0.014, EventPropagator=odeint, mPoints=1000
Event: Type=Grad, Name=dGrad2,tStart(s)=0.0, EventDuration(s)=7.2e-3, EventPropagator=odeint, mPoints=128, gPulseShape=Trapezoid, gPulseWidth(s)=7e-03, gRiseTime(s)=0.1E-3, gFallTime(s)=0.1E-3,Gx(T/m)=0.20
Event: Type=delay, Name=tau2, tStart(s)=0.00104049516952, EventDuration(s)=0.001, EventPropagator=odeint, mPoints=1000
Event: Type=AcqWin, Name=acq, tStart(s)=0.00204049516952, EventDuration(s)=2.048, EventPropagator=odeint, mPoints=2048, ReceiverPhase(deg)=90

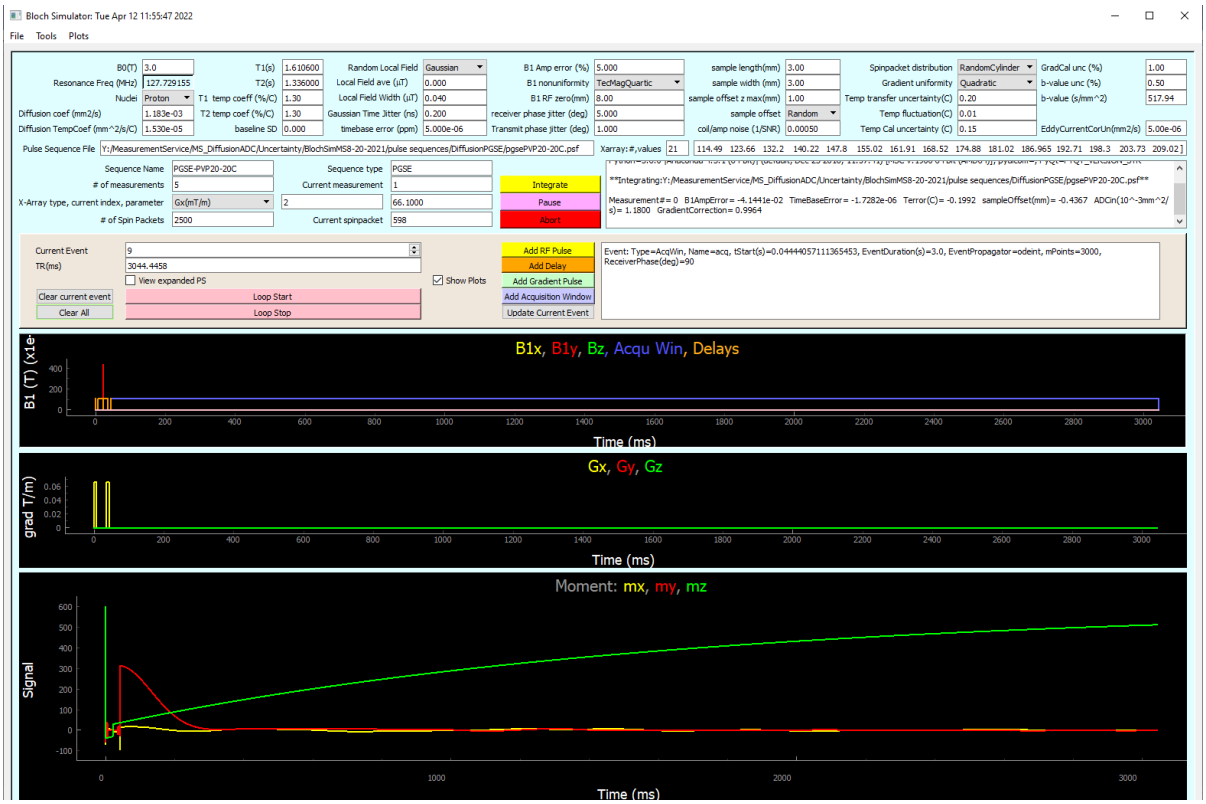

Fig. A3.1 Screen shot from Monte Carlo simulation showing a PGSE pulse sequence and simulated free induction decay